Philipps Universität Marburg

Antigen 43-mediated biotin display and fabrication of bacteria-driven microswimmers

Dissertation

Zur Erlangung des Doktorgrades

der Naturwissenschaften

(Dr. rer. nat.)

dem Fachbereich Biologie

der Philipps-Universität Marburg

vorgelegt

von

Oliver Schauer

aus Gießen

Marburg, September 2018

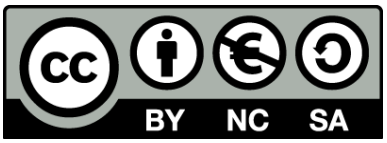

Die Untersuchungen zur vorliegenden Arbeit wurden von September 2014 bis August 2018 am Max-Planck-Institut für terrestrische Mikrobiologie in Marburg unter der Leitung von Prof. Dr. Victor Sourjik durchgeführt.

Vom Fachbereich Biologie der Philipps Universität Marburg

als Dissertation angenommen am: 30.10.2018

Erstgutachter: Prof. Dr. Victor Sourjik
Zweitgutachter: Prof. Dr. Michael Bölker

Weitere Mitglieder der Prüfungskommission:

Prof. Dr. Anke Becker
Prof. Dr. Martin Thanbichler

Tag der mündlichen Prüfung: 01.11.2018

Die während der Promotion erzielten Ergebnisse wurden in folgender Originalpublikationen veröffentlicht:

Schauer O, Mostaghaci B, Colin R, Hürtgen D, Kraus D, Sitti M, Sourjik V (2018) Motility and chemotaxis of bacteria-driven microswimmers fabricated using antigen 43-mediated biotin display. *Sci Rep* 8(1):9801.

Alapan Y, Yasa O, **Schauer O**, Giltinan J, Tabak AF, Sourjik V, Sitti M (2018) Soft erythrocyte-based bacterial microswimmers for cargo delivery. *Science Robotics* 3(17).

“Try and leave this world a little better than you found it and when your turn comes to die, you can die happy in feeling that at any rate you have not wasted your time but have done your best.”

Robert Baden-Powell

Content

Abbreviations

aa	amino acids
CFP	cyan fluorescent protein
ddH_2O	sterile ultra-pure water
DNA	deoxyribonucleic acid
dNTP	deoxyribonucleotide triphosphate
EDTA	ethylene diamine -tetra-acetic acid
GFP	green fluorescent protein
IPTG	isopropyl-β-D-1-thiogalactopyranoside
mCherry	monomeric red fluorescent protein mCherry
OD_{600}	optical density at 600 nm
RFU	relative fluorescence units
rpm	Rotation per minute
SEM	standard error
STD	standard deviation

Abstract

Controlled attachment of bacterial cells to biotic and abiotic surfaces without affecting their fitness is of great interest in biotechnological applications, such as patterning surfaces with cell-based biosensors, cell-cell attachment in syntrophic communities and fabrication of bacteria-driven biohybrid microswimmers. For years genetically modified outer membrane proteins and autotransporters were used to functionalize the bacterial cell surface with peptides and small proteins used for peptide library screening, bioremediation and biocatalysis. In this study we modified *Escherichia coli* (*E. coli*) to autonomously display biotin on its cell surface via the engineered autotransporter antigen 43 (Ag43) and thus to bind to streptavidin modified surfaces. We could show that a biotin acceptor peptide (BAP) at the N-terminus of Ag43 is biotinylated in the cytoplasm, translocated to the cell surface and accessible to free or surface bound streptavidin. Flow cytometry measurements and fluorescence microscopy imaging of cells stained with fluorescently labelled streptavidin indicate that the biotinylation is strongly dependent on the intracellular levels of biotin and the biotin protein ligase BirA. Moreover, the staining pattern of Ag43 suggests that the majority of Ag43 is located at the cell poles. In addition, we modified Ag43 with the LOV2 domain of *Arabidopsis thaliana*, to control the accessibility of the displayed biotin through light controlled photocaging. To examine the effect of attachment on the fitness of *E. coli*, we used laser-assisted adsorption by photobleaching (LAPAP) to micro-pattern an abiotic surface with biotin. Such immobilized cells were able to grow for several generations and released their daughter cells into the medium. Aside from Ag43 alternative display mechanisms including OmpA (outer membrane protein A), INP (ice nucleating protein), AIDA-I (autotransporter) and FliC (flagellin), were investigated for biotin display, although only modified flagellin showed pronounced attachment to streptavidin.

In a second part we used the Ag43 based biotin display system to fabricate bacteria-driven biohybrid microswimmers (bacteriabots). Bacteriabots combine synthetic cargo

with motile bacteria that enable propulsion and steering. Although fabrication and potential use of such bacteriabots have attracted much attention, existing methods of fabrication require an extensive sample preparation that can drastically decrease the viability and motility of bacteria. Moreover, chemotactic behavior of bacteriabots in a liquid medium with chemical gradients has remained largely unclear. To overcome these shortcomings, we used our Ag43 based biotin display system to bind cells to streptavidin-coated cargo. We show that the cargo attachment to these bacteria is greatly enhanced by motility and occurs predominantly at the cell poles, which is greatly beneficial for the fabrication of motile bacteriabots. We further performed a systematic study to understand and optimize the ability of these bacteriabots to follow chemical gradients. We demonstrate that the chemotaxis of bacteriabots is primarily limited by the cargo-dependent reduction of swimming speed and show that the fabrication of bacteriabots using elongated *E. coli* cells can be used to overcome this limitation.

Zusammenfassung

Die kontrollierte Anheftung von Bakterienzellen an biotische und abiotische Oberflächen, ohne Beeinträchtigung ihrer Fitness, ist von großem Interesse für biotechnologische Anwendungen, wie zum Beispiel bei der Strukturierung von Oberflächen mit zellbasierten Biosensoren, der Zell-Zell-Bindung in syntrophen Gemeinschaften und der Herstellung von biohybriden Mikroschwimmern angetriebenen von Bakterien. Seit Jahren werden genetisch modifizierte äußere Membranproteine und Autotransporter benutzt, um die bakterielle Zelloberfläche mit Peptiden und kleinen Proteinen zu funktionalisieren die für das Screening von Peptidbibliotheken, Bioremediation und Biokatalyse verwendet werden können. In dieser Arbeit haben wir *Escherichia coli* (*E. coli*) modifiziert, um mit Hilfe von Autotransporter Antigen 43 (Ag43) autonom Biotin auf der Zelloberfläche zu präsentieren und somit an Streptavidin-modifizierten Oberflächen anzuheften zu können. Wir konnten zeigen, dass ein Biotin-Akzeptor-Peptid (BAP) am N-Terminus von Ag43 im Zytoplasma biotinyliert, an die Zelloberfläche transloziert und für freies oder oberflächengebundenes Streptavidin zugänglich war. Durchflusszytometrie-Messungen und fluoreszenzmikroskopische Aufnahmen von Zellen, die mit fluoreszenzmarkiertem Streptavidin angefärbt wurden, zeigten, dass die Biotinylierung stark von der intrazellulären Konzentration von Biotin und der Biotin-Protein-Ligase BirA abhängig ist. Darüber hinaus deutet das Färbemuster von Ag43 darauf hin, dass Ag43 größtenteils an den Zellpolen lokalisiert ist. Zusätzlich modifizierten wir Ag43 mit der LOV2-Domäne von *Arabidopsis thaliana*, um die Zugänglichkeit des präsentierenden Biotins durch lichtgesteuerte Photoaktivierung zu kontrollieren. Um die Fitness von angehefteten *E. coli* Zellen zu untersuchen, verwendeten wir die lasergestützte Adsorption durch Photobleichung (LAPAP) und konnten dadurch abiotische Oberfläche im Mikrometerbereich mit Biotin strukturieren. Solche immobilisierten Zellen waren in der Lage für mehrere Generationen zu wachsen und ihre Tochterzellen in das umgebende Medium freizusetzen. Neben Ag43 wurden alternative Membranproteine

wie OmpA (*outer membrane protein A*), INP (*ice nucleating protein*), AIDA-I (Autotransporter) und FliC (Flagellin) auf die Möglichkeit untersucht Biotin zu präsentieren, wobei nur modifiziertes Flagellin eine ausreichende Bindung zu Streptavidin aufwies.

Im zweiten Teil dieser Arbeit verwendeten wir das auf Ag43 basierte Biotin-Präsentationssystem um biohybride Mikroschwimmer herzustellen die von Bakterien angetriebenen werden (*Bacteriabots*). *Bacteriabots* bestehen aus einer synthetischen Ladung die mittels Bakterien angetrieben und gesteuert wird. Obwohl die Herstellung und potentielle Verwendung solcher *Bacteriabots* viel Aufmerksamkeit auf sich gezogen hat, erfordern bestehende Herstellungsverfahren immer noch eine umfangreiche Probenvorbereitung, die die Fitness und Motilität von Bakterien drastisch verringern kann. Darüber hinaus ist das chemotaktische Verhalten von *Bacteriabots* in einer Flüssigkeit mit chemischen Gradienten weitgehend unerforscht. Um diese Defizite anzugehen verwendeten wir das auf Ag43 basierte Biotin-Präsentationssystem, um Zellen und eine mit Streptavidin beschichtete Ladung miteinander zu verbinden. Wir konnten zeigen, dass die Beladung von Batterien strak von deren Motilität abhängt und vorwiegend an den Zellpolen auftritt, was für die Herstellung von motilen *Bacteriabots* sehr vorteilhaft ist. Des Weiteren untersuchten wir in wie weit die verwendeten Bakterien einem chemischen Gradienten folgen können und versuchten diese Fähigkeit zu optimieren. In diesem Zusammenhang konnten wir demonstrieren, dass die Chemotaxis von *Bacteriabots* primär durch die Beladung verursachte Verringerung der Geschwindigkeit limitiert ist und dass die Verwendung von langgestreckten *E. coli* Zellen für die Herstellung von *Bacteriabots* diese Limitierung überwinden können.

1 Introduction

1.1 Bacterial cell surface display systems

The cell surface of bacteria harbors a variety of membrane proteins including receptors, enzymes, transporters and cell adhesion proteins. Moreover, cell surface appendages like flagella, pili, curli and fimbriae are assembled from many subunits and protrude far into the extracellular space. Since these proteins can be genetically modified[1], they can be used to target recombinant proteins (passenger proteins) to the surface of living cells and therefore expose them to the extracellular environment. This has the advantage that molecules, proteins or bigger structures that cannot cross the cell envelope can be used to interact with the passenger protein. Together with a high abundance of up to 10^5–10^6 membrane proteins per cell[2] makes it useful for various biotechnological applications[3], including the display of antigens for vaccine-delivery systems[4], enzymes for whole-cell biocatalytic systems[5] and protein libraries for screening purposes [6]. In the past such surface display systems were established for eukaryotic cell lines[7], yeast[8, 9], gram positive[10, 11] and gram negative bacteria[12, 13]. However, the most frequently used organism is *Escherichia coli (E. coli)*, which is the most accessible bacterium for genetic engineering and broadly used for producing recombinant proteins. Here Appendix-Table 1 gives a comparative overview over the used cell surface display proteins and the corresponding passenger proteins.

The most commonly used proteins for surface display are outer membrane proteins and autotransporter proteins (Figure 1). Both are integral outer membrane proteins and span the outer membrane with antiparallel β-sheets. Surface display precursor proteins are produced in the cytoplasm and due to their N-terminal signal peptide are translocated via the SecYEG complex across the cytoplasmic membrane[14]. During translocation a signal peptidase cleaves off the signal peptide and releases the mature protein into the periplasm. In the case of outer membrane proteins periplasmic chaperones associate with the protein and keep it in an unfolded state, until it is embedded into the outer

membrane, via the BAM complex[15]. The peptide or protein of interest that will be displayed (passenger protein) is typically located at the C-terminus or a loop protruding from the outer membrane protein, which is exposed to the extracellular space. On the other hand the type V secretion system of autotransporters involves the Sec system for crossing the inner membrane. The C-terminal domain of these proteins create a porin–like structure in the outer membrane facilitated by their inherent auto chaperone domain and periplasmic chaperones[16]. The N-terminal passenger domain is translocated to the cell surface with an additional ~50 amino acid linker region spanning the β-barrel pore[17]. In case of autotransporters the protein of interest is typically located within or at the N-terminus of the passenger domain.

One of the most used outer membrane proteins is a chimera of the first 29 amino acids of Lpp, the major *E. coli* lipoprotein, which includes its natural signal sequence, and the transmembrane domain (amino acids 46 to 159) of the outer membrane protein A (OmpA)[18, 19]. The N-terminus of OmpA was used to display heterologous proteins like scFv antibody, β-lactamase[20] or cellulases[21, 22]. Autotransporter proteins are widely used to display entire protein domains, which retains their functionality and ability to dimerize[23, 24]. Prominent representatives for autotransporter proteins are AIDA-I from pathogenic *E. coli* (DAEC) strains[25, 26] and antigen 43 (Ag43)[24, 27] from *E. coli* K12 which are involved in cell auto-aggregation and translocate naturally a 797 amino acid and 498 amino acid passenger domain across the outer membrane. Lipoproteins, like truncated derivatives of the ice nucleation protein (INP) of *Pseudomonas syringae*[28], have been reported to display the largest passenger proteins among the surface display systems for *E. coli*[1, 13]. In contrast to the above described insertion of β-sheets into the outer membrane, lipoproteins form a covalent linkage between its relatively hydrophobic N-terminus and a lipid moiety[29, 30]. Besides integral membrane proteins, cell surface appendages like fimbriae and flagella are used to display recombinant peptides far beyond the cell surface, which prevents an interference with membrane proteins, lipopolysaccharides (LPS), extracellular polymeric substances (EPS) and other outer membrane associated molecules. An additional advantage is that fimbria and flagella are composed of numerous identical subunits, facilitating dense accumulation of displayed peptides[31]. However, since the construction of these filaments depends on a

defined conformation of their subunits, a conformational change through an incorporated peptide can be detrimental for its integrity. Additionally, the flagellin subunits FliC and flagellar cap protein FliD are translocated through the central channel of the flagellum[32], with a diameter of about 2 nm, which limits the introduction of peptides to under 60 amino acids[33, 34]. Structural analysis of the flagellin subunit FliC identified variable regions, which allow the deletion of up to 187 amino acids without loss of function or polymerisation of the flagellum[35]. Westerlund-Wikstrom, *et al.* (1997)[36] could demonstrate that larger proteins like the 302 amino acid YadA adhesin can be displayed by replacing such variable regions.

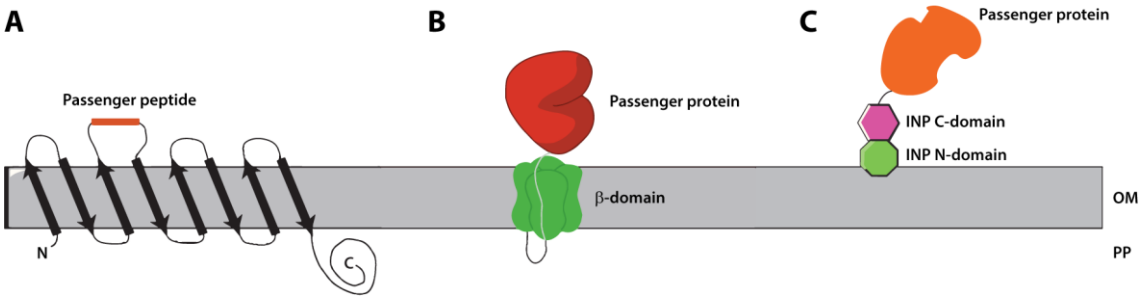

Figure 1 Schematic representations of typical *E. coli* surface display systems. Obtained and modified from van Bloois, *et al.* (2011)[13] **(A)** OmpA with a passenger peptide (orange) inserted into a surface exposed region. The transmembrane antiparallel β-sheets are shown as arrows. **(B)** An autotransporter-based display scaffold used for the surface presentation of an N-terminally fused passenger enzyme (orange). **(C)** N and C domains of the ice nucleation protein with truncation of the entire internal repeating domain. PP: periplasm, OM: outer membrane.

1.1.1 Antigen 43

Antigen 43 (Ag43) is with 50,000 copies per cell one of the most abundant outer membrane proteins of *E. coli* and belongs to the autotransporter family[27, 37, 38]. The gene *agn43* encodes for the 1,039 amino acid protein, which has the typical domain architecture of autotransporter and comprises of an N-terminal signal sequence, a secreted passenger domain (α domain) and a β-domain comprising an autochaperone domain and a C-terminal integral outer membrane β-barrel domain(Figure 2A). The signal sequence targets Ag43 to the inner membrane and directs its translocation across the membrane via the Sec system into the periplasmic space[14, 16]. The passenger domain of Ag43 is secreted to the outer cell surface and forms a twisted L-shaped β-helical structure with a length of about 100 Å[39, 40]. The L-shaped structure facilitates self-association of Ag43 by hydrogen bonds forming between two parallel strands and

consequential leads to auto-aggregation between cells which express it (Figure 2B)[41]. The autochaperone domain together with periplasmic chaperones (DegP, FkpA, Skp and SurA) and accessory factors (Bam complex) presumably translocate and incorporate the C-terminal β-barrel domain into the outer membrane by forming a β-barrel pore, through which the passenger domain is secreted[42-44]. According to immunofluorescence studies Ag43 is homogeneously distributed over the cell surface[41]. However, Jain*, et al.* (2006)[45] could demonstrate that the localization of various autotransporters, including AIDA-I, a close homologue to Ag43, are highly dependent on the composition of the outer membrane, the lipopolysaccharide length and the autotransporter abundance (Figure 2C,D), suggesting that also the localization of Ag43 can vary.

The expression of *agn43* features phase variation and is dependent on the competitive binding between the repressor OxyR and the deoxyadenosine methyltransferase (Dam)[46]. The expression state of a cell can be inherited by the next generation yet the switch between the phases is reversible. The deletion of *oxyR* or *dam* leads to locking the cells in the On or Off phase, respectively[47, 48]. This phase variation creates phenotypic heterogeneity within a clonal population and leads to a selective autoaggregation of cells in the On phase. Several studies could demonstrate that this Ag43 mediated cell-to-cell interaction enhances the formation of *E. coli* biofilms[49, 50], which is supported by the increased expression of Ag43 during biofilm growth compared to exponential and stationary planktonic cultures[51].

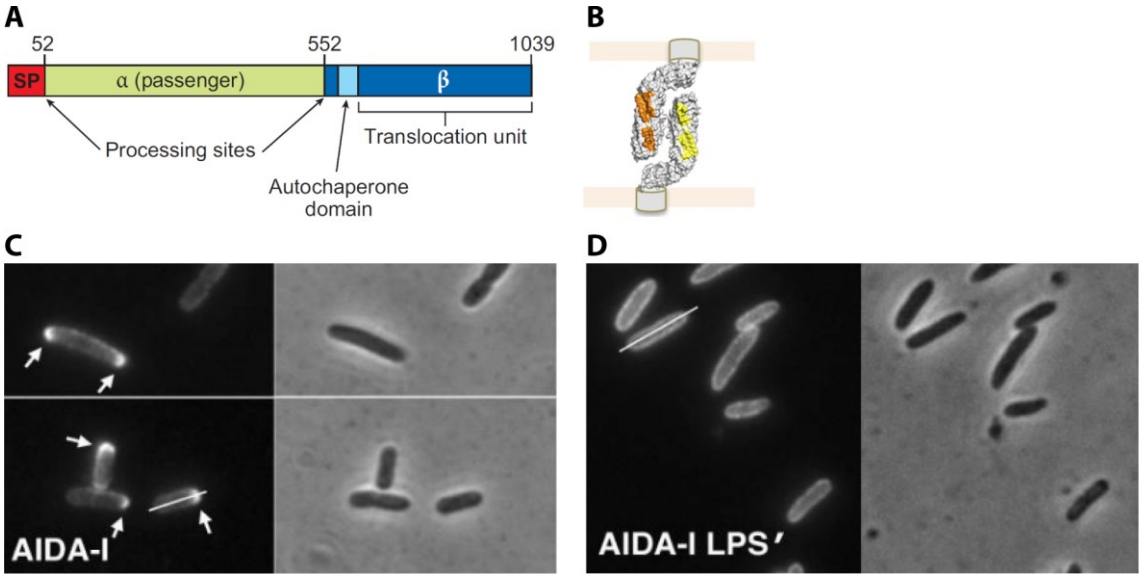

Figure 2 Domain organization of Ag43 and differential localization of AIDA-I. Obtained and modified from van der Woude, *et al.* (2008)[27], Heras, *et al.* (2014)[39] and Jain, *et al.* (2006)[45]. **(A)** Schematic representation of the protein domains of Ag43. Shown are the signal peptide (red), the α-domain (green), the β-domain (blue), and the autochaperone domain (light blue). Numbers designate the numbers of amino acids at the domain boundary. **(B)** Model of Ag43 self-assembly in a head-to-tail conformation. The interacting surfaces of the α-domain (shown in yellow and orange) are easily accessible to neighboring molecules. **(C, D)** The localization of autotransporter AIDA-I, expressed from a plasmid, on the surface of *E. coli* 2443 cells (strain 2443 ompT pIB264), which express a complete LPS (C) and on the surface of *E. coli* K-12 (strain MBG263/pIB264), which express an incomplete LPS (D). Scale bar: 5 µm.

1.2 The use of biotin in biotechnological applications

Biotin, also known as vitamin H, can be found in organisms as free D-(+)-biotin, covalently bound to proteins or as biocytin an occurring intermediate from biotin metabolism. It is typically bound to multiple enzymes as prosthetic group and is involved as cofactor in carbon dioxide transfer like in fatty acid synthesis or gluconeogenesis[52]. In eukaryotic organisms biotin is involved in chromatin remodeling, since specific lysine residues in histones can be biotinylated by biotinidase and holocarboxylase synthetase[53]. In research and biotechnology the genetically modification of proteins allows for their specifically biotinylation, which is widely used to detect their localization in the cell or to isolate them from a complex environment. This is possible through the strong interaction between biotin and the protein streptavidin, which can be coupled to various dyes or surfaces.

1.2.1 The natural biotinylation system of *E. coli*

In *E. coli* the genes required for the syntheses of biotin (vitamin H) are encoded in the biotin biosynthetic operon (*bio*). The operon is controlled by the demand and availability of biotin in the cell[54, 55]. Extracellular biotin is imported into the cell through YigM, a secondary active transporter and a less efficient nonspecific transport[56]. Free biotin in the cell is inactive and has only a biological function when it is covalently bound to biotin acceptor proteins. This biotinylation is mediated through the 35.5 kDa biotin protein ligase BirA[57, 58], which activates biotin with ATP to a biotinoyl-5'-AMP intermediate and subsequently forms an amide linkage between the carboxyl group of biotin and the ε-amino group of a specific lysine within the acceptor protein (Figure **3**A)[59]. The only naturally biotinylate protein in *E. coli* is the biotin carboxyl carrier protein (BCCP), a subunit of the acetyl coenzyme A carboxylase (ACC). ACC uses the biotin as cofactor to catalyze the first step of the fatty acid synthesis, the carboxylation of acetyl-CoA to malonyl-CoA[60]. BirA is a bifunctional protein which, besides biotinylating BCCP, is a transcriptional repressor of the *bio* operon (Figure 3B,C)[61]. In the absence of BCCP, the BirA-biotinoyl-5'-AMP complex is thermodynamically very stable, which promotes the complex to dimerize[62] and bind to the operator site of the *bio* operon[63]. This allows BirA to balance the intracellular concentration of biotin and BCCP for efficient biotinylation[64]. The recognition and biotinylation by BirA is probably mediated through a structural feature within BCCP[59], positioning the biotin accepting lysine within the active site of BirA. Screening of synthetic peptides revealed that a consensus sequence of 13 amino acids is sufficient to specifically biotinylated the peptide[65], although the primary structure of this peptide showed low resemblance with the natural recognition side.

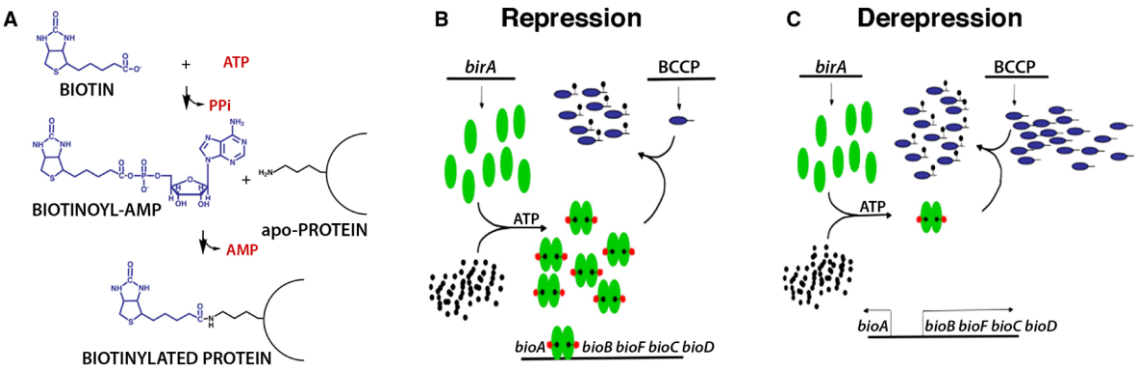

Figure 3 General model of *bio* operon regulation. Obtained and modified from Solbiati, *et al.* (2010)[66]. **(A)** The biotin protein ligase reaction. **(B, C)** General model of repression and derepression of *E. coli bio* operon transcription by BCCP supply. Green ovals denote BirA, tailed blue ovals are BCCP, black dots are biotin, and black dots with red pentagons are bio-AMP.

1.2.2 Streptavidin, its analogues and their interaction with biotin

Streptavidin, a homotetramer from *Streptomyces avidinii*, can form with biotin a stable bond over a wide range of temperatures and pH values, therefore it has been extensively studied for biotechnological applications. Since biotin can be used as a prostatic group and has a side chain that is easily conjugated to different moieties, it is used to immobilize molecules like DNA, RNA, proteins, nanoparticles or quantum dots, to a variety of substrates[67-69]. Moreover, biotinylation of proteins is a well-known process and is used to functionalize specific proteins in a mixed pool like the cytoplasm of the cell[70, 71]. Biotin is, with a size of 0.244 kD, a small molecule which has a minor effect on the properties of the attached protein. The posttranslational biotinylation of proteins is typically achieved by fusing a 15 amino acid biotin acceptor peptide[65, 72] at the N-terminus, C-terminus or within the protein of interest. In the presence of the *E. coli* enzyme biotin protein ligase (BirA) the lysine in the BAP sequence is specifically biotinylated. Here BirA can either be expressed within the cell simultaneously to the protein of interest or can be added externally to, for example, a cell lysate. The specificity of the BirA based biotinylation allows its use in various prokaryotic and eukaryotic systems without modifying endogenous proteins[73-75].

The interaction between streptavidin and biotin is highly specific and one of the strongest non-covalent bonds in nature, with a dissociation constant of 10^{-13} M to 10^{-15} M[76-78] and a binding strength of 5 pN to 170 pN[79]. To bind biotin efficiently, four

streptavidin monomers form a 52.8 kDa homotetramer, where each monomer has a binding site for one biotin molecule. Biotin is confined in the hydrophobic binding pocket of streptavidin by van der Waals interaction[80], eight hydrogen bonds[81] and an electronic polarization mediated through a cooperative effect of hydrogen bonds surrounding the binding side[82-84].

Streptavidin, avidin and NeutrAvidin are functional and structural analogues with a high affinity to biotin[85, 86]. Avidin is a glycosylated protein present in the egg white of oviparous vertebrates. NeutrAvidin is a commercial available deglycosylated derivate of avidin[87]. Besides the glycosylation of avidin the main difference between these three proteins is that avidin[77] is a basic protein with a high isoelectric point (pI) of 10.5, whereas streptavidin[77] with a pI of 5-6 and NeutrAvidin[87] with a pI of 6.3 are mildly acidic proteins. Owing to their lower charge, streptavidin and NeutrAvidin have a lower nonspecific protein–protein interaction at pH 7.4 than avidin.

1.2.3 Modifying the cell surface with biotin

In recent years efforts have been made to modify the surface of eukaryotic cell lines[88, 89], yeast[75, 90], gram positive[91] and gram negative[92-94] bacteria with biotin, since the interaction with streptavidin conjugated with molecules or immobilized on surfaces can be used for the identification and quantification of membrane proteins[88, 89, 91, 92], the isolating of rare cell populations from a complex cell mixture[95], electron microscopic and magnetic resonance tomographic imaging[90, 96], cell adhesion[94] and the display of non-natural molecules[75]. Depending on the organism, various methods were used, falling into the following three categories: chemical biotinylation of membrane proteins, enzymatic biotinylation of recombinant membrane proteins and biotinylated antibodies targeting membrane associated epitopes. The most widely used methods to chemically bind biotin to surface proteins are the use of sulfosuccinimidyl biotin which cross-links with exposed primary amine groups of proteins[92, 97-99] and N-biotinyl-L-lysine which reacts with oxidized glycosides of lipopolysaccharides[100]. This modification of the cell surface is mainly used to adhere cells stably on streptavidin coated surfaces like for example a rapid immobilization of eukaryotic cells to a substrate[101] or the attachment of

bacteria to nanoparticles used in the fabrication of bacteria-driven microswimmers[102, 103].

For the surface display of biotin, an outer membrane protein or motif targeting the outer membrane is used to translocate a typically 15 amino acid biotin acceptor peptide, which is enzymatically biotinylated either intracellularly or extracellularly by the biotin protein ligase BirA[65, 72] from *E. coli*. In eukaryotic cell lines modified membrane proteins like the growth factor receptor (EGFR)[104] and the platelet-derived growth factor receptor (PDGFR)[90] or the raft-targeting motif of the Lck kinase are used for the translocation[96], whereas in yeast the anchor domain of the flocculation protein Flo1p (Flo428) of *Saccharomyces cerevisiae* is used[75, 105]. The use of biotinylated antibodies is mainly used for *E. coli,* targeting the lipid A of the lipopolysaccharide[94] or OmpA[93]. The last two methods associate biotin to a specific protein or molecule on the cell surface, which allows their detection and cell sorting based on the used streptavidin conjugated ranging from fluorescent dyes[95] to small particles like quantum dots[106] and magnetic nanoparticles[96].

1.3 Bacteria propelled microswimmers

Cell-driven biohybrids have been studied widely over the last decade due to their potential biomedical applications, including the targeted active delivery of cargo, such as drugs, genes, or imaging contrast agents[94, 107-114]. Here, unicellular organisms, such as bacteria or algae, or cells of higher eukaryotes (*e.g.*, cardiomyocytes or spermatozoa), are used to propel the biohybrid swimmers in stagnant or low-velocity physiological fluids. Especially bacteria-driven microswimmers (bacteriabots) are a versatile tool due to the diversity of their sensory and tactic behaviors, high and robust motility in liquid media at diverse environmental conditions (*e.g.*, variable temperature, pH, oxygen concentration etc.) and therapeutic[115] and targeting[116] capabilities for specific diseases[117], as well as the potential for tailored genetic modifications bringing desired attributes. Recent studies have shown that bacteriabots based on *Escherichia coli, Serratia marcescens* or *Salmonella enterica* serovar Typhimurium can in principle follow chemoattractant gradients[118-122], including gradients toward cancerous cells[103, 109]. However, reliable application of such bacteriabots, in biomedicine and beyond,

requires better fundamental understanding of their chemotactic behavior, considering that the attachment of single or multiple bacteria to synthetic bodies (Figure 4), such as microparticles[112, 117, 119-121, 123], microsheets[124], microemulsions[94], and microtubes[125], is likely to affect their taxis performance compared to the free swimming bacteria.

Bacteriabots generally consist of motile bacteria which are attached to synthetic cargo (*e.g.*, microparticle). Although electrostatic or hydrophobic interactions provide the simplest ways to attach bacterial cells to the cargo[112, 123, 126], such attachment may not be specific and reliable enough to maintain their integrity, especially in biological fluids with high concentrations of proteins, ions and possible fluidic shear forces[115]. In contrast, protein-protein or protein-ligand interactions like between biotin/streptavidin[79], spytag/spycatcher[127], Jun/Fos[128] etc. are highly specific and very strong. Most commonly the attachment of cells decorated with biotin to streptavidin coated nanoparticles has been utilized in the fabrication of bacteriabots[94, 118, 129]. Although the bacterial cell surface could be functionalized with biotin through several methods as described before (section 1.2.3), the yield and efficiency of motile bacteriabots fabricated using these methods remained low, because several functionalization and washing steps negatively affect bacterial motility and viability. Moreover, the specificity of these methods is rather limited[130].

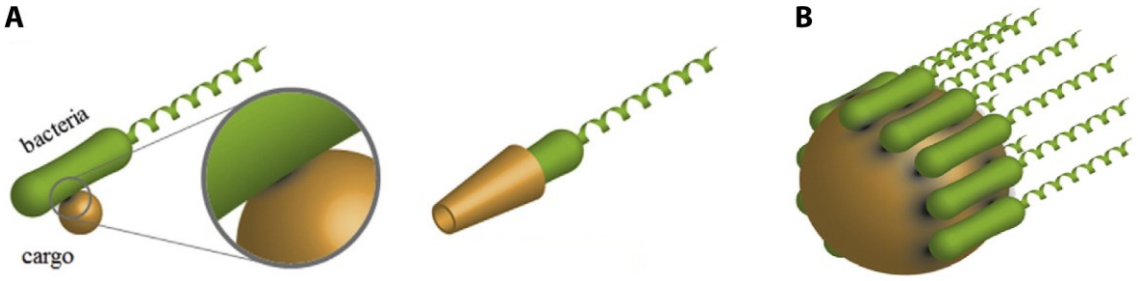

Figure 4 Attachment of single or multiple bacteria to synthetic cargo. Obtained and modified from Hosseinidoust, *et al.* (2016)[115]. Single-cell **(A)** and multi-cell **(B)** biohybrid systems with spherical or cone cargo.

1.4 Chemotaxis of *E. coli*

Like most organisms, bacteria are dependent on finding niches with optimal conditions for survival and growth. The ability of bacteria to sense and follow gradients of environmental stimuli, including nutrients, signal molecules, beneficial or harmful chemicals, pH, redox potential and temperature[131], is mediated through receptor proteins and a signaling cascade translating such stimuli into a change in motility[132]. Bacteria evolved a variety of surface depended motility systems, including swimming, swarming, gliding and twitching, whereas surface independent motility is restricted to swimming[133]. The rotation of flagella protruding from the cell surface, helical structures made of many flagellin subunits and powered by a membrane bound motor complex[134].

In case of the peritrichous *E. coli*, the model organism for bacterial chemotaxis[135], the propulsion of the cell is controlled by the direction of their flagellar motor rotation, with counterclockwise rotation resulting in the bundling of the multiple flagella, which powers more-or-less straight runs, and clockwise rotation leading to a partial disintegration of the bundle and cell tumbling[136]. In a homogeneous environment bacteria explores the environment in a random walk like manner (Figure 5A), achieved through runs lasting between one and two second followed by a tumble lasting about 0.1 s[137]. Similar to other chemotactic bacteria, swimming *E. coli* cells make temporal comparisons of their environment and modulate the run length dependent on whether the environment becomes more or less favorable, thus biasing the random walk towards the favorable direction (Figure 5B)[137-139]. The underlying chemotaxis signaling network (Figure 5C) of *E. coli* consists of five receptors (Tar, Tsr, Tap, Trg, and Aer), which are arranged in chemoreceptor clusters together with two cytoplasmic proteins, the adaptor CheW and the kinase CheA[140, 141]. Further cytoplasmic signaling proteins are the response regulator CheY, its phosphatase CheZ, and the receptor methylation/demethylation enzymes CheR and CheB. The main function of the sensory clusters is to process environmental stimuli and to provide a coordinated output – the level of CheY phosphorylation – controlling the direction of flagellar motor rotation. The wide dynamic range of stimuli discriminations in *E. coli* chemotaxis is maintained by the activity-dependent methylation of chemotaxis receptors. Receptor methylation compensates stimulus-induced changes in activity of the receptor-associated kinase

CheA, so that bacteria can adapt to constant background stimulation. Additionally, due to its delayed occurrence, receptor methylation also serves as a short-term memory, enabling the aforementioned temporal comparisons of environmental conditions.

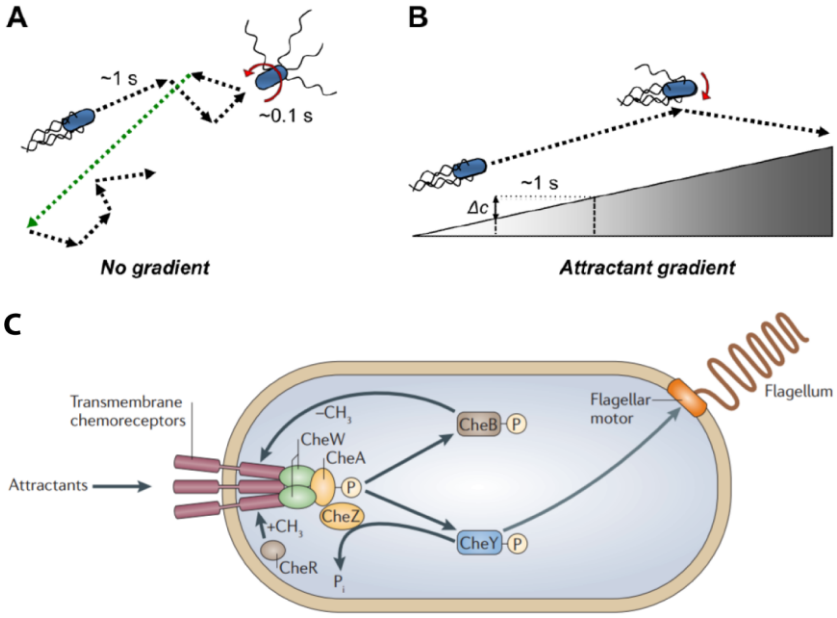

Figure 5 Chemotaxis strategy of *E. coli* and the underlying signaling network. Obtained and modified from Sourjik, *et al.* (2012)[142] Porter, *et al.* (2011)[143]. See text for more details.

1.5 Scope of this dissertation

In different fields of biotechnology a strong and specific attachment between bacterium and biotic or abiotic surfaces are needed. Up to this day different methods have been used, to a certain extent successfully to mediate such surface attachment, including unspecific interactions, the chemical modification of bacteria and the genetically modification of outer membrane proteins with functional peptides and small proteins. However most methods used so far either lack reliable attachment, specificity or require elaborate sample preparation which is accompanied by decreased fitness of the bacteria.
In this study we address this problem by constructing systems displaying biotin autonomously on the cell surface of *E. coli* and evaluating the attachment to surface bound streptavidin, including its potential for bacteriabot fabrication. Moreover, we investigate how chemotaxis of bacteria is affected when attached to synthetic cargo and apply our findings to overcome eventual limitations in bacteriabot fabrication.

2 RESULTS

2.1 Characterization of biotinylated peptides displayed on the bacterial cell surface

The aim of this study was the construction of a genetically engineered *E. coli* strain capable of directed and specific attachment to biotic and abiotic surfaces. We showed that the engineered autotransporter antigen 43 can be used to display biotin on the bacterial cell surface and characterize the biotin-streptavidin mediated attachment.

2.1.1 Modified autotransporter Ag43 displaying biotinylated peptides

For displaying biotin on the cell surface of *E. coli* we genetically modified the N-terminus of the endogenous Ag43 with an 15 amino acid biotin acceptor peptide (BAP)[65], which can be biotinylated intracellularly by the native biotin ligase BirA[72]. After successful translocation through the inner cell membrane and insertion into the outer membrane, the biotinylated N-terminus of Ag43 should be displayed on the cell surface[24] and thus accessible to extracellular molecules (Figure 6). To assess which position in Ag43 is best suitable for introducing BAP we made three constructs. Ag43-90aa-BAP had the BAP placed at the N-terminus of Ag43, Ag43-BAP-90aa had the BAP placed 90 amino acids downstream of the N-terminus, whereas for Ag43-BAP, the first 90 amino acids were missing. At the same site as BAP, we added a FLAG epitope for detecting the presence of the construct on the cell surface and a TEV protease restriction site to release and verify the extracellular localization of the biotin modified peptide. For visualization we stained biotin with NeutrAvidin (analogue of streptavidin) conjugated to a green fluorophore (NeutrAvidin-biotin staining), whereas the FLAG epitope was immunostained with a secondary antibody conjugated to a red fluorophore (see Material and Methods for details).

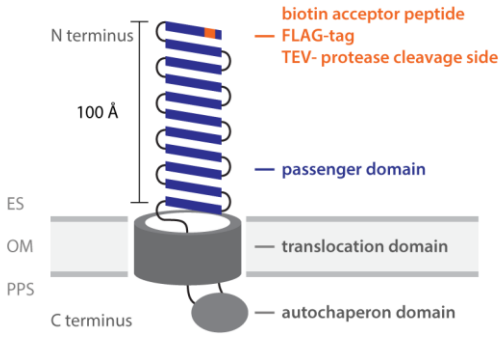

Figure 6 Design of the Ag43 based biotin display system. Schematic model of the Ag43-mediated peptide display. The N-terminus of Ag43 was modified with a FLAG epitope tag and a biotin acceptor peptide (BAP). ES: extracellular space, OM: outer membrane, PPS: periplasmic space.

The modified passenger domain of the recombinant Ag43 could be detected on the surface of most cells via FLAG-tag antibody staining of the outer membrane (Figure **7**A). In case of Ag43-BAP-90aa and Ag43-BAP the same cells also showed pronounced NeutrAvidin-biotin staining. The incubation of stained cells with TEV protease released the bound fluorescently labeled NeutrAvidin from the cell surface within 15 minutes (Figure 7C). This indicated that BAP was biotinylated in the cytoplasm, translocated to the cell surface and accessible to exogenous fluorescently labeled NeutrAvidin. However placing BAP at the full-length N-terminus of Ag43 (Ag43-90aa-BAP) showed weak staining, indicating that not all positions in Ag43 are accessible to BirA or NeutrAvidin. To promote the accessibility of surface bound NeutrAvidin we decided to use in all further described experiments the construct with the shortened Ag43 N-terminus, Ag43-BAP. Furthermore, quantification of the fluorescence microscopy images of Ag43-BAP stained with fluorescently labeled NeutrAvidin showed that in up to 35 % of the cells the protein was located at the cell poles, whereas the majority of cells had a rather uniform distribution (Figure 7B).

The quantification of biotinylated Ag43-BAP using flow cytometry allowed us to assess the limitations of the system and to optimize the biotin display (Figure 7C). Since the biotinylation is mainly dependent on biotin and BirA, we externally increased their availability and used the NeutrAvidin-biotin staining to assess the amount of biotin present on the cell surface. The addition of biotin to the growth medium increased the staining up to 4.4 fold. The further overexpression of BirA increased the biotinylation to about 9 fold compared to cells grown without biotin. This indicates that the BAP

biotinylation was partly limited by the availability of biotin and that the overexpression of BirA can drastically increase biotinylation. In order to determine if all translocated BAP was biotinylated, we incubated cells with exogenously added BirA and biotin after cell harvest. The further increase in the biotinylation suggested that even in presence of biotin in the growth medium and an increased intracellular level of BirA, *E. coli* biotinylated only a fraction of Ag43-BAP.

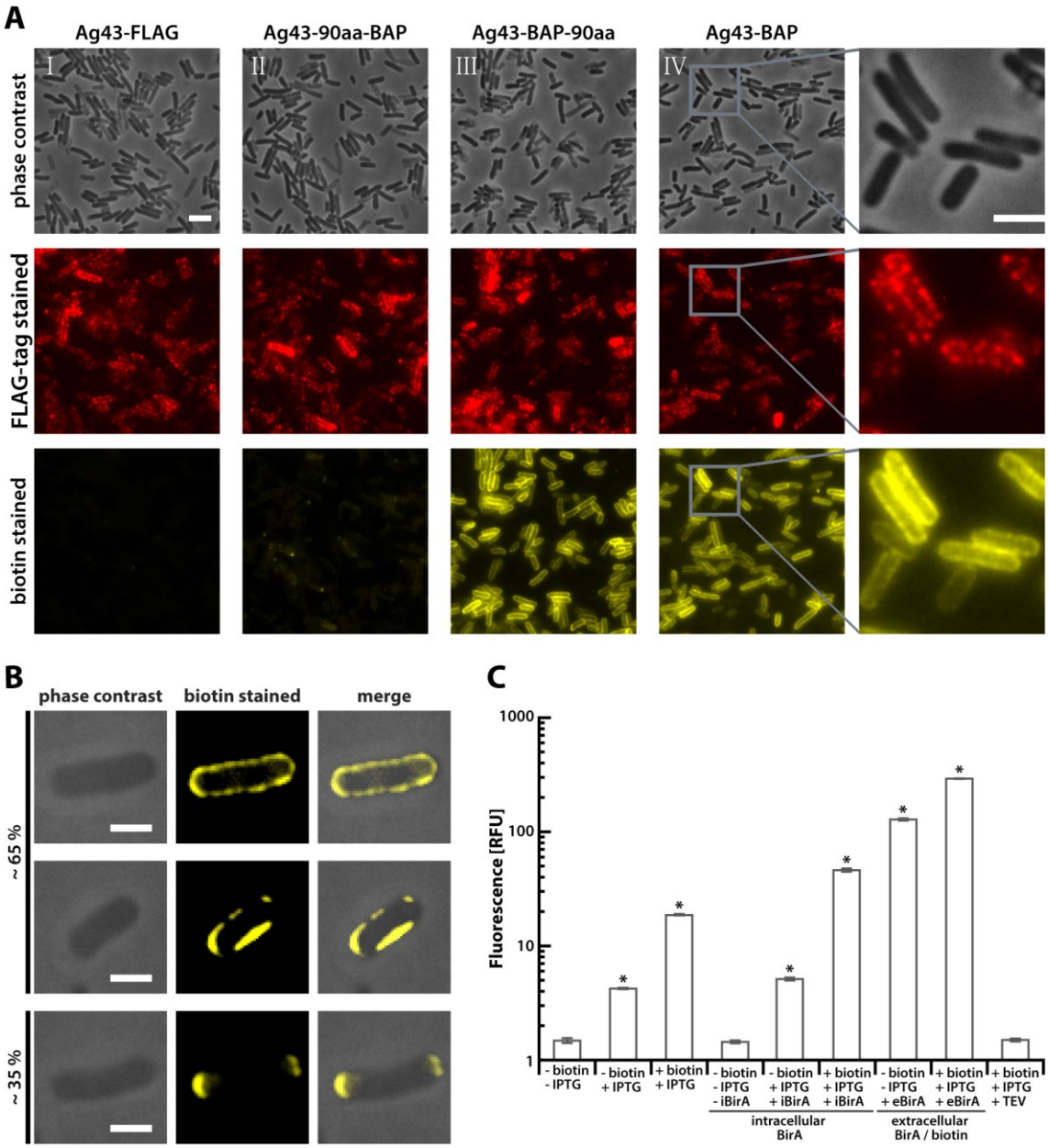

Figure 7 Quantification and localization of biotinylated Ag43-BAP displayed on the cell surface of *E. coli*. *E. coli* cells carrying a recombinant Ag43 on IPTG inducible plasmid were grown with 1 µM biotin and 100 µM IPTG in the growth medium, if not indicated differently. **(A)** *E. coli* cells carrying Ag43-FLAG with and without BAP variants (see text for more details) were analyzed using anti-FLAG immunostaining (red) and NeutrAvidin-biotin staining (yellow) for detecting recombinant Ag43-FLAG and surface-displayed biotin, respectively, and subsequent fluorescence microscopy. Scale bar: 4 µm. **(B)** Fluorescence images of *E. coli* cells carrying Ag43-BAP that were incubated with fluorescently labeled NeutrAvidin (yellow). Scale bar: 2 µm. **(C)** *E. coli* cells carrying Ag43-BAP, and BirA on a plasmid induced with arabinose (iBirA), were cultivated, washed and subsequently incubated with or without exogenous BirA / biotin (eBirA). TEV protease was added after NeutrAvidin-biotin staining for 15 min when indicated (TEV). Biotinylation was quantified via anti-biotin immunostaining measured by flow cytometry, as described in Material and Methods. Statistical analysis was performed using a two-sample t-test with unequal sample size and unequal variance, yielding highly significant differences between all datasets above 2 RFU (with asterisk indicating $P < 0.001$). Data are from six independent experiments.

2.1.2 Specific cell-cell attachment mediated through NeutrAvidin

Since the biotinylated peptide could be displayed on the cell surface, we investigated under which conditions the strong biotin-NeutrAvidin interaction causes cell-cell attachment. Different concentrations of NeutrAvidin were added to cell suspensions displaying biotin and determined the formation of cell aggregates after 30 min via bright-field microscopy. The addition of 1 µg/ml NeutrAvidin to cell suspensions with an OD_{600nm} of 0.0375 lead to cell-cell aggregation, which was absent at 10 µg/ml and 0.1 µg/ml of NeutrAvidin (Figure 8). Likewise aggregation was also seen by mixing untreated and NeutrAvidin saturated cells in a ratio of 5 to 1. In the presence of excess free biotin, the aggregation could be blocked, supporting that the cell-cell attachment is mediated by NeutrAvidin binding to displayed biotin of two neighboring cells. No aggregation was observed when cells were grown in TB medium (Figure 8), whereas it was clearly visible when biotin was added to this medium or cells were grown in a rich medium like LB medium. This supports the assumption that the availability of biotin in the growth medium influences the amount of displayed biotin per cell and thereby the specific aggregation via NeutrAvidin.

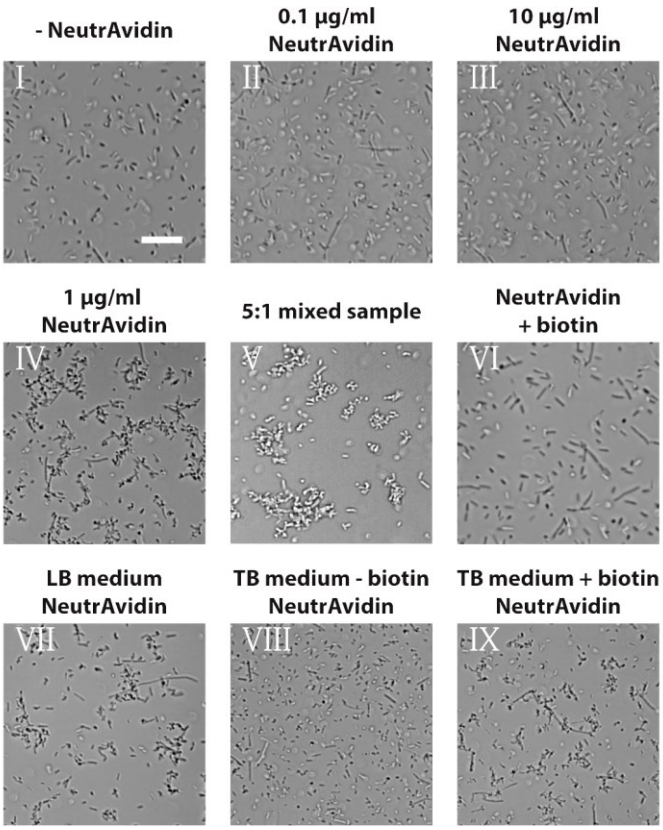

Figure 8 Dependence of cell-cell attachment on NeutrAvidin and biotin. (I-IX) *E. coli* cells carrying Ag43-BAP on IPTG inducible plasmid were grown with 1 µM biotin and 100 µM IPTG in TB medium, if not indicated differently. Cell suspensions were incubated with 1 µg/ml NeutrAvidin (II-IV, VI-IX), if not indicated differently. (VI) Cells were incubated with 1 µg/ml NeutrAvidin, 1 µM biotin and incubated for 30 min. (V) Untreated cells and cells coated with NeutrAvidin were mixed in a ratio of 5 to 1. The formation of cell aggregates was determined after 30 min of incubation via bright-field microscopy. Scale bar: 20 µm.

2.1.3 Attachment of cells on microparticles

To validate that NeutrAvidin can mediate the attachment between cells but also to defined surfaces, *E. coli* expressing Ag43-BAP was incubated for 30 min with streptavidin coated microparticles. Similar to the attachment behavior seen before, Ag43-BAP enabled cells to attach to microparticles, whereas in the absence of BAP or the addition of excess biotin, no attachment was visible (Figure 9A). By mixing two different colored strains we could demonstrate that a microparticle can hold multiple cell types in close proximity (Figure 9B).

At high concentration of cells and microparticles the attachment leads over time to the formation of aggregates Figure 9C). The size of the aggregates can be controlled by the addition of biotin since it blocks the formation of new biotin-streptavidin bonds.

Furthermore, non-motile cells (flagellin deletion mutant, Δ*flic*) formed smaller and more equally distributed aggregates, indicating that cell motility has an effect on cell-particle attachment and aggregation.

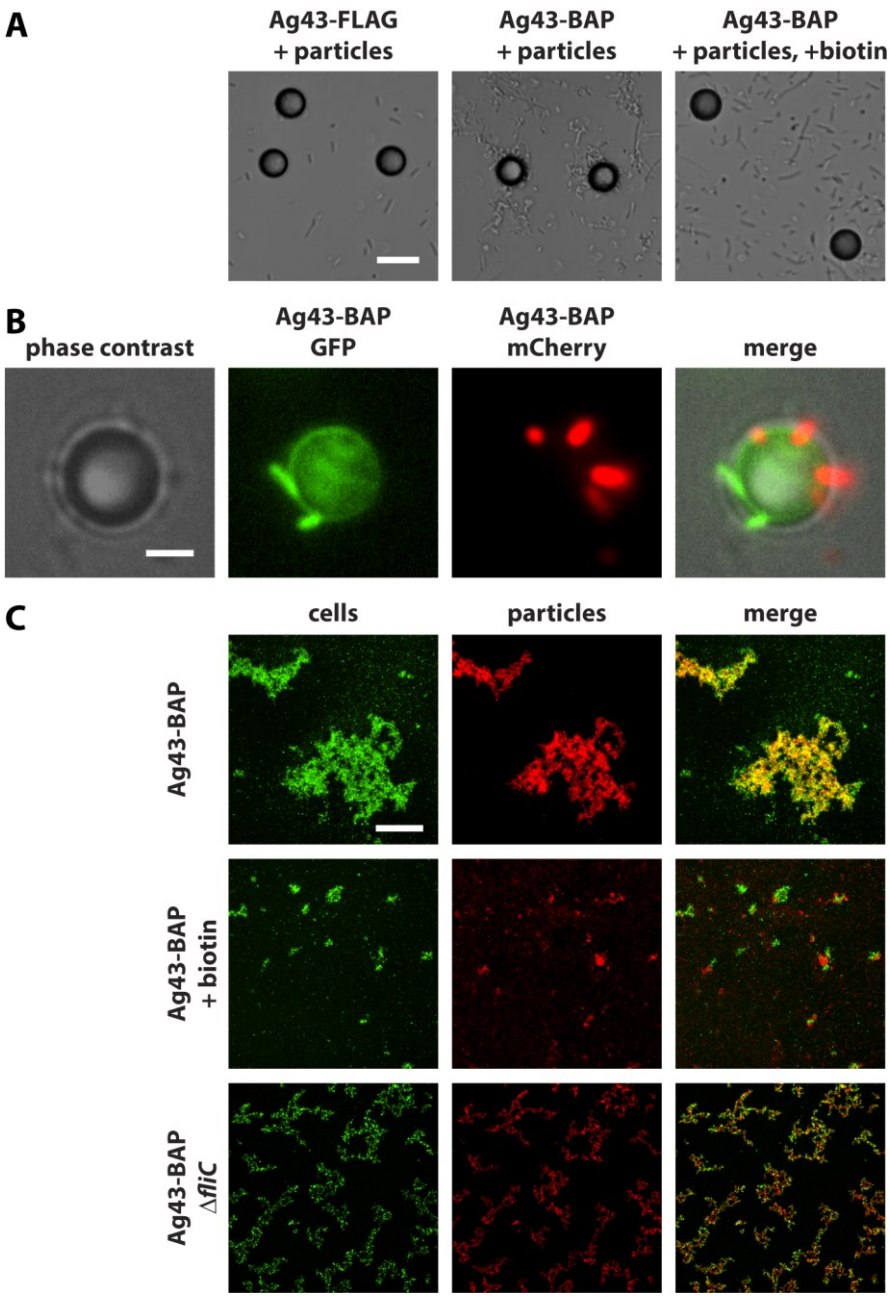

Figure 9 Cell attachment on streptavidin coated particles. *E. coli* cells carrying a recombinant Ag43 on IPTG inducible plasmid were grown with 1 µM biotin and 100 µM IPTG in TB medium. **(A)** Cells carrying Ag43-FLAG with and without BAP were incubated for 20 min with streptavidin-coated 10-µm polystyrene particles. If indicated 1 µM biotin was added before incubation. Attachment was visualized via bright-field microscopy. Scale bar: 20 µm. **(B)** Cells carrying Ag43-BAP and an inducible GFP (green) or mCherry (red) construct were mixed and incubated for 20 min with streptavidin-coated 10-µm polystyrene (PS) particles. Attachment was visualized via fluorescence microscopy. Scale bar: 4 µm. **(C)** Motile wild-type *E. coli* cells (WT) and non-motile Δ*fliC* carrying Ag43-BAP and an inducible GFP construct (green) were incubated for 6 h with streptavidin-coated red fluorescent 2-µm silica particles (red). If indicated 1 µM biotin was added before incubation. Aggregation was visualized via fluorescence microscopy. Scale bar: 150 µm.

2.1.4 Role of motility in cell-particle attachment

Based on the previous results we had a closer look at how cells are attached to particles and which effect the cell motility has on the cell-particle attachment. The complexes between cell and microparticle could be visualized in great detail using either confocal fluorescence microscopy or scanning electron microscopy (Figure 10A). The images indicate that cells preferentially attach via their pole to the microparticles. To confirm this observation and whether motility has an effect on it, we performed statistical analysis. We analyzed the attachment pattern of motile cells (wild-type) and non-motile cells (Δ*flic*) via fluorescence microscopy and defined a polar attachment when the particle was located within the first fifth of the cell. Wild-type cells had a more pronounced polar attachment compared to the non-flagellated strain that was used as a control (Figure 10B), suggesting that this is at least partially due to head-on collisions of swimming cells with the microparticles during the attachment process. However, preferential localization of the recombinant Ag43 to the *E. coli* cell pole might also contribute to polar attachment (Figure 7B), since significant polar preference was observed even for the non-flagellated cells.

To better understand the importance of motility for attachment, we compared the attachment kinetics of motile and non-motile bacteria. Cells and microparticles were mixed and analyzed every 2 min via flow cytometry to distinguish microparticle-attached cells, from free cells and microparticles. The attachment of wild-type cells reached after ~6 min of incubation its half-maximal value and approaching saturation after 20 min, when free particles became depleted (Figure 10C). Excess of free biotin in this process completely blocked attachment, confirming specificity of bacteria-particle interactions. In contrast, the attachment of non-motile cells lacking flagella reached its half-maximal value after ~39 min of incubation. To clarify if this difference was partially due to the lack of motility, and not due to unspecific adhesion of cells via flagella[144], the swimming speed of wild-type *E. coli* was decreased by dissipating the proton motor force of the cell with the help of carbonylcyanide-m-chlorophenylhydrazone (CCCP). Wild-type cells treated with CCCP had an even more pronounced decrease in the attachment rate compared to non-motile cells, whereas the effect of CCCP on the attachment rate of non-motile cells was minor. The overall worse

attachment of the CCCP-treated wild type compared to non-flagellated cells suggests that in absence of motility, flagella might partly hinder the biotin-streptavidin mediated cell-particle attachment[145]. Altogether, these data clearly show that motility promotes (polar) attachment, primarily through heads-on collisions of bacteria with microparticles.

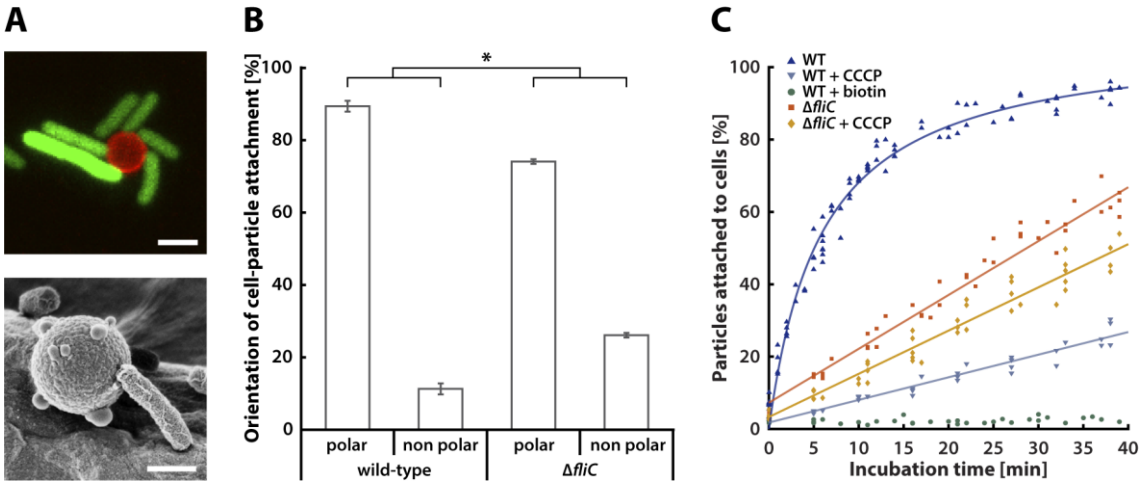

Figure 10 Effect of cell motility on particle attachment. Motile wild-type *E. coli* cells (WT) and non-motile Δ*fliC* cells carrying the recombinant Ag43-BAP on IPTG inducible plasmid and an arabinose inducible GFP construct (green) were incubated for 20 min with streptavidin-coated 2.2-µm PMMA particles (red), at a mixing ratio of 1:30. **(A)** Images of particle-attached cells acquired via confocal laser scanning microscopy (top) or scanning electron microscopy (bottom), with scale bars being 2 µm and 1 µm, respectively. For better visualization, cells were elongated by inhibiting cell division using cephalexin to the TB medium for one hour before harvesting. **(B)** Corresponding quantification of the polar and non-polar cell-particle attachment of WT (for 786 attached cells) and Δ*fliC* (for 1115 attached cells) cells were analyzed via fluorescence microscopy. Statistical analysis was performed using a two-sample *t*-test with unequal sample size and unequal variance, with asterisk indicating $P < 0.005$. Error bars show SEM of three independent experiments. **(C)** Kinetics of particle attachment quantified using flow cytometry. Where indicated, CCCP was added during incubation to reduce cell motility. As a negative control, biotin was added in excess to inhibit the cell-particle attachment. Statistical analysis, performed using a two-sample *t*-test with unequal sample size and unequal variance, showed that difference between all datasets was highly significant ($P < 0.00001$).

2.1.5 Spatial arrangement of cells on micro-patterned biotin surfaces

Since it could be shown that cells can bind to streptavidin coated microparticles, we further investigated to which extent cells can be arranged spatially on a given surface. In order to fabricate a surface with a well-defined biotin pattern, we used laser assisted protein adsorption by photobleaching (LAPAP) allowing surface pattering in micrometer scale[146, 147]. Here fluorescein labelled biotin was bound to a BSA coated glass surface by means of free radicals generated after laser assisted fluorescein

photobleaching[148]. The position and distribution of the biotin modification was controlled by the residence time of the bleaching laser. The bound biotin could be visualized by incubating the surface with fluorescently labeled NeutrAvidin (Figure **11**A) and showed, as expected, a Gaussian distribution (Figure 11B), reflecting the transverse electromagnetic profile of the laser beam[149]. Cells which displayed biotin and were subsequently coated with NeutrAvidin could bind to the biotin modified BSA (BSA-biotin), as well as Streptavidin coated microparticles (Figure 11C). As shown in Figure 11D the position and strength of attachment can be controlled by positioning (the six bright spots) or moving (the lines between the spots) the laser over the surface. From top to bottom the photobleaching was performed one, two and three times for each lane respectively, which led to a noticeable difference in NeutrAvidin and particle density. Together with the absence of attachment in control samples lacking either biotinylated BSA, NeutrAvidin or microparticle, shows that the attachment is highly specific.

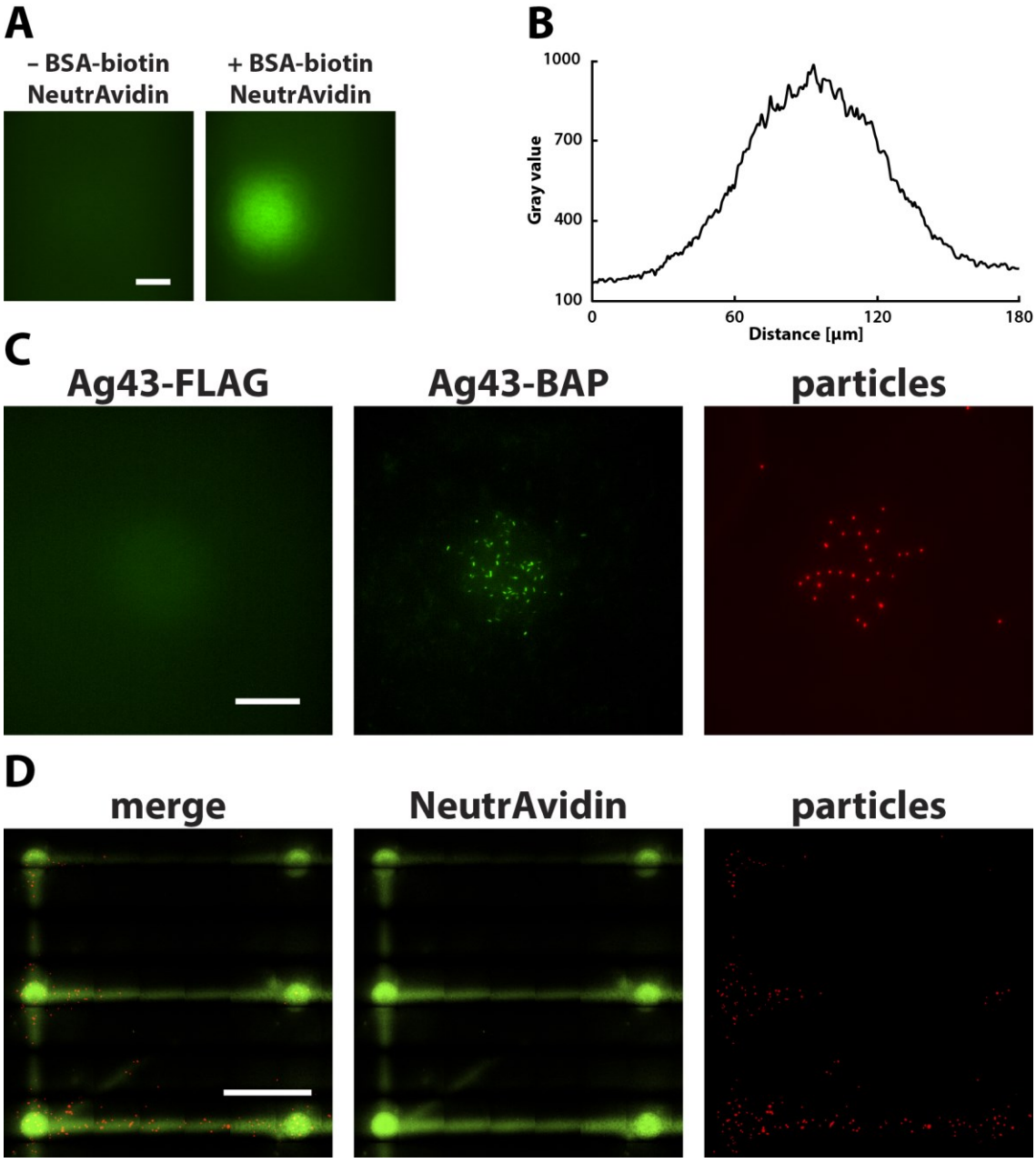

Figure 11 Micro-pattering surfaces with biotin via LAPAP. Glass surfaces were coated with BSA and subsequently fluorescein labelled biotin was immobilized by laser assisted fluorescein photobleaching (see Material and Methods for details). **(A)** Glass surfaces coated with and without BSA were biotinylated (+/-BSA-biotin). After LAPAP treatment the surface was treated with fluorescently labeled NeutrAvidin (green) and analyzed via fluorescence microscopy. Scale bar: 40 µm. **(B)** Intensity profile of the fluorescent NeutrAvidin spot in image A called + BSA-biotin NeutrAvidin. **(C)** After LAPAP treatment the surface was incubated for 30 min with streptavidin-coated 2.2-µm PMMA particles (red), NeutrAvidin coated *E. coli* cells carrying an arabinose inducible GFP (green) and Ag43-FLAG with or without BAP on IPTG inducible plasmid, as indicated. Attachment was visualized via fluorescence microscopy. Scale bar: 40 µm. **(D)** After LAPAP treatment the surface was incubated for 30 min with fluorescently labeled NeutrAvidin (green) and streptavidin-coated 1.4-µm PMMA particles (red). Attachment was visualized via fluorescence microscopy. Scale bar: 400 µm.

Based on the previous experiments, we asked whether cells attached to a modified glass surface are metabolic active, hence can grow and divide. We observed that, after cell division both daughter cells stayed attached when the mother cell was directly attached to the biotinylated glass surface (Appendix-Figure 1). In order to keep the number of attached cells constant, we decided to mediate the attachment between surface and cell via microparticles, to facilitate the release of the non-attached daughter cell after cell division. We first attached streptavidin coated microparticles to the biotin modified glass surface and subsequently incubated them for 30 min with cells displaying biotin. After the removal of free swimming cells, up to 6 cells were attached to one 1.4 µm microparticle (Figure 12). Time-lapse experiments were performed at 30 °C in TB medium and showed that attached cells were able to grow and only one daughter cell remained attached after cell division. The generation time of attached cells was 2.86 h ± 0.54 h (± SEM, n = 101), comparable to cells grown in shaking flasks (Appendix-Figure **2**), further demonstrating that cells stayed metabolically active after attachment, which is important for the second part of this study.

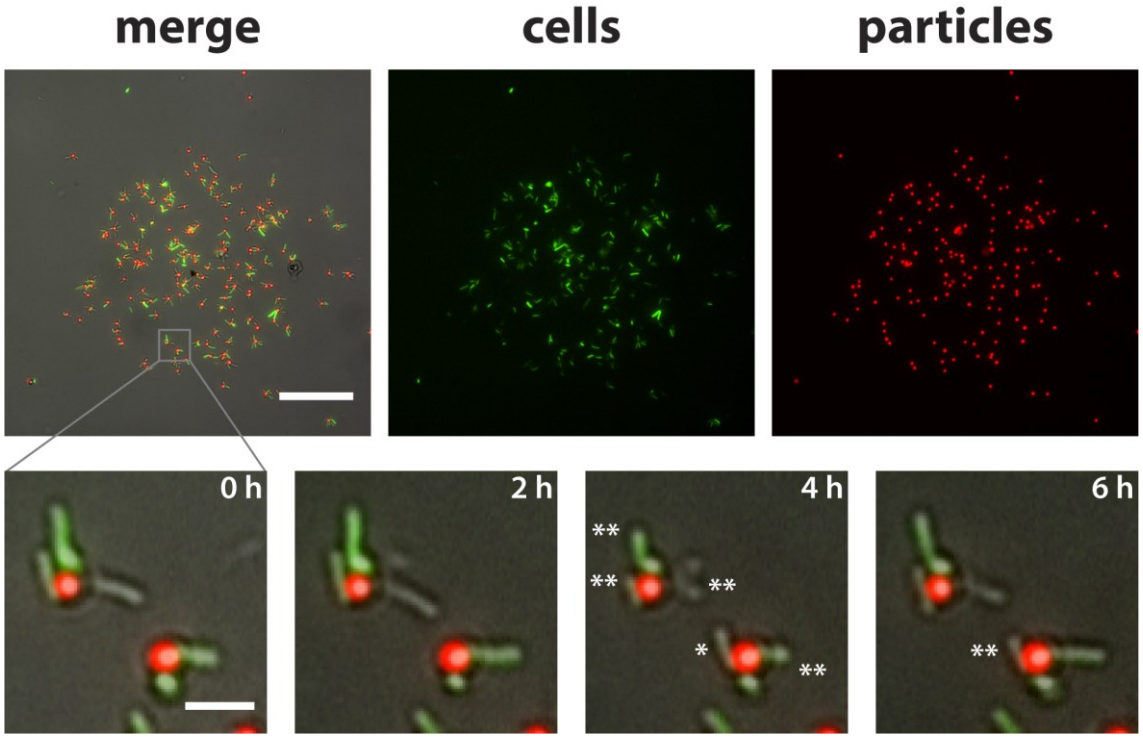

Figure 12 Growth of cell attached to the surface of a particle. The Glass surface was biotinylated via LAPAP as described before and incubated for 30 min with streptavidin-coated 1.4-µm PMMA particles (red). Subsequently, *E. coli* cells carrying Ag43-BAP on IPTG inducible plasmid and an arabinose inducible GFP construct (green) were incubated with the immobilized particles and after 30 min unattached cells were removed, whereas attached cells were grown and imaged under the microscope for 6 in TB medium at 30 °C. New attaching cells are marked as * and dividing cells as **. Scale bar: 40 µm and 4 µm for full image and image segment, respectively.

2.1.6 Alternative biotin display systems

Besides modifying Ag43 for displaying biotin on the cell surface, we investigated the potential of other well studied display systems including three membrane proteins: the outer membrane protein A (Lpp-OmpA)[19] of *E. coli*, the ice nucleation protein (INPNC)[28] of *Pseudomonas syringae* and the autotransporter AIDA-I (AIDA) of *E. coli*[150, 151], as well as the flagellar filament structural protein FliC[152] of *E. coli*. For Lpp-OmpA and INPNC the BAP was introduced at the C-terminus of the protein, whereas for AIDA it was placed at the N-terminus (see Material and Methods for a detailed description). The FliC-BAP construct was based on the design of Lu, *et al.* (1995)[153], which introduces into a variable region of FliC[35] the active side of thioredoxin consisting of a short disulfide-bonded loop that protrudes from the protein. Within this loop we inserted the BAP. For all three membrane proteins we were unable to detect the recombinant protein via FLAG-tag antibody staining but only AIDA-BAP showed,

compared to Ag43-BAP, a weak biotin display (Figure 13A). However, further experiments with FliC-BAP showed that the attachment behavior was similar to Ag43-BAP, including NeutrAvidin mediated cell-cell attachment and binding to streptavidin coated microparticles (Figure 13B). Moreover, we did not notice a decrease in cell motility, indicating that biotinylated FliC proteins got incorporated into the flagellum without affecting its functionality. Since no NeutrAvidin-biotin staining of the flagellum was visible, it seems that the number of biotinylated FliC per flagellum was too low to be detected and further experiments like a western blot analysis of isolated flagella have to be performed to validate our findings.

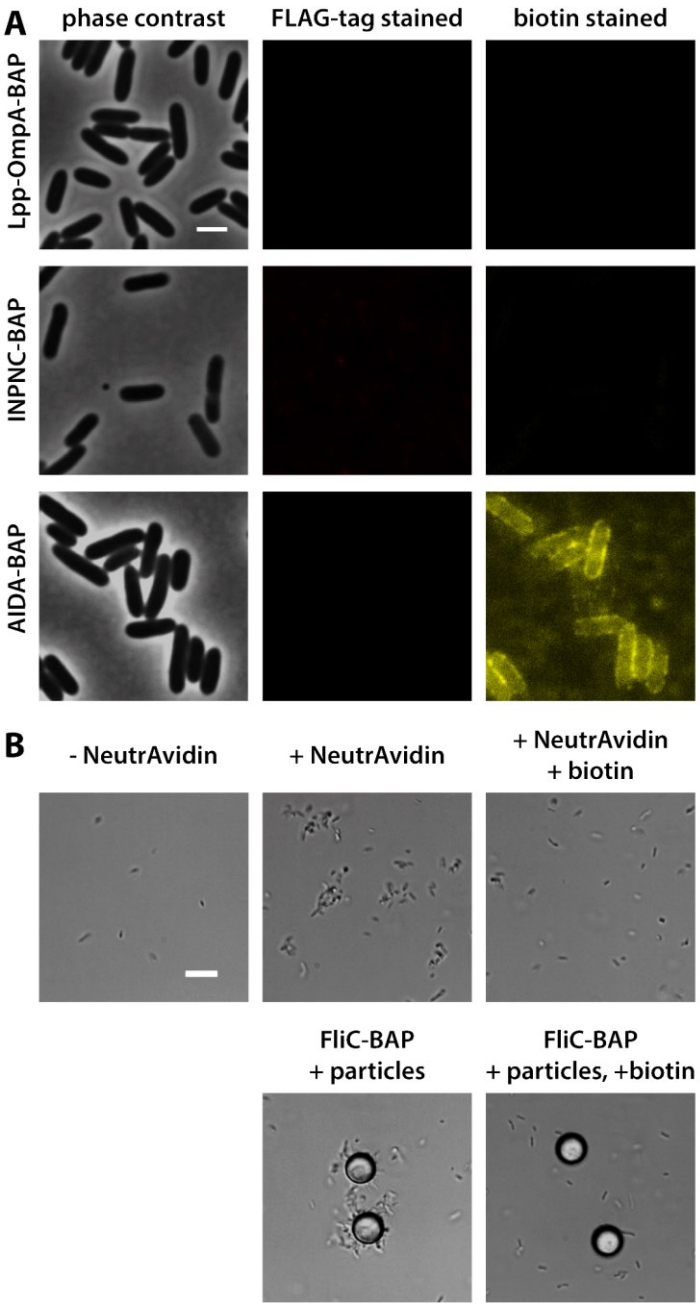

Figure 13 Investigating alternative biotin display systems. (A) *E. coli* cells carrying Lpp-OmpA-BAP, INPNC-BAP and AIDA-BAP on IPTG inducible plasmid were grown with 1 µM biotin and 100 µM IPTG in TB medium and analyzed using anti-FLAG immunostaining (red) and NeutrAvidin-biotin staining (yellow) for detecting the FLAG-tag and surface-displayed biotin, respectively. Staining was visualized via fluorescence microscopy. Scale bar: 2 µm. **(B)** *E. coli* cells carrying FliC-BAP on IPTG inducible plasmid were grown with 1 µM biotin and 100 µM IPTG in TB medium and were incubated for 20 min with 1 µg/ml NeutrAvidin, 1 µM biotin and streptavidin-coated 10-µm polystyrene (PS) particles, as indicated. Attachment was visualized via bright-field microscopy. Scale bar: 20 µm.

2.1.7 Photocaging displayed biotin via LOV2 domain

To control the accessibility of biotin displayed on a post translational level, we used the LOV2 domain of *Avena sativa*[154] to photocage BAP on the cell surface. In the field of optogenetics the light-oxygen-voltage-sensing domain (LOV domain) is widely used to control the accessibility of active sites via a light induced conformational change within the protein[155]. The LOV2 domain consists of 143 amino acids, including a C-terminal 24 amino acid α-helix (Jα) and harbors a blue-light sensitive flavin mononucleotide (FMN) cofactor. Upon blue-light absorption (absorption maximum at 450 nm) the FMN chromophore binds covalently to the protein and leads to the unfolding of the Jα-helix, which reveals the C-terminus of the domain[156]. The chromophore binding and therefore the unfolding of the Jα-helix is thermally reversible in the dark, with a photocycle lifetimes of ~80 sec[157]. This effect of light induced conformational change of the Jα-helix is widely used to externally control the accessibility of effector domains introduced into the C-terminus of the protein[158]. To achieve this level of control we integrated the LOV2 domain into Ag43-BAP right in front of BAP (Ag43-BAP-LOV2), neighboring the Jα-helix (Figure 14A). In order to assess the photocaging of biotin we stained the cells with fluorescently labeled NeutrAvidin in the dark (dark state) or under blue light (light state) for 20 min and analyzed the fluorescence intensity via fluorescent microscopy. The comparison of cells kept in the dark and cells illuminated with blue light showed a stronger NeutrAvidin-biotin staining when cells were exposed to blue light (Figure 14B). However, also in the dark state a clear staining of some cells was visible, indicating that the ability of the LOV2 domain to photocage biotin is limited. This might contribute to the natural unfolding of the Jα-helix even in the dark, leading to the exposure if biotin. Further optimization needs to be performed to obtain a reliable and tight control of attachment through light exposure, including shortening the Jα-helix to improve the encapsulation of the biotinylated BAP in the dark state.

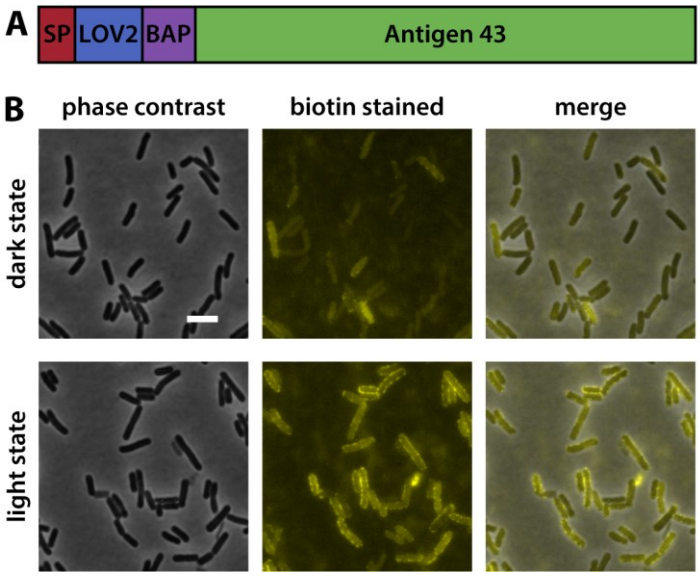

Figure 14 The LOV2 domain can photocage biotin on the cell surface of *E .coli*. (A) Gene map of the Ag43-BAP-LOV2 construct. Signal peptide (SP), light-oxygen-voltage-sensing domain (LOV2) and biotin acceptor peptide (BAP). **(B)** *E. coli* cells carrying Ag43-BAP-LOV2 on IPTG inducible plasmid were grown with 1 µM biotin and 100 µM IPTG in TB medium. Cells were incubated with fluorescently labeled NeutrAvidin (yellow) in the dark (dark state) and under blue light (light state) for 20 min. The NeutrAvidin-biotin staining was visualized via fluorescence microscopy. Scale bar: 4 µm.

2.2 Motility and chemotaxis of bacteriabots fabricated using antigen 43-mediated biotin display

In the second part of this study, we characterized the motility and chemotaxis of bacteria-driven microswimmers (bacteriabots) fabricated using the previously described antigen 43-mediated biotin display system and demonstrated that the chemotaxis of bacteriabots is primarily limited by the cargo-dependent reduction of swimming speed.

2.2.1 Swimming behavior of cells attached to microparticles

As we could show in the previous chapter Ag43-BAP can mediate a rapid and stable attachment between bacteria and streptavidin coated microparticles, which made it ideal for the fabrication of bacteriabots. We first characterized the dependence of bacteriabot movement on the number of attached bacteria (Figure 15A). We observed that in cases, when only one cell was attached to a microparticle, bacteria almost exclusively pulled the microparticle (Figure 15A panel I) and only in rare cases and for a short period of time cell pushed the particle. For cases when two bacteria were attached to the same particle and their long cell axes aligned, the swimming behavior was similar to the particle pulled by a single cell, but the overall movement was markedly slower (Figure **15**A panel II). This was also observed in very rare cases where two particles were aligned alternating between tree cells (Figure 15A panel III). However, when the axes of the two cells were not aligned (Figure 15A panel IV) or when more than two cells were attached to a microparticle (Figure 15A panel V), the swimming behavior was largely compromised, with very little processive motion, likely due to the misalignment of the forces exerted by individual bacteria on the same particle. Thus, the simplest constellation consisting of one bacterial cell per microparticle provides the most efficient and fastest particle propulsion. In order to determine an optimal proportion between microparticles and cells, we analyzed the swimming behavior of bacteriabots at particle to cell mixing ratios of 1:240, 1:30 and 1:3.75 (Figure 15B). At a mixing ratio of 1:30 the majority of observed bacteriabots consisted of one bacterial cell per particle, with the highest number and swimming speed of motile bacteriabots. In subsequent experiments we used this ratio for bacteriabot fabrication.

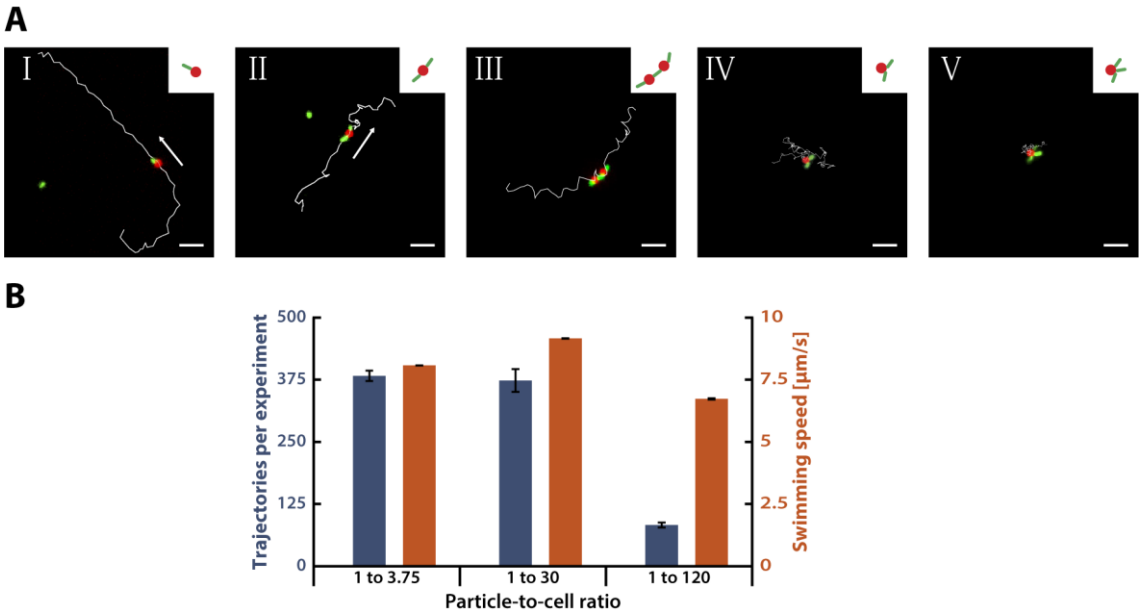

Figure 15 Motility of the fabricated bacteriabots. Motile wild-type *E. coli* cells (WT) carrying the recombinant Ag43-BAP on IPTG inducible plasmid and an arabinose inducible GFP construct (green) were incubated for 20 min with streptavidin-coated 2.2-µm PMMA particles (red). **(A)** Exemplary trajectories of bacteriabots with one, two and three attached WT *E. coli* cells, analyzed using time-lapse fluorescence microscopy. Acquisition time of depicted trajectories was 6.5 s (panel I), 7.4 s (panel II), 9.1 s (panel III), 13 s (panel IV), and 5.4 s (panel V). Scale bar: 8 µm. **(B)** Bacteriabots were fabricated with a particle-to-cell mixing ratio of 1:240, 1:30 and 1:3.75, as indicated. Number of trajectories and mean swimming speed were calculated from individual 2D trajectories of the particles. Error bars show STD of seven independent experiments.

2.2.2 Dependence of bacteriabot motility on particle size and cell length

To analyze the effects of particle attachment on bacterial motility, we tracked two-dimensional (2D) swimming trajectories of *E. coli* cells that were either free swimming (Figure 16A) or attached to 1.4-µm or 2.2-µm diameter particles (Figure 16B,C). As shown above bacteriabots with more than one bacterium have a reduced motility and since bacteriabots are not buoyant, they sediment if not propelled efficiently. Thus these bacteriabots stayed at the bottom of the observation chamber and were not recorded in all following experiments. Therefore we consider that the majority of measured bacteriabots have only one bacterial cell attached. For consistency reasons, the measurements were performed within 30 min to 90 min after placing the sample into the observation chamber. Free-swimming *E. coli* had a mean swimming speed of 15.71 ± 0.02 µm/s (± SEM), which was reduced to 12.83 ± 0.02 µm/s upon attachment of 1.4-µm particles and to 9.76 ± 0.02 µm/s upon attachment of 2.2-µm particles (Figure **16**B,C). Even more pronounced reduction was visible in the fraction of bacteria with the

highest swimming speed (>20 μm/s) (Figure 16A-C). Such reduction of the cell swimming speed is consistent with the increase in the rotational and translational friction coefficients caused by the addition of a spherical particle, which could be computed by modeling flagellar propulsion using resistive force theory[159-161] (Appendix-Figure 3, Appendix-Table 2, section 4.9.1). To clarify whether the motility of free swimming and attached cells decreases over time, we analyzed the swimming speed and chemotactic drift (more information about the chemotactic drift in section 2.2.3) in time intervals from 30 to 60 min, 60 to 90 min and 90 to 120 min after placing the sample into the observation chamber. Although cell motility in our assay decreased gradually over time, this decrease was slow and similar for free swimming cells (Figure 16F) and bacteriabots (Figure 16G), indicating that particle attachment has no negative effect on the energy state of the cell.

We then wondered how swimming properties of the *E. coli*-based bacteriabots could be enhanced. We hypothesized that the swimming properties of elongated *E. coli* cells would be less affected by the particle attachment and therefore suitable for bacteriabot fabrication. *E. coli* cells can be easily artificially elongated by growing them in presence of cephalexin, a β-lactam antibiotic that reversibly blocks the cell division by binding to the transpeptidase FtsI which is involved in septum division[162,163]. Therefore, the cell length can be altered by the duration of cephalexin treatment. Such elongated *E. coli* cells are able to perform chemotaxis[164] and are known to have more, and possibly also longer, flagella, although the increase in the number of flagella might not be linearly proportional to the increase in the cell length[160]. We thus expected that – at a given particle size – the cephalexin-treated cells have a more favorable balance between the size of the cell body (and the number of flagella) and the particle size. Our calculations indeed predicted smaller reduction of the swimming speed for elongated cells upon attachment of the same-sized particle (Appendix-Figure 3, section 4.9.1).

Cells treated with cephalexin for 60 min, with an average length of approximately 9 μm, had a mean swimming speed of 14.66 ± 0.06 μm/s, similar to the speed of normal cells with an average size of approximately 3 μm (Figure 16D). However, consistent with our prediction, particle attachment had much less effect on the swimming speed of

elongated cells, which only decreased to 12.08 ± 0.04 μm/s for 2.2-μm particles (Figure **16**E). Similarly, the fraction of fast-swimming cells was also little affected. Furthermore, the mode of microparticle propulsion was apparently different between normal and elongated cells. As mentioned above (Figure 15A panel I), normal-sized cells predominantly pulled the microparticles, while pushing propulsion was apparently unstable and almost immediately reversed by a tumble. In contrast, elongated cells could mediate both pulling and pushing propulsion (Figure 16H). The efficiency of the two modes of propulsion by the elongated cells was nearly equal, with pulling population being observed in 46% of cases, and the mean swimming speed during pulling and pushing runs being 14.9 ± 3.0 μm/s and 18.1 ± 5.2 μm/s, respectively. In further contrast to particle propulsion by normal-sized cells, particle-loaded elongated cells changed their swimming direction by stopping and reversing their swimming orientation rather than by tumbling (Figure 16H), which is in agreement with previous studies[160, 164].

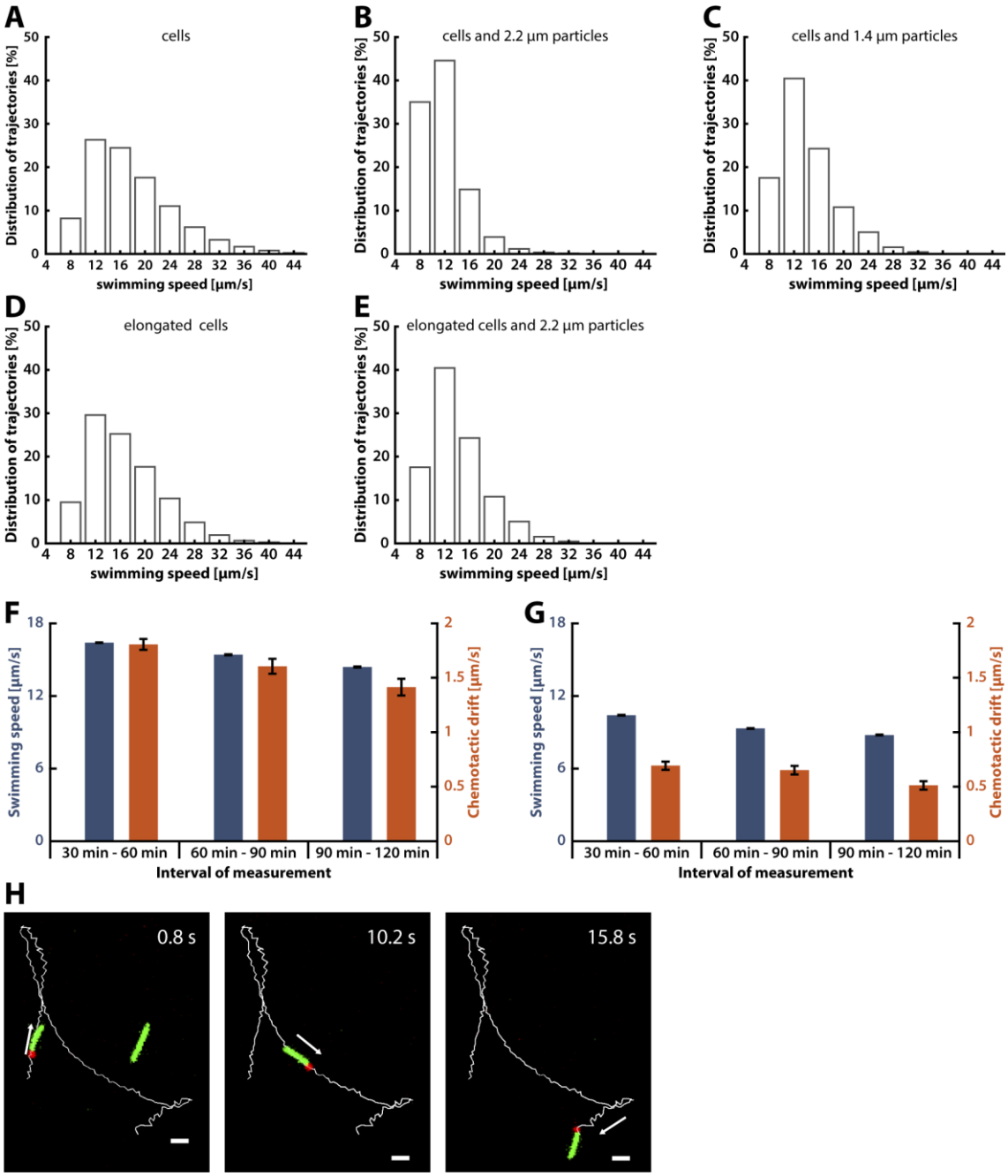

Figure 16 Motility of bacteriabots based on normal and elongated cells. (A-E) Distribution of swimming speed within populations of normal or elongated *E. coli* cells, with or without PMMA microparticles, as indicated. Average swimming speed of individual cells was determined based on 2D trajectories recorded using fluorescence microscopy, as described in Material and Methods. Numbers of analyzed trajectories were 109192, 30724, 44698, 10601, and 10744 for cells, cells with 2.2-µm particles, cells with 1.4-µm particles cells, elongated cells, and elongated cells with 1.4-µm particles, respectively. **(F, G)** Mean swimming speed and chemotactic drift were calculated from individual 2D trajectories (see Material and Methods for more details) of normal cells without (F) or with 2.2-µm particles (G). Measurements were performed at different time intervals (as indicated) after placing the sample into the observation chamber. Error bars show STD of four independent experiments. Numbers of analyzed trajectories for the three indicated time intervals were 53901, 25954, 17058 for free-swimming cells and 20165, 13343, 8674 for cells with 2.2-µm particles. **(H)** Examples of 2D trajectories of bacteriabots based on elongated *E. coli* cells. Scale bar: 8 µm.

To further investigate how the swimming dynamics of normal and elongated bacteria was altered by an attached microparticle, we determined the time autocorrelation of direction of motion as well as the mean square displacement (MSD) of bacteria with and without attached microparticles. The autocorrelation of directional motion for elongated cells was decaying much more slowly with the distance than for normal cells (Figure 17A), and their MSD curves (Figure 17B) indicated more efficient, superdiffusive spreading. Both of these observations could be explained by the lower reorientation per change of direction for elongated cells and by the higher persistence in their direction of motion during runs (i.e., lower rotational diffusion) (Figure 16H and Figure 17C). The attachment of particles led to decreased autocorrelation of direction and persistence for both normal and elongated cells, suggesting that an attached particle increases the reorientation of the cell, either by causing larger reorientations during tumbles or reduced directional persistence during runs.

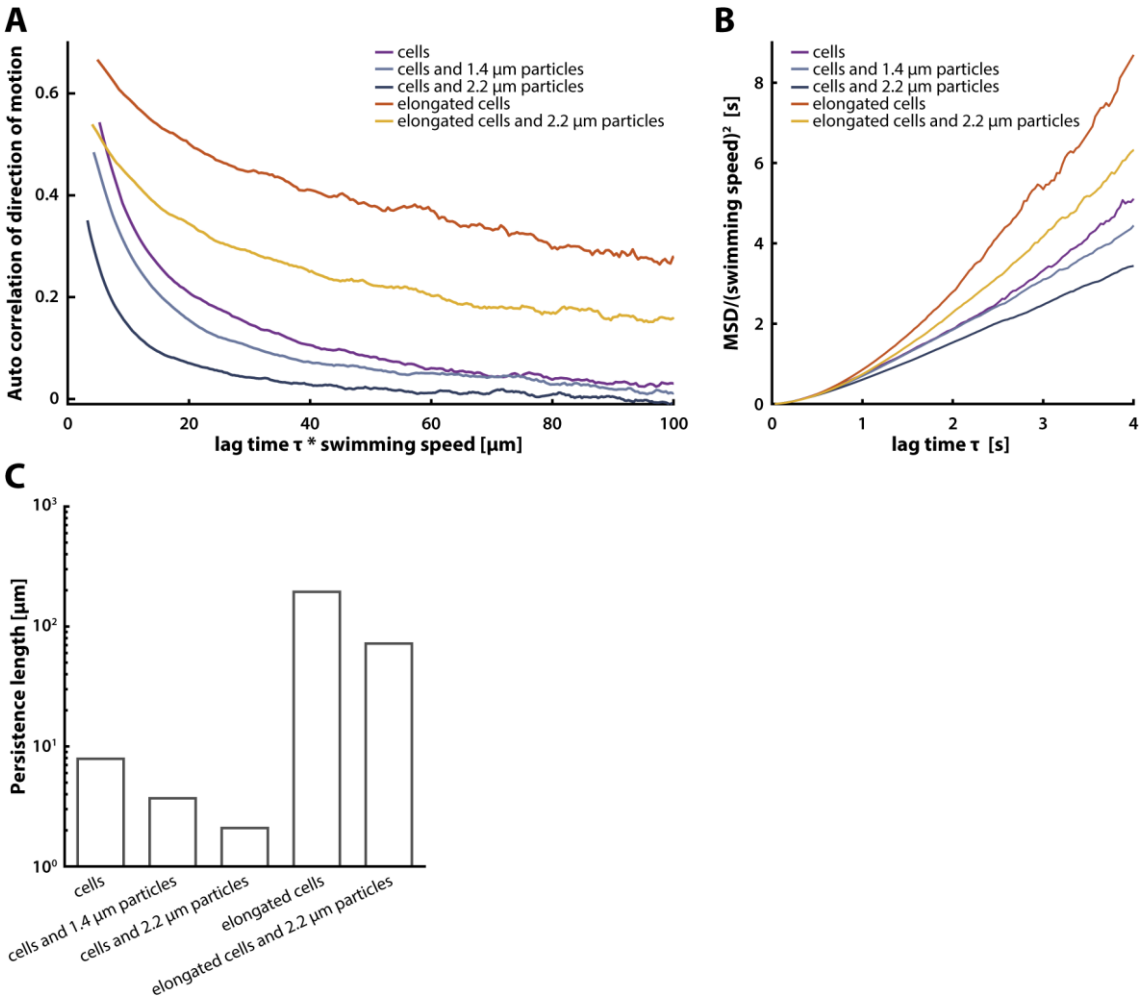

Figure 17 Mean-square displacement (MSD) and persistence length of free cells and bacteriabots. The trajectory data of normal or elongated *E. coli* cells, with or without PMMA microparticles, are identical to the data from Figure 16A-E. **(A)** Autocorrelation of direction of motion, calculated from the trajectory data as described in Material and Methods. **(B)** MSD normalized by the square of the swimming speed was calculated from the trajectory data as described in Material and Methods. **(C)** The persistence length was obtained by fitting the curves of panel A as described in Material and Methods.

2.2.3 Chemotaxis of bacteriabots: increased swimming speed is beneficial for cargo delivery

To investigate the capability of bacteriabots based on normal or elongated cells to perform chemotaxis, we monitored their behavior in the presence of a chemical gradient formed in a microfluidic channel (see Material and Methods for more details). For normal free-swimming bacteria, the mean chemotactic drift in a linear gradient of 0 to 200 µM MeAsp over 2 mm channel length was 1.55 ± 0.03 µm/s (Figure 18A), within the range of previously reported values[165]. The chemotactic drift decreased to 1.28±0.03 µm/sec and 0.63±0.03 µm/sec for normal bacteria attached to 1.4 µm and

2.2 µm particles, respectively. This strong decrease was apparently due to the lower swimming speed of bacteriabots, since plotting the chemotactic drift as a function of the swimming speed for individual cells showed comparable – and even better – drift of bacteriabots at a given speed compared to free cells (Figure 18B). Overall, the dependence of the chemotactic drift on the swimming speed was very steep, scaling as v_0^{α} with α ranging from 2.5 to 3.4 (Appendix-Figure 4A), which is markedly steeper than α = 2 expected from the general theory of bacterial chemotactic motion[135] (Appendix-Figure 4B). This is likely explained by other factors that contribute to the chemotactic drift being a function of swimming speed, such as the tumbling angle[166], or signal amplification by the chemotaxis pathway[135], which depends on the expression of chemotaxis and flagellar genes, and therefore correlates with the swimming speed.

Regarding elongated cells, their mean chemotactic drift was with 2.4±0.1 µm/sec and 1.62±0.07 µm/sec, for free and attached cells respectively, significantly higher than those of normal cells (Figure 18A). Interestingly, elongated cells showed nearly the same dependence of the chemotactic drift on swimming speed with and without attached particles, which was higher than for free-swimming normal cells but comparable to that of the normal cells carrying particles (Figure 18B). Consistently, the mean chemotactic bias (the chemotactic drift normalized by the squared swimming speed) was similar for bacteriabots and elongated cells and lower for free-swimming normal cells (Figure 18C).

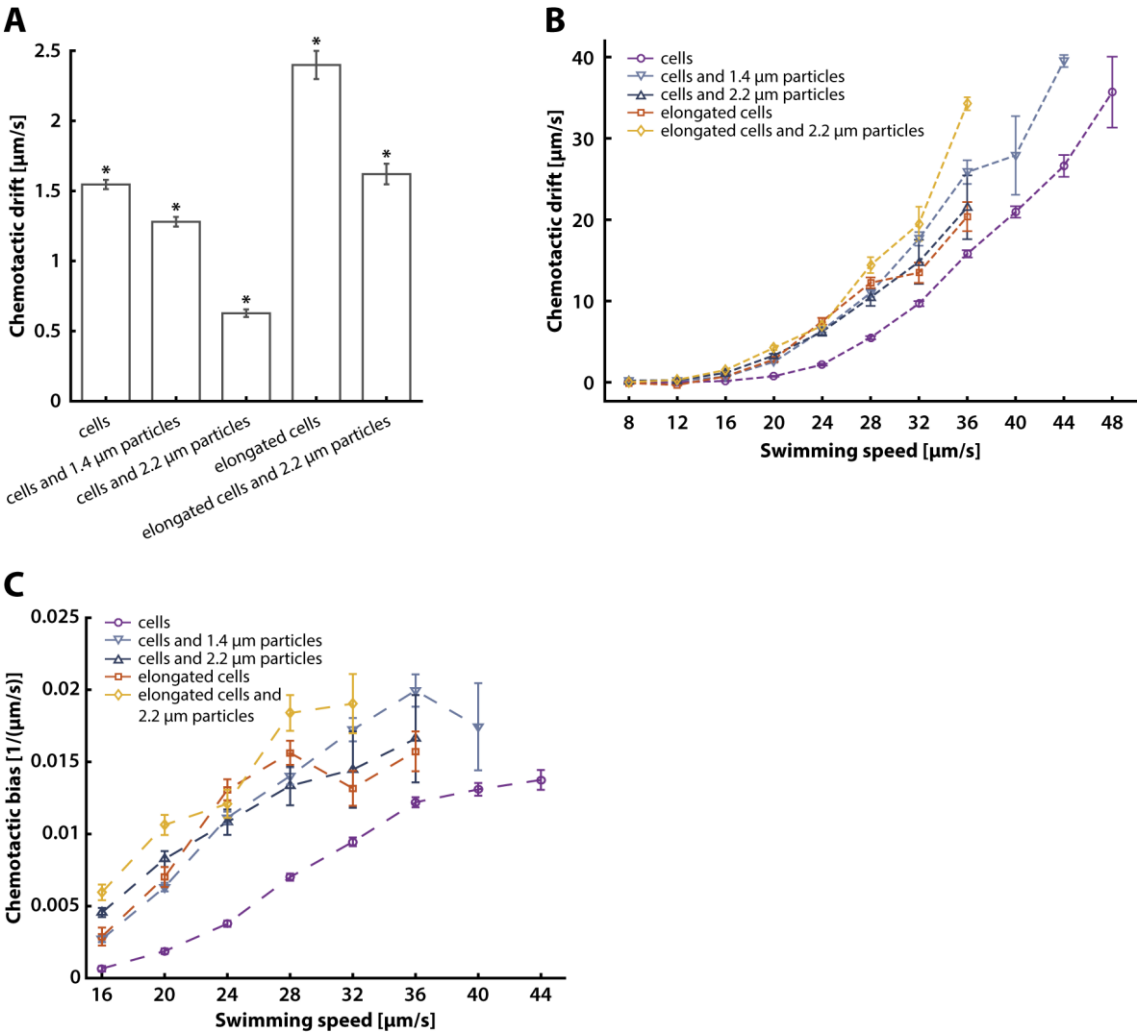

Figure 18 The chemotactic drift of free-swimming cells and bacteriabots. (A-C) Mean chemotactic drift (A), chemotactic drift as a function of the swimming speed (B) and chemotactic bias as a function of the swimming speed were calculated from individual 2D trajectories of cells with or without particles, as indicated (see Material and Methods for more details). Statistical analysis in (A) was performed using a two-sample *t*-test with unequal sample size and unequal variance, yielding highly significant differences between all datasets (with asterisk indicating $P < 0.00001$). Error bars show SEM. Numbers of analyzed trajectories were 109192, 44698, 30724, 10601, and 10744 for cells, cells with 1.4-µm particles, cells with 2.2-µm particles cells, elongated cells, and elongated cells with 1.4-µm particles, respectively. (C) Chemotactic bias, defined as chemotactic drift normalized by the swimming speed, v_{ch}/v_0^2, was calculated as described in Material and Methods. Error bars show SEM.

As stated earlier, bacteriabots need to maintain their function in biological fluids to be of use for biomedical applications. One distinct property of biological fluids is their higher viscosity, up to 5 mPa·s in case of blood[167] compared to < 1 mPa·s for water. Therefore, we tested motility of bacteriabots when the viscosity of the medium was raised above 4 mPa·s by addition of methyl cellulose. The speed of both free swimming cells and bacteriabots was unchanged or even slightly increased at this higher viscosity

(Figure 19A, B), which could be explained by the resistive force theory (section 4.9.1). Notably, the observed dependence of chemotactic drift on swimming speed was unaffected by an increased medium viscosity (Figure 19C, D).

These results suggest that the swimming speed is by far the major determinant of the bacteriabot's capability to perform chemotaxis, irrespective of the cell length, cargo attachment or medium viscosity, and they show that cell elongation can enhance chemotaxis of bacteriabots

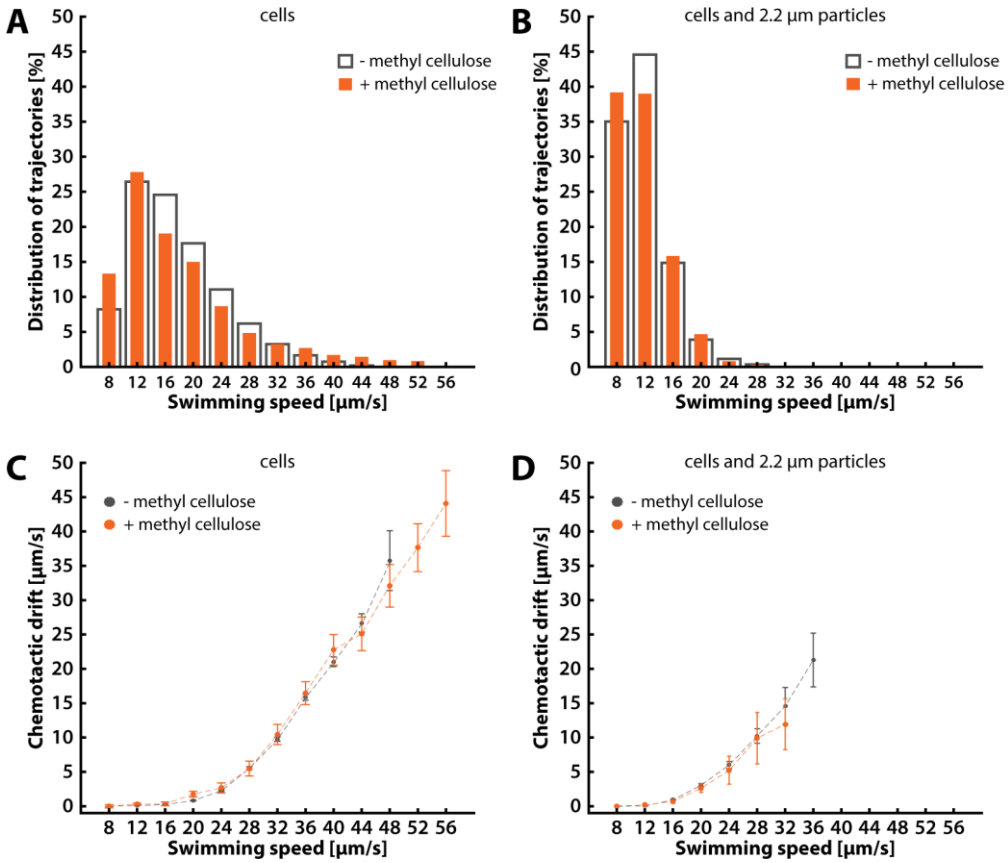

Figure 19 Motility of free swimming cells and bacteriabots at two different viscosities. (A-D) Distributions of swimming speed (A, B) and of chemotactic drift as a function of the swimming speed (C, D) were calculated from individual 2D trajectories for free swimming *E. coli* cells and cells attached to 2.2 µm particles (see Material and Methods for more details). Cells were measured in motility buffer with and without the addition of 0.25 % w/v 4000 cP methyl cellulose (~4.3 mPa·s at 32°C)[168]. In the more viscous fluid, average chemotactic drift was 3.44 ± 0.22 µm/s (± SEM) for free swimming cells, and 0.42 ± 0.09 µm/s for bacteriabots. Numbers of analyzed trajectories in buffer without and with methyl cellulose were 109192, 3068 for free-swimming cells and 30724, 2924 for bacteriabots. Error bars show SEM.

3 DISCUSSION

Specific adhesion to biotic and abiotic surfaces is essential for the survival of microorganisms, since processes like reproduction, acquisition of nutrients or formation of multicellular structures are dependent on it, and is mostly mediated through adhesins on the cell surface. In biotechnological applications the same adhesins and their cognate surfaces, as well as receptor-ligand interactions are used to immobilize manly eukaryotic cells. However, the controlled attachment of bacteria to biological and well defined artificial surfaces is less explored. In this study we constructed and evaluated the antigen 43-mediated biotin display on the cell surface of *E. coli*, in order to bind streptavidin modified surfaces for cell-cell attachment, immobilization of cells in confined patterns and bacteriabot fabrication. Moreover, we performed systematic measurements of such bacteriabots, to analyze the effect cargo has on the motility and chemotaxis of attached bacteria.

3.1 Characteristics and use of antigen 43-based biotin display

Rapid and stable cell-cell or cell-surface attachment is of great interest for various applications, however common methods used today rely on external modifications of the cell surface, which is accompanied by extensive sample preparation and can affect the fitness of the cell. Instead, we decided to genetically engineer *E. coli* to autonomously display biotin on its cell surface using a modified version of autotransporter Ag43 carrying the biotinylation peptide BAP. Besides, the engineered Ag43-BAP allowed the introduction of additional features to the display system, such as a TEV protease restriction site for a targeted release from the attached surface and the LOV2 domain to alter the accessibility of biotin by light controlled photocaging. Although *E. coli* can synthesize biotin[55], the amount needed to biotinylate all produced Ag43-BAP proteins seems to exceed its biotin synthesis capacity. We could partially overcome this limitation by adding biotin to the growth medium and an overexpression

of BirA, which has been shown in previous studies to greatly promote the biotinylation of heterologously expressed proteins in eukaryotic and bacterial cells[75, 169, 170]. The need for addition of biotin to the growth medium could be bypassed by increasing biotin production of the cell through overexpression of the biotin synthase BioB[170].

In contrast to previous studies[24, 41, 171], which found that Ag43 was distributed evenly over the bacterial surface, we observed that in up to one third of the cells Ag43-BAP was localized at the poles. This could be attributed to its overexpression or an artefact of the biotin straining with streptavidin, since it can bind up to four biotin molecules and therefore might promote the clustering and change the localization of Ag43. However, studies on the closely related autotransporters AIDA-I and IcsA, demonstrated that a polar localization or an evenly distribution over the bacterial surface is dependent on the strain, structure of the lipopolysaccharide (LPS) and expression level of the autotransporter[45]. Similar experiments on Ag43-BAP could give insights on the conditions controlling its degree of a polar localization.

One of the difficulties of making especially small molecules accessible at the bacterial cell surface is to overcome the LPS layer. In K-12 strains of *E. coli*, which synthesize an incomplete LPS, this monolayer is about ~20 Å thick and can limit the accessibility of displayed peptides[172, 173]. This might explain why the display of biotin by means of OmpA, INP and AIDA-I showed no biotin straining, despite reports showing successful display of various proteins at the cell surface[13]. If the lack of staining is caused by NeutrAdinin not reaching the surface exposed biotin, using strains producing shorter LPS or a different staining method could give better results. On the other hand, the successful biotin display based on Ag43 with a passenger domain of about 100 Å and FliC forming flagella demonstrates that cell surface protrusions can overcome the bacterial LPS layer. This becomes even more important in organisms with a thicker LPS layer, including *E. coli* strains harboring a complete LPS, increasing this layer up to 370 Å[174, 175]. Besides LPS, it also has been shown that fimbriae and capsules can physically shield the cell surface and therefore sterically prevent the accessibility of Ag43[171, 176, 177].

As Ag43 can be expressed and exposed on the surface in a broad range of gram negative bacteria, including *Salmonella enterica, Burkholderia cepacia, Pseudomonas aeruginosa, Pseudomonas fluorescens, Klebsiella pneumoniae, Enterobacter cloacae* and *Serratia liquefaciens*[24, 176], this display system is principally compatible with various biomedical applications, like bacteriabots based on these species[178, 179]. Indeed, harnessing the ability of different bacterial species to sense and respond to a wide range of chemical compounds, pH, temperature, oxygen level[180] and other physiological signals present in for example the human body[181], together with the ability of some bacteria to change their morphology or to invade cell tissue, becomes relevant in biomedical applications where autonomous bacteriabots are of great interest[178, 179].

The modification of the bacterial cell surface has been used widely in biotechnological applications, including the construction of different whole-cell biocatalysis and bioremediation systems[182]. However, such systems relay on that the display of the catalytic enzymes through outer membrane proteins, the ability of the protein to fold correctly in the extracellular space and the incorporation of required cofactors[13]. This difficulty might be addressed by producing biotinylated variants of the proteins of interest under native conditions, their purification and subsequent attachment on biotin displaying cells coated with streptavidin. Such system would only add a 15 amino acid peptide to the protein and on the same cell surface a combination of different proteins could be displayed effortlessly.

Lastly, we could show that the Ag43-BAP mediated cell-cell and cell-surface attachment was dependent on the amount of displayed biotin and surface bound streptavidin. In addition, the attachment could be blocked by excess free biotin, which demonstrates the specificity and robustness of this system. This enables, together with surface modifying techniques like LAPAP, a fast and easy way to functionalize abiotic surfaces with defined patterns and density of living cells at micrometer resolution. Moreover, we could show that attached cells are metabolic active, which makes this method suitable for applications where immobilized cells have to be viable over long periods of time in a confined space, like in cell based biosensors or for screening purposes. In this regard, extended experiments examining the survival and adaptation of

such surface bound cells to changes of environmental conditions, would be of great interest for long time cultivation.

An emerging field in metabolic engineering and synthetic biology are engineered microbial consortia, because metabolic incompatible or complex biosynthetic pathways could be divided between different organisms, which would reduce the metabolic burden of each cell and frees up energy for the cells central metabolism[183]. Attempts have been made to co-cultivate and characterize microbial communities ranging from simple co-cultivation experiments of two distinct species[184] to microdroplet co-cultivation of environmental samples[185] and tailored microbial ecosystems dependent on bi-directional communication or cross feeding[186]. Nevertheless, the majority of these systems rely on a stable ratio between strains over a long period of time. This remains challenging, since typically one strain overgrows the other. However, a defined strain ratio could be maintained for surface bound cells, since their offspring would be released from the surface and blocked from reattachment, as we could show previously for our system. Such stable cell layers might also been used to grow either single strains or co-cultures continuously in a microfluidic system under flow and to collect accruing pathway products.

3.2 Fabrication of bacteriabots with Ag43-BAP

There is an increasing interest in various applications of bacteria to deliver microscopic cargos and several studies have shown that such bacteria-powered microswimmers can be principally used to move cargo in environmental gradients[112, 118-122]. However, the applicability of bacteriabots remained limited, partly due to the lack of protocols for specific and fast loading of cargo. In this study, we developed and characterized a system for efficient generation of bacteriabots via biotin-streptavidin interaction. Although this interaction was already used to construct bacteriabots[94, 120, 123], previous biotin functionalization of the bacterial cell surface required time consuming preparations with either biotin-conjugated antibodies targeting outer membrane proteins or the lipopolysaccharide[118], or a chemical modification of the surface via biotin-NHS ester[102]. Because bacterial flagella are fragile, multistep preparation procedures can largely decrease the motility of the cell due to the exposure to chemicals and shear

forces and thus decrease the applicability of the resulting bacteriabots. An increase in sample preparation complexity requires an extensive quality control, to ensure sufficient biotinylation of the surface or stable attachment of biotinylated molecules like antibodies. Especially in applications where detached bacteria interfere with downstream processes, a reliable cell attachment is important. To address these shortcomings in the fabrication and application of bacteriabots, we first developed a fast, specific, and efficient approach for microparticle attachment. It relies on Ag43 to display biotin on *E. coli* surface and utilizes bacterial motility to greatly accelerate the attachment of streptavidin-coated cargo particles. The attachment of particles using this Ag43-BAP approach showed high efficiency and yield, achieving fifty percent of particles loaded on cells within 6 min. Not all particles observed were loaded with bacteria which can be attributed to the particles used which vary in streptavidin functionalization. This became apparent when even under high excess of modified cells a subpopulation of particles remained cell free and therefore were considered as nonfunctional. This suggests that at about 94 % particle coverage all viable particles are occupied by a bacterial cell.

Furthermore, we could demonstrate that cell surface appendages interfere with the cell-particle attachment and that attachment was strongly enhanced by cell motility. The attachment of wild-type cells impaired in motility via CCCP was significantly reduced compared to the case of non-motile Δ*fliC* cells, indicating that flagella physically hinder the approach of cell and particle. This suggests that the removal of cell surface appendages like pili, fimbriae or curli fibers could increase attachment not only for *E. coli* but also for other bacteria used in bacteriabot fabrication. In addition, we observed that the attachment was strongly enhanced by cell motility, suggesting that the rather straight motion of motile cells promotes heads-on collision and attachment to the particle. The heads-on collisions between motile cells and particles could also partly explain strong bias towards polar attachment observed in the wild-type cells, although the enrichment of Ag43 at the cell pole may further contribute to this bias. Such polar attachment of cargo is beneficial for the movement of bacteriabots, because it ensures alignment of the center of mass with the propulsion direction and stabilizes the ballistic motion of the bacteriabot. Furthermore, as proposed by Behkam*, et al.* (2008)[187] and

Hosseinidoust, *et al.* (2016)[115], the polar attachment of cell and a defined patterning of a microparticle (janus particle) might allow multiple aligned cells attached on one side of the particle to cooperatively propel such a bacteriabot (Figure 20). We observed an example of such a cooperative motion for cases when a particle was placed between two polar attached cells and their long cell axes were aligned. In contrast, bacteriabots with multiple nonaligned cells tumbled more often and had shorter periods of straight motion, demonstrating that attachment of multiple bacteria to the same particle hinders particle motion rather than facilitating it. This effect may be partly due to the misalignment between the axes of individual cells, and thus of generated propulsion forces as well as uncoordinated tumbling events between the different cells. However, even in cases when the axes of multiple cells were aligned, their motility was lower than upon attachment of a single cell, likely because of the steric hindrance of the flagella bundle but also due to uncoordinated switching of flagella in individual cells. Thus, random attachment of multiple bacteria to the same microparticle may be generally undesirable for cargo loading.

Interestingly the cell shape seems to greatly influence the mode of bacteriabot propulsion, since regular cells mainly pulled the particle, whereas elongated cells pulled and pushed the particle. This might especially important for bacteriabot fabrication with larger cargo, since the flagella bundle, in case of pulling cells, has to cope with the cargo and might be disturbed when the cargo size increases, as a single filament escaping the flagella bundle is sufficient for its disintegration[188].

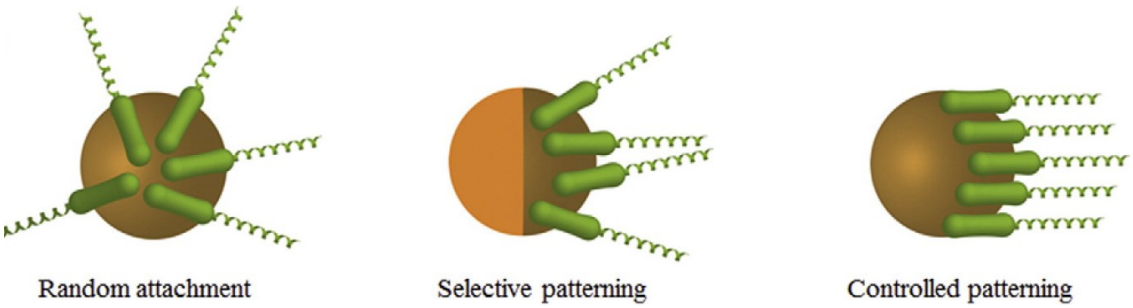

Figure 20 Patterning and orientation of bacteria on microparticles. Obtained and modified from Hosseinidoust, *et al.* (2016)[115].

3.3 Motility and chemotaxis of the fabricated bacteriabots

The bacteria used in bacteriabot fabrication do not only propel the cargo but are also used to detect and respond to environmental signals. Up until now mainly chemotaxis and the response to pH of bacteriabots fabricated from *Serratia marcescens*[119, 121, 189], *Salmonella typhymurium*[121] and *E. coli*[190] have been investigated. However, the mobility and tactic movement of bacteriabots is still not well understood. In order to evaluate the usefulness of our attachment system for bacteriabot fabrication and to elucidate how the motility and chemotaxis of cells attached to cargo are affected, we tracked and analyzed in detail the movement of bacteriabots. We observed that the chemotactic efficiency of bacteriabots was exclusively limited by their swimming speed. In general, the dependence of the chemotactic drift on the swimming speed was very steep, even steeper than expected from the theory of bacterial chemotactic motion[135]. The capability of both cells and bacteriabots to perform chemotaxis is thus extremely sensitive to their swimming speed, meaning that even minor speed reduction due to cargo loading would have substantial effect on the chemotactic efficiency. Consistent with that, although at equal swimming speeds the chemotactic efficiency of the bacteriabots was even higher than for regular-sized free-swimming *E. coli* cells, their average chemotactic drift was largely reduced, because bacteriabots are on average slower than free swimming cells. This was particularly pronounced upon attachment of the larger, 2.2-µm, particles, but was also visible for smaller 1.4-µm particles. Bacteriabots maintained their swimming speed in media with increased viscosity and thus the dependence of chemotactic drift and swimming speed stayed unchanged, which is promising for applications in biological fluids.

Together, the steep dependences of the chemotactic drift on the swimming speed and of the swimming speed on the load imply that the effective size of cargo that can be carried by the chemotactic bacteriabots based on normal *E. coli* cells is limited to approximately 2 µm. However, we could circumvent this limitation by using *E. coli* cells that were elongated by treatment with cephalexin, an antibiotic blocking cell division. Such elongated cells have a mean swimming speed similar to that of normal cells, which could indicate that they possess longer flagella, although their increased number of flagella[190] could also play some role. Nevertheless, the chemotactic drift in

linear gradients apparently increased upon cell elongation, likely due to the higher persistence length of these elongated cells, in consensus with the previous work of Guadayol*, et al.* (2017)[160]. Most importantly, the swimming speed of elongated cells – and therefore their chemotaxis – was much less affected by the particle attachment. Our study thus suggests that elongated cells are superior compared to normal *E. coli* cells for bacteriabot fabrication. This seems to be partly due to the more favorable relation between the size[126] and number of flagella in these cells[160] relative to the size of the cargo particle. Besides, high motion persistence, lower rotational diffusion and the shifted center of mass of the bacteriabot towards the propelling elongated cell probably allows for the observed stable pulling and pushing of the particle.

In the work of Alapan*, et al.* (2018)[191] we could show that *E. coli* cells displaying biotin through Ag43-BAP can be used to attach them via a biotin-avidin-biotin binding complex to red blood cells (RBCs; erythrocytes), demonstrating that the cargo of bacterial microswimmers is not only restricted to synthetic particles. Furthermore such biocompatible RBCs were loaded with superparamagnetic nanoparticles and anticancer doxorubicin drug molecules, whereby the swimming direction of these microswimmers could be guided via an external electromagnetic field. Remarkably the attachment between bacterium and RMC was strong enough for a single bacterium to push and deform a 4 to 5 µm erythrocyte through a 2 µm gap without breaking. Based on our experience with smaller synthetic nanoparticles this system might also benefit from using elongated cells for propelling the RBCs. In addition to the magnetic steering of the microswimmers, the chemotaxis of the bacteria could be used to direct them in gradients of environmental stimuli. The combination of both guidance systems could be used to first bring the cargo into a defined region of interest using magnetic steering followed by an autonomous detection and following of a distinct environmental gradient via the bacterial chemotaxis.

3.4 Concluding remarks

An emerging field in biotechnology is the use of bacterial cell surfaces as a scaffold to display various tailored peptides or proteins produced by the cells themselves. Besides applications concerning sensing of environmental molecules, whole-cell biocatalysis or binding of specific molecules, the modification of the cells surface is used to attach bacteria to biotic an abiotic surfaces. However the efficiency and usefulness of such an immobilization relies strongly on the binding strength as well as the binding speed and the effect an attachment method has on the fitness of the cell. In this respect we developed the Ag43 mediated biotinylation of the bacterial cell surface, which is in principal compatible with applications using the strong interaction between biotin and streptavidin to modify or attach cells. Since this interaction is widely used in different research areas, this biotinylation method may be easily integrated into already existing systems, as demonstrated for the fabrication of bacteriabots and the immobilization of cells on microfabricated surfaces.

In regard of bacteriabot fabrication we showed that the displayed biotin mediates fast and stable attachment to particles and that the chemotaxis of cells is primarily limited by the decrease in the swimming speed upon microparticle attachment. This limitation could be largely circumvented by controlled elongation of *E. coli* cell body, which enables both faster particle propulsion and much more efficient chemotaxis, thus holding high potential for future biomedical applications. Aside from the attachment of cells to a synthetic microparticles[192], this system was used to fabricate erythrocyte (RBC)-based bacterial microswimmers[191], where the cell-RBC attachment was strong enough to actively deform the erythrocyte via the propulsion force generated by the bacterium.

4 Material and Methods

4.1 Materials

4.1.1 Chemicals, enzymes, antibodies and consumables

Chemicals, enzymes, antibodies and consumables used in this study and the corresponding suppliers are listed in Table 1, Table 2, Table 3 and Table 4.

Table 1 Chemicals used in this study.

Chemicals	Supplier
Agar bacteriology	Applichem, Germany
Agarose ultra-pure	Biozym, Germany
Albumin Fraktion V (BSA)	Carl Roth, Germany
Ampicillin	Applichem, Germany
L-(+)-Arabinose	Roth, Germany
BactoTM Tryptone	BD Biosciences, Germany
D-(+)-Biotin	Carl Roth, Germany
BactoTM Yeast extract	BD Biosciences, Germany
$CaCl_2$ x 2 H_2O	Carl Roth, Germany
Carbonylcyanide-m-chlorophenylhydrazone (CCCP)	Sigma-Aldrich, Germany
Chloramphenicol	Applichem, Germany
Dimethyl sulfoxide (DMSO)	Sigma-Aldrich, Germany
EDTA	Merck, Germany
D-Glucose	Applichem, Germany
Glycerol	GERBU Biotechnik, Germany
HEPES	Sigma-Aldrich, Germany
Isopropyl-β-D-thiogalactoside (IPTG)	Carl Roth, Germany
Kanamycin sulphate	Sigma-Aldrich, Germany
Lithium acetate	Sigma-Aldrich, Germany
Magnesium sulfate ($MgSO_4$)	Sigma-Aldrich, Germany
Manganese(II) chloride ($MnCl_2$)	Sigma-Aldrich, Germany
Methyl cellulose (4000 cP)	Sigma-Aldrich, Germany
α-Methyl-DL-aspartate (MeAsp)	Sigma-Aldrich, Germany
Potassium phosphate dibasic (K_2HPO_4)	Sigma-Aldrich, Germany
Potassium chloride (KCl)	Sigma-Aldrich, Germany
Potassium phosphate monobasic (KH_2PO_4)	Sigma-Aldrich, Germany
2-Propanol	Carl Roth, Germany
Sodium chloride (NaCl)	Carl Roth, Germany

Yeast Extract	Applichem, Germany

Table 2: Enzymes used in this study

Enzymes	Supplier
Restriction enzymes and buffer	Thermo Fisher Scientific, Germany and New England Biolabs, Germany
T4 DNA-Ligase and buffer	Thermo Fisher Scientific, Germany
Phusion® DNA Polymerase	New England Biolabs, Germany
ProTEV Plus (TEV protease)	Promega, USA
BirA biotin-protein ligase reaction kit	Avidity, USA

Table 3: Antibodies used in this study

Antibody	Supplier
monoclonal mouse anti-FLAG® M2 antibody	Sigma Aldrich, Germany
monoclonal mouse anti-biotin BTN.4 antibody	Thermo Fisher, Germany
anti-mouse goat IgG conjugated to Cy3	Thermo Fisher, Germany

Table 4: Consumables used in this study

Consumables	Supplier
Coverslip	Carl Roth, Germany
GeneJET DNA Purification Kit	Thermo Fisher Scientific, Germany
GeneJET Gel Extraction Kit	Thermo Fisher Scientific, Germany
GeneJET Plasmid Miniprep Kit	Thermo Fisher Scientific, Germany
Microscope slide	Marienfeld, Germany
1.4-µm Poly(methyl methacrylate) particles	PolyAn, Germany
2.2-µm Poly(methyl methacrylate) particles	PolyAn, Germany
10-µm Polystyrene particles	Sigma-Aldrich, Germany
2-µm Silica particles	Chemicell, Germany
Silicone elastomer Kit (SYLGARD® 184)	Dow Corning, USA
8-Well microplates	Ibidi, Germany
96-Well microplates	Ibidi, Germany

4.1.2 Media

Media were autoclaved for 20 min at 121 °C and 2 bar. To solidify medium, 1.5 % (w/v) agar was added prior to autoclaving.

LB (Luria-Bertani Broth)-medium:

Chemicals	Final concentration
tryptone	10 g/l
yeast extract	5 g/l
NaCl	5 g/l

Chemicals were resolved in deionised water.

TB (Tryptone Broth)-medium:

Chemicals	Final concentration
tryptone	10 g/l
NaCl	5 g/l

Chemicals were resolved in deionised water and pH was adjusted to 7.0.

4.1.3 Media additives

Protein expression was induced by adding 100 µM isopropyl-β-D-thiogalactopyranoside (IPTG) or 0.005% L-(+)-arabinose to the growth medium. Antibiotics used in this study are listed in Table 5.

Table 5 Antibiotics used in this study.

Antibiotics	broth	agar
Ampicillin	100 µg/ml	200 µg/ml
Chloramphenicol	34 µg/ml	34 µg/ml
Kanamycin	50 µg/ml	50 µg/ml

4.1.4 Buffer solutions

Phosphate buffer:

Chemicals	Final concentration
K_2HPO_4	0.2 g/l
Na_2HPO_4	1,15 g/l
NaCl	8 g/l
KCL	0.2 g/l

Chemicals were resolved in deionised water and pH was adjusted to 7.4.

Motility buffer:

Chemicals	Final concentration
K_2HPO_4	10 mM
KH_2PO_4	10 mM
NaCl	67 mM
EDTA	0.1 mM
Glucose	1 %
BSA	0.5 %

Chemicals were resolved in deionised water and pH was adjusted to 7.

TAE-buffer:

Chemicals	Final concentration
Tris base	40 mM
Na-acetate	40 mM
EDTA	1 mM

Chemicals were resolved in deionised water.

TB buffer:

Chemicals	Final concentration
HEPES	10 mM
$MnCl_2$	55 mM
$CaCl_2$	15 mM
KCl	250 mM

Chemicals were resolved in deionised water.

4.1.5 Oligonucleotides

Oligonucleotides were synthesized by Eurofins. Oligonucleotides used in this study are listed in (Table 6).

Table 6 Oligonucleotides used in this study

Oligonucleotides	Nucleotide Sequence (5'-3')
-125_fwd	TGCCACCTGACGTCTAAGAA
160_rev	ATTACCGCCTTTGAGTGAGC
Ag43_EcoRI_rev	CTTTCGCTAAGGATGATTTCTGGAATTCTTAGAAGGTCACATTCAGTGT
Ag43_NdeI_fwd	CAACATATGAAACGACATCTGAATACCTG
Ag43ss_SalI_SacI_rev	CTAGAGCTCGTCGACAACGATGTCAGCAGCCAGCA
Ag43ss_SalI_SpeI_SacI_rev	CTAGAGCTCACTAGTGTCGACAACGATGTCAGCAGCCAGCA
AIDA_linker_HindIII_fwd	CAAAAGCTTGGCGGAGGTTCTGGAGGAGGGTCTGGAGGAGCAGGTAATACTCTTACCGT
araC_NheI-fwd	GTTGCTAGCTTATGACAACTTGACGGCTA
BAP_EcoRI_rev	CTAGAATTCTTATTCATGCCACTCGATCTTCTGGGCTTCGAAGATGTCGT
BAP_SalI_rev	CTTGTCGACTTCATGCCACTCGATCTTCT
BAP_XhoI_fwd	CTACTCGAGGGCCTGAACGACATCTTCGAAGCCCAGAAGATCGAGTGGCA
BirA_E/NsiI/MfeI-rev	GTCCAATTGATGCATGAATTCTTATTTTTCTGCACTACGCA
BirA_RBS_HindIII_fwd	GTAAAGCTTAGGAGAAATTAACTATGAAGGATAACACCGTG
Cerulean_HindIII_rev	GTTAAGCTTTTACTTGTACAGCTCGTCCA
Cerulean_RBS_SphI_fwd	GAAGCATGCAAGGAGAAATTAACTATGGTGAGCAAGGGCGAG
FliC_711_NotI_XmaI_fwd	AATCCCGGGGCGGCCGCCAGTTCTCCAACCG
FliC_711_XmaI_rev	CTACCCGGGATCGTTATCACCACCGGTGA
FliC_EcoRI_rev	GTTGAATTCTTAACCCTGCAGCAGAGAC
FliC_NdeI_fwd	GAACATATGATGGCACAAGTCATTAATAC
INPNC_BamHI_rev	GATGGATCCTTTAACTTCGATCCAGTCGT
INPNC_XbaI_fwd	GTATCTAGAATGACCCTGGACAAAGCTCT
Link_FLAG_fwd	GATCCGGCGGAGGTTCTGGAGGAGGGTCTGGAGGAGACTACAAAGACGATGACGACAAGC
Link_FLAG_rev	TCGAGCTTGTCGTCATCGTCTTTGTAGTCTCCTCCAGACCCTCCTCCAGAACCTCCGCCG
Linker_SacI_rev	CTAGAGCTCTCCTCCAGACCCTCCTCCAG
MCS_fwd	GGCTAGCCATATGTCTAGAGGATCCCTCGAGG
MCS_rev	AATTCCTCGAGGGATCCTCTAGACATATGGCTAGCCTGCA
OmpA_BamHI_rev	GTAGGATCCGTTGTCCGGACGAGTGCCGA
OmpA_BamHI_rev	GTAGGATCCGTTGTCCGGACGAGTGCCGA
pBAD_XhoI_EcoRI_NheI_rev	GTTGCTAGCTTAGAATTCCTCGAGCCAAAAAAACGGGTATGGAG
SacI_XhoI_TEV_NsiI_fwd	CCTCGAGAATCTGTATTTCCAGGGCAACACCACGCTGAATGGTGGCGAACAGTGGATGCA
SacI_XhoI_TEV_NsiI_rev	TCCACTGTTCGCCACCATTCAGCGTGGTGTTGCCCTGGAAATACAGATTCTCGAGGAGCT
T5_op_NheI_fwd	CATGCTAGCAAATCATAAAAAATTTATCT
T5_op_RBS_NdeI_rev	CCTCATATGTAATTCCTCCTTGTGTGAAATTGTTAT
T5_RBS_Aflll_fwd	CTACTTAAGAAAAAATTTATCTGCTTTCAGGAAAATTTTTCTGTATAATA
T5_RBS_NcoI_rev	CATCCATGGTTAATTTCTCCTTTGAATCTATTATACAGAAAAATTTTCCT
T7-TTTT_EcoRI_rev	GTAGAATTCCCGCAATTCCCAATTCCAGG
T7-TTTT_MfeI_fwd	CTTCAATTGCTTCCGATCCCCAATTCCTG
TarAss_NdeI_fwd	CAACATATGAAAGCTACTAAACTGGTACT
TEV_XhoI_HindIII_fwd	TCGAGGAGAATCTGTATTTCCAGGGCA
TEV_XhoI_HindIII_rev	AGCTTGCCCTGGAAATACAGATTCTCC
Trx_NotI_rev	AATGCGGCCGCCAGGTTAGCGTCGAGGAA
Trx_XmaI_fwd	CTACCCGGGATGAGCGATAAAATTATTCA

4.1.6 Bacterial strains

Bacterial strains used in this study are listed in Table 7.

Table 7 *E. coli* strains used in this study.

Strain	Genotype	Source
DH5α	F– endA1 supE44 thi-1λ-recA1 gyrA96 relA1 deoRΔ(lacZYA-argF)U169	Invitrogen, USA
MG1655	F- (λ-) rph-1	[193]
ΔfliC	MG1655 ΔfliC, Kms	This study

4.2 Molecular biological methods

4.2.1 Polymerase chain reaction (PCR)

The amplification of specific DNA fragments from DNA templates was performed by PCR using oligonucleotides (primer) flanking the region of interest. A standard PCR reaction mixture and program are listed in Table 8 and Table 9.

Table 8 Standard PCR reaction mixture

Final concentration	Component
0.2 mM	dNTPs
2 mM	MgSO4
1 µM	forward primer
1 µM	reverse primer
0.015 U/µl	Phusion DNA polymerase
0.1-0.5 ng/µl	template DNA
1x	5x Phusion HF buffer

Table 9 Standard PCR program

Time	Temperature	Step	
2 min	95 °C	initial DNA denaturation	
30 s	95 °C	DNA denaturation	30 cycles
30 s	65 °C	primer annealing	
30 s/kb	72 °C	elongation	
5 min	72 °C	final elongation	

For further cloning steps the PCR product was purified with the GeneJET DNA Purification Kit, according to the manufacturers' protocol.

4.2.2 Restriction digestion and ligation of DNA fragments

The restriction of DNA-molecules was performed by restriction enzymes. The amount of restriction enzyme and the used restriction buffer were chosen according to the manufacturers' recommendation. The restriction mixture consisted of 25-250 ng DNA, the corresponding buffer and the chosen restriction enzymes. The mixture was incubated for 1 h at 37 °C and purified with the GeneJET DNA Purification Kit or GeneJET Gel Extraction Kit, according to the manufacturers' protocol.

The ligation of linearized plasmid and DNA-fragment was performed by mixing them in a molar ratio of 1:6. The ligation mixture contained 50 ng linearized vector, the corresponding amount of the DNA-fragment, T4 DNA ligase buffer, 0.04 U/µl T4 DNA ligase and was incubated for 30 min at room temperature. The required amount of DNA was determined using the following formula:

$$\frac{\text{ng vector} \times \text{kb insert}}{\text{kb vector}} \times \text{molar ratio} \left(\frac{\text{insert}}{\text{vector}}\right) = \text{ng insert}$$

4.2.3 Agarose gel electrophoresis

The agarose gel electrophoresis was used to separate DNA-fragments according to their size. DNA-probes were mixed with DNA-loading dye (New England Biolabs, Germany) and loaded on a 1 % agarose gel (1 % agarose in TAE-buffer; 0.005 % Midori Green, Biozym, Germany). The DNA-fragments were separated by 90 V in a gel chamber filled with TAE-buffer and analysed via UV-light.

4.2.4 Determination of DNA concentration by spectrophotometric estimation

The purity and concentration of DNA were determined via NanoDrop2000 Spectrophotometer. Here the absorption spectrum of the solution between 220 to 350 nm was detected. The quotient 260 nm/280 nm was a measure of DNA purity. A quotient of 1.5 corresponded to a 50 % DNA/protein-solution, whereas a quotient of 2 corresponded to pure DNA. For an estimation of the DNA concentration the following formula was used: $\mathrm{OD}_{260} * 50\ \mu\mathrm{g/ml} = \text{DNA concentration in } \mu\mathrm{g/ml}$

4.2.5 Plasmid construction

Plasmids named pOSK (Figure 21) were derived from pREP4 (Qiagen, Germany), and include the gene for the transcriptional regulator AraC and the arabinose-inducible promotor pBAD[194] driving the expression of *birA*, *mCherry* or *gfp*. Plasmids named pOSA were derived from pSB1A3 (Registry of Standard Biological Parts, USA) and include an IPTG-inducible T5 promotor[195] controlling the expression of recombinant Ag43, FliC, AIDA-I, OmpA and INP. The proteins were modified with the following peptide sequences: a TEV protease restriction site (ENLYFQS) included a flexible linker region placed in front (GGGSGGGSGG), a FLAG-tag epitope (DYKDDDDK) and a biotin acceptor peptide (GLNDIFEAQKIEWHE). A detailed description of the plasmids can be found in Table 10.

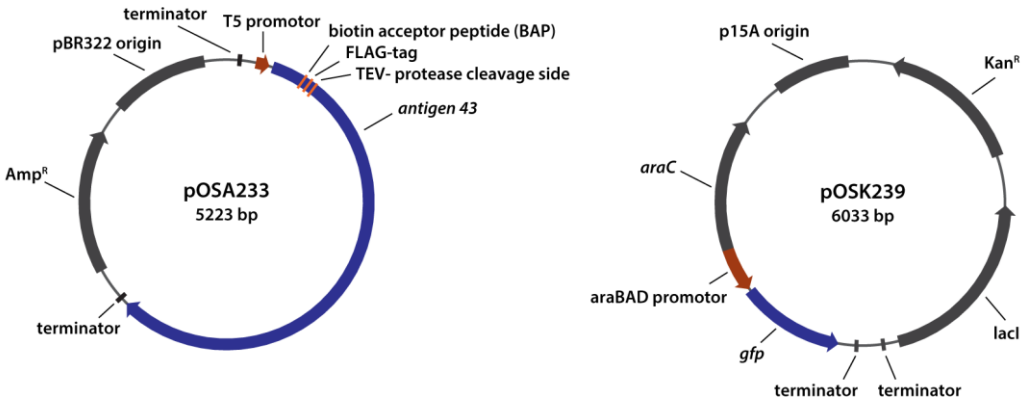

Figure 21 Representation of the expression system used in this study.

Table 10 Plasmids used in this study.

Plasmid	Resistance	Induction	Description	Source
pOSA73 (FliC-BAP)	Amp^R	IPTG	BAP and the active side of thioredoxin replace 741-1067 nt of the coding region of FliC	[153]
pOSA117 (Lpp-OmpA-BAP)	Amp^R	IPTG	29 nt of the lipoprotein Lpp signal peptide, 138-474 nt of OmpA followed by FLAG epitope and BAP	[19]
pOSA147 (INPNC-BAP)	Amp^R	IPTG	BAP, FLAG epitope and TEV protease restriction site were placed at the end of the truncated derivative of the ice nucleation protein (INPNC) derived from BBa_K523008	Reg. of Stand. Biol. Parts, USA)
pOSA176 (AIDA-BAP)	Amp^R	IPTG	BAP, FLAG epitope and TEV protease restriction site were placed between the PelB signal sequence and 2541-3858 nt of the AIDA-I translocator domain	[150]
pOSA200 (Ag43-FLAG)	Amp^R	IPTG	FLAG epitope and TEV protease restriction site replaced 171-312 nt of the coding region of Ag43	This study
pOSA217 (Ag43-90aa-BAP)	Amp^R	IPTG	BAP, FLAG epitope and TEV protease restriction site were placed at 170 nt of the coding region of Ag43	This study
pOSA224 (Ag43-BAP-90aa)	Amp^R	IPTG	BAP, FLAG epitope and TEV protease restriction site were placed at 313 nt of the coding region of Ag43	This study
pOSA233 (Ag43-BAP)	Amp^R	IPTG	BAP, FLAG epitope and TEV protease restriction site replaced 171-312 nt of the coding region of Ag43	This study
pOSA247 (Ag43-BAP-LOV2)	Amp^R	IPTG	LOV2 domain, BAP, FLAG epitope and TEV protease restriction site replaced 171-312 nt of the coding region of Ag43	This study
pOSK226	Kan^R	Arabinose	*lacI, araC*, pBAD promotor, *cfp, birA*	This study
pOSK237	Kan^R	Arabinose	*lacI, araC*, pBAD promotor, *mCherry*	This study
pOSK239	Kan^R	Arabinose	*lacI, araC*, pBAD promotor, *gfp*	This study
pREP4	Kan^R		Expression plasmid, *lacI*	Qiagen, Germany
pSB1A3	Amp^R		Expression plasmid	Registry of Standard Biological Parts, USA
pCP20	Cm^R, Amp^R		Flp recombinase	[196]

4.2.6 Isolation of plasmid DNA

For isolation of plasmid DNA the bacteria were grown on agar plates, harvested and transferred into a reaction tube. The cell lyses and plasmid extraction were carried out by using the GeneJET Plasmid Miniprep Kit, according to the manufacturers' protocol.

Plasmid DNA was stored at 20 °C. DNA sequencing was performed by Eurofins MWG Operon (Germany), to verify the correctness of newly constructed plasmids.

4.2.7 Preparation and transformation of chemical competent *E. coli*

The preparation of $CaCl_2$ competent *E. coli* cells was done according to the protocol of Inoue*, et al.* (1990)[197]:

E. coli was grown in 125 ml SOB-medium at room temperature and vigorous shaking (180 rpm), to an OD_{600nm} of 0.6. Then the culture was placed on ice for 10 min and harvested at 12000 rpm for 10 min in a chilled centrifuge. The cell pellet was gently resuspended in 40 ml ice-cold TB buffer, incubated on ice for 10 min and spun down as above. The cells were resuspended in 10 ml ice-cold TB buffer, supplemented with 7 % (v/v) DMSO and incubated on ice for 10 min. Then aliquots of 100 µl cell suspension were dispensed in reaction tubes and immediately chilled by immersion in liquid nitrogen. The competent *E. coli* cells were stored at -80 °C.

For transformation of *E. coli* with plasmid DNA, either 10 ng purified plasmid or 15-30 µl of a ligation mixture was mixed with 100 µl $CaCl_2$ competent *E. coli* cells and incubated for 30 min on ice. Afterwards the mixture was heat shocked for 45 s at 42 °C and subsequently set on ice for 2 min. Then the cells were incubated in 1 ml LB-medium for 1 h at 37 °C. Afterwards the cells were spread on a LB agar plate, containing the antibiotic selective for the transformed plasmid. The plate was incubated till single colonies were visible. Single colonies of transformants were transferred to a new selective agar plate. The presence of the plasmid was analysed by polymerase chain reaction (PCR).

4.3 Microbiological and cell biological methods

4.3.1 Cultivation of *E. coli*

Cells were grown at 34 °C and 275 rpm in TB medium, supplemented with the appropriate antibiotics and with or without the addition of 1 µM D-(+)-biotin. The cell growth was monitored with a Tecan Infinite M1000 Pro Microplate Reader (Tecan,

Switzerland). Cell cultures were inoculated with a 1:100 diluted overnight culture. After 2 hours of cultivation, the expression of recombinant proteins was induced by the addition of 100 µM isopropyl-β-D-thiogalactopyranoside (IPTG) and 0.005% L-(+)-arabinose. Cells were cultivated for additional 2 to 2.5 hours until an OD_{600} of 0.6 was reached. Where indicated, 10 µg/ml cephalexin was added to the culture for 60 min before harvesting cells. Cells were washed and resuspended in motility buffer.

4.3.2 Immuno- and NeutrAvidin-biotin staining

The detection of recombinant Ag43 and of the surface-displayed biotin was performed via immunostaining and biotin staining. For immunostaining, the cell suspension (OD_{600} of 2.0) was incubated with 1 µg/ml monoclonal mouse anti-FLAG® M2 antibody or 1 µg/ml monoclonal mouse anti-biotin BTN.4 antibody for 1 hour at room temperature. After washing three times, cells were resuspended in motility buffer and incubated with 1 µg/ml anti-mouse goat IgG conjugated to Cy3 for 1 hour at room temperature. For NeutrAvidin-biotin staining, the cell suspension (OD_{600} of 2.0) was incubated with 1 µg/ml NeutrAvidin conjugated to DyLight™ 488 (Thermo Fisher, Germany) for 45 min at room temperature. The fluorescence images were acquired at 488 and 587 nm for DyLight™ 488 and Cy3 stained cells, respectively, using a Nikon Eclipse Ti-U fluorescence microscope (Nikon Instrument, Japan) with 100x objective and Zyla 4.2 Plus sCMOS camera (Andor Technology Ltd, UK). Quantification of biotinylation was performed using a BD LSRFortessa SORP cell analyzer (BD Biosciences, Germany). Extracellular biotinylation of Ag43-BAP was performed by incubating the cell suspension (OD_{600} of 2.0) with 0.1 mg/ml BirA in motility buffer supplemented with 10 mM ATP, 10 mM MgOAc and 50 µM d-biotin for 1 hour at 30 °C. Samples were subsequently washed tree times with motility buffer and stained via NeutrAvidin, DyLight™ 488 conjugate. The cleavage of surface displayed BAP from Ag43 was performed by incubating the cell suspension (OD_{600} of 0.1) with 0.01 units/µl TEV protease, 1 mM DTT and ProTEV buffer for 15 min at 30 °C.

4.4 Bacteriabot fabrication

Cells were prepared as described above and resuspended to a final OD_{600} of 0.0375 in motility buffer. The cell suspension was mixed in a ratio of 1:30 (in numbers) with 1.4-µm or 2.2-µm Red4 streptavidin PMMA particles (1.5×10^3 particles/µl) and incubated for 20 min at room temperature. The kinetics of cell-particle attachment was analyzed using a BD LSRFortessa SORP cell analyzer. Where indicated, carbonylcyanide-m-chlorophenylhydrazone (CCCP) was added during incubation.

4.5 Microscopy

4.5.1 Widefield fluorescence microscopy

The fluorescence imaging of cells and particles was performed at 488 nm using a Nikon Eclipse Ti-U fluorescence microscope (Nikon Instrument, Japan) using a 40x objective and a dual emission image beam splitter with 525/50 nm and 647/57 nm mounted emission filters (Optosplit II; Cairn Research, UK) connected to an iXon3 897 EMCCD camera (Andor Technology Ltd, UK) at 10 frames per second. This setup enabled dual-color time-lapse microscopy of green fluorescent cells and red fluorescent particles. From these data, the propulsion orientation (push or pull) of the cell and the respective swimming speed was determined. The same data set was used to analyze the particle attachment along the cell body, with a particle attached within the first fifth of the cell body being considered as polar attachment.

4.5.2 Confocal laser scanning microscopy and scanning electron microscopy

The cell-particle attachment was visualized using a Zeiss Axio Observer Laser Scanning Microscope (LSM) 880 (Zeiss, Germany) using a 40x objective. Samples were illuminated using a 488 nm Argon and 561 nm DPSS laser. Z-stack projections were analyzed using the Zeiss ZEN System imaging software (Zeiss, Germany). Samples were also imaged using a Supra 55VP scanning electron microscope (Zeiss, Germany) using an accelerating voltage of 3 kV and an in-lens detector.

4.6 Laser assisted protein adsorption by photobleaching

The fabrication of well-defined biotin patterns on a glass surfaces was performed via laser assisted protein adsorption by photobleaching (LAPAP)[146, 147]. Glass surfaces were incubated with a 1 % BSA solution for 20 min, washed three times and covered with 100 µg/ml Biotin-(5-fluorescein)-conjugate (Sigma-Aldrich, Germany). The fluorescein labelled biotin was photobleached for 100 msec using a 515 nm DPSS laser (Acal BFi, Germany), leading to the generation of free fluorescein radicals binding to the BSA surface[148]. Subsequently the biotinylated surface was washed tree times and incubated for 20 min with 1 µg/ml NeutrAvidin, 1.4-µm Red4 streptavidin PMMA particles (1.5×10^3 particles/µl) or a cell suspension.

4.7 Microfluidics assay

The swimming behavior of cells and bacteriabots fabricated as described above was analyzed using a poly-di-methylsiloxane (PDMS) microfluidic device consisting of two large reservoirs (0.5 ± 0.1 cm^2 $\times$ 50 ± 2 µm) connected by an observation chamber (2 mm in length and 1 mm in width), constructed by standard photolithography techniques as described previously[165, 198]. The SU-8 master was prepared on a silicon wafer, casted with freshly mixed PDMS (silicone elastomer kit SYLGARD® 184, 1:10 cross-linker to base ratio, Dow Corning, USA) and let to be polymerized overnight at 65 °C. Microfluidic devices were bonded on a glass slide after oxygen plasma treatment. The microfluidic chamber was filled with a solution containing 1 M lithium acetate and 1% denatured BSA, preventing particles from adhering to its walls. After 15 min both reservoirs were filled with motility buffer containing cells or bacteriabots, where one reservoir contained additionally 200 µM α-methyl-DL-aspartate (MeAsp). A linear gradient of MeAsp formed across the observation chamber within an hour[198]. Fluorescence imaging of cell and bacteriabots (particles) was performed at 488 nm and 587 nm, respectively, using a Nikon Eclipse Ti-U fluorescence microscope (Nikon Instrument, Japan) with a 40x objective and a Zyla 4.2 Plus sCMOS camera (Andor Technology Ltd, UK) at 33 frames per second.

4.8 Particle-tracking

Cells and bacteriabots were tracked using Fiji[199], with a custom-written particle-tracking plugin using centroid localization algorithm to detect particles and identification of the closest particle in next frame for trajectory linking[200]. The instantaneous velocity $\boldsymbol{v}_i(t)$ (in 2D) of the object *i* was also determined by linear fit of the trajectory position $\boldsymbol{r}_i(t)$ on a 10-frames long sliding window around time point *t*. Further processing via MATLAB (MathWorks, USA) yielded the population-averaged swimming speed $\boldsymbol{v}_0$, chemotactic drift $\boldsymbol{v}_{ch}$, chemotactic bias $\frac{\boldsymbol{v}_{ch}}{v_0^2}$, the mean square displacement $\langle \Delta r^2(t) \rangle$ and the auto-correlation of direction of motion $C_v(t)$, as:

$$v_0 = \sum_i \sum_t^{T_i} |\, \boldsymbol{v}_{i(t)}| \;\Big/ \sum_i T_i \qquad [1]$$

$$\boldsymbol{v}_{ch} = \sum_i \sum_t^{T_i} \boldsymbol{v}\_i(t) \;\Big/ \sum_i T_i \qquad [2]$$

$$\langle \Delta r^2(t) \rangle = \sum_i \sum_{t'}^{T_i - t} \left(\boldsymbol{r}_i(t + t') - \boldsymbol{r}_i(t') \right)^2 \Big/ \sum_i (T_i - t) \qquad [3]$$

$$C_v(t) = \sum_i \sum_{t'}^{T_i - t} \frac{\boldsymbol{v}_i(t + t') \cdot \boldsymbol{v}_i(t')}{\overline{v_i^2}} \Big/ \sum_i (T_i - t) \qquad [4]$$

Here, T_i is the duration of trajectory *i*. Only trajectories longer than 20 frames and for which the average swimming speed $\overline{v_i} = \frac{\sum_t^{T_i} |\, \boldsymbol{v}_i(t)|}{T_i}$ was higher than 5 µm/s were considered, to avoid artifacts arising from spurious detections and from non-swimming objects, respectively. Furthermore, trajectories were sorted according to their average swimming speed to plot data in Figure 18B,C using equation [1, 2] for each subset of trajectories. In Figure 17B, the mean-square displacement of each trajectory was calculated using equation [3] and normalized by the respective v_0^2. Auto-correlation of direction of motion in Figure 17A was calculated for all trajectories using the equation

[4], lag times were multiplied by the respective swimming speed $\boldsymbol{v}_0$. Persistence length ξ was computed by fitting the autocorrelation according to $C_v(t) = C_0 e^{-v_0 t/\xi} + A_0$.

4.9 Bioinformatic methods

In the context of the publication Schauer*, et al.* (2018)[192] the modeling part of this study was done by Dr. Remy Colin.

4.9.1 Calculation of swimming speed dependence on cargo using the resistive force theory for flagellar bundle

By rotating its corkscrew-shaped flagellar bundle, *E. coli* propels itself in water, which appears as an extremely viscous liquid at the cell's length scale – *i.e.* the Reynolds number is low. In this situation, resistive force theory[161] can be applied to compute the propulsion speed of the cell as a function of the geometries of the flagellum and the cell body as well as the characteristics of the flagellar motor.

Following the works of Purcell[159], the symmetries of flows at low Reynolds number yield a linear set of relations between, on the one hand, the velocity (v) and rotation frequency (ω) of the flagellar bundle and, on the other hand, the force (F_{thrust}) and torque (N_{fl}) it generates:

$$-F_{thrust} = A\,v - B\,\omega \qquad [5a]$$

$$N_{fl} = -B\,v + D\,\omega \qquad [5b]$$

Since no net force is exerted on the cell (or bacteriabot), these force and torque equate the viscous force and torque experienced by the cell body (with its attached bead when relevant), which also moves at speed v and rotate at angular velocity Ω.

$$F_{thrust} = A_0\,v \qquad [6a]$$

$$N_{fl} = -D_0\,\Omega \qquad [6b]$$

Here, A, B, D and A_0, D_0 are the elements of the so-called propulsion matrices of respectively the flagellar bundle and the cell body. Notably, B measures the conversion

of rotation into translation (and vice-versa) thanks to the corkscrew shape of the bundle, and A (resp. A_0) and D (resp. D_0) are the translational and rotational friction coefficients of the bundle (resp. body). For the bundle modeled as a rigid helix, they can be calculated using resistive force theory[161] and depend only on the geometry of the organelle and the viscosity of the fluid, as:

$$A = K_n\, l \sin\psi \left(\tan\psi + \frac{\gamma_k}{\tan\psi}\right) \quad [7a]$$

$$B = K_n\, l\, R \sin\psi \ (1 - \gamma_k) \quad [7b]$$

$$D = K_n\, l\, R^2 \sin\psi \left(\frac{1}{\tan\psi} + \gamma_k \tan\psi\right) \quad [7c]$$

with

$$\tan\psi = 2\pi\frac{R}{\lambda} \quad [8]$$

$$K_n = \frac{4\pi\eta}{\ln\left(1.8\frac{\lambda}{r}\right) + 1/2} \quad [9]$$

where l, R and λ are the helix length, radius and pitch respectively, ψ is the pitch angle relative to the swimming axis, r is the radius of the bundled filaments (composed of three or more 13 nm[201] thick flagella) and γ_k is the ratio of the tangential (K_t) to perpendicular (K_n) friction coefficients of the bundled filament (Appendix-Figure 4B). All values for *E. coli* bundle used here are listed in Appendix-Table 2.

The cell body and its bead cargo are modeled by an equivalent cylindrical rod of length L_{eff} and diameter d_{eff} as follows:

$$L_{eff} = L_c + d_b \quad [10a]$$

$$d_{eff} = \frac{L_c}{L_{eff}}\, d_c + \frac{d_b}{L_{eff}} d_b \quad [10b]$$

with L_c and d_c indicating cell body length and diameter, and d_b the bead diameter (Appendix-Figure 4A). Defining the aspect ratio $p = L_{eff}/d_{eff}$, the friction coefficient of this equivalent rod is[202]:

$$A_0 = 2\pi\,\eta \frac{L_{eff}}{\ln p - 0.207 + 0.98/p}. \qquad [11]$$

Equations [5] and [6] can be solved to yield the swimming speed as a function of the motor rotation speed $\omega^m = |\Omega| + |\omega|$, considering that for *E. coli,* $D \ll D_0$ and $B^2 \ll (A + A_0)D_0$,[160]:

$$v = B \frac{\omega^m}{(A + A_0)} \ . \qquad [12]$$

When cells are elongated or attached to beads, the friction coefficients A_0 and D_0 increase. From equation [12] we gather a first obvious effect of an increase of A_0 on swimming speed. The rotation speed ω^m could also change due to an increase of the total torque experienced by the motors. Indeed, the torque-rotation speed characteristic curve was measured for the *E. coli* motor[203]. In first approximation, the motor rotation speed is more-or-less constant, as long as the torque necessary to rotate the flagellum and its load ($N^m = |D\omega| + |D_0\Omega|$) stays below a saturation value, above which the motor can only generate a constant torque and thus rotates more slowly. We first assume that in all our experiments the load is below saturation and the rotation speed stays constant.

The predicted swimming speed was computed from equations [7], [10], [11] and [12]. Using the parameters displayed in Appendix-Table 2, a relatively good agreement was found with the experimental values (Appendix-Figure 3B). Notably, the values of predicted swimming speed for different conditions ranked as the experimental ones. For the cephalexin-treated cells, it was necessary to assume that flagellar length increased to account for the relatively high swimming speed that was experimentally observed. Normal cells loaded with the 2.2-µm beads had a swimming speed lower than expected from the prediction, which could indicate that ω^m started to decrease because of a high load. Since D_0 scales as L_{eff}^3 [202], the total load on the motors of cephalexin treated cells

is expected to be even higher, but the increased flagella number should keep the torque per motor below saturation, explaining why a constant ω^m accounts for the swimming speeds in this case.

Note that the predicted swimming speed does not depend on the viscosity of the fluid. We indeed observed that the swimming speed was largely unaffected by raising the viscosity of the medium to ~4.3 mPa·s using methyl cellulose (Figure 19). It might have even increased slightly for the wild type cells, a phenomenon often reported[168] and assumed to come from the viscoelastic properties of the fluid[204], which is however beyond the scope of our model.

APPENDIX

Appendix-Figures

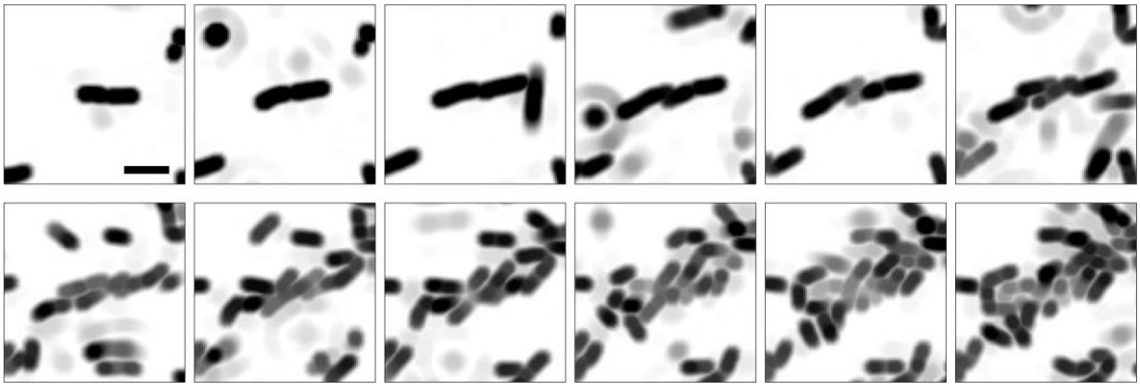

Appendix-Figure 1 Cells directly immobilized on a coated glass surface. Glass surfaces were coated with BSA and subsequently fluorescein labelled biotin was immobilized by laser assisted fluorescein photobleaching (see Material and Methods for details). After LAPAP treatment the surface was incubated for 30 min with streptavidin-coated *E. coli* cells carrying Ag43-BAP and imaged under the microscope for 6 in TB medium at 30 °C. Scale bar: 4 µm.

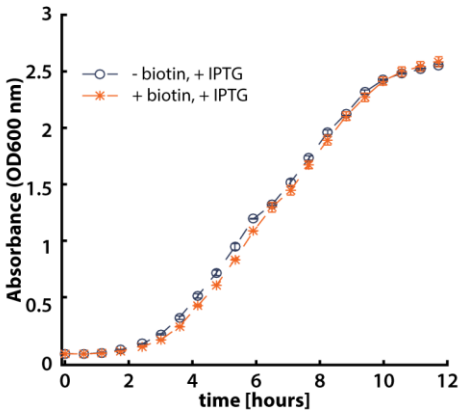

Appendix-Figure 2 Growth curves of *E. coli* cells carring Ag43-BAP. *E. coli* cells carrying a recombinant Ag43-BAP on IPTG inducible plasmid were grown with or without 1 µM biotin and/or 100 µM IPTG in TB medium, as indicated. Cells were subsequently incubated with or without BirA / biotin. Growth curves were obtained from three independent experiments. Cell density was measured via absorbance at 600 nm. Error bars show SEM.

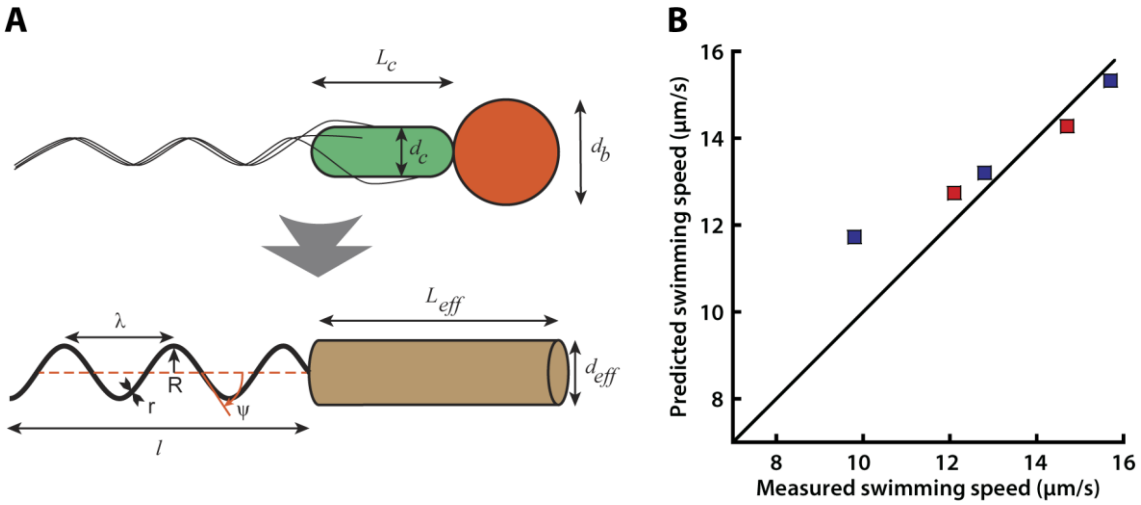

Appendix-Figure 3 Analysis of cargo effects on swimming speed using resistive force theory. (A) Schematic representation of a swimming bacteriabot used for theoretical analysis. The cell body of length L_c and diameter d_c and attached bead of diameter d_b was modeled by an equivalent cylinder with the effective length L_{eff} and diameter d_{eff} (see Supporting Text for calculations). The flagellar bundle was modeled by a single helix, the thickness of which represents several single flagella. **(B)** Swimming speeds predicted by the resistive force theory (see Supporting Text for calculations) as a function of the measured swimming speed, compared to the experimental data for the five conditions studied (blue: normal cells, red: cephalexin-treated cells). In the context of the publication Schauer, *et al.* (2018)[192] this analysis was done by Dr. Remy Colin.

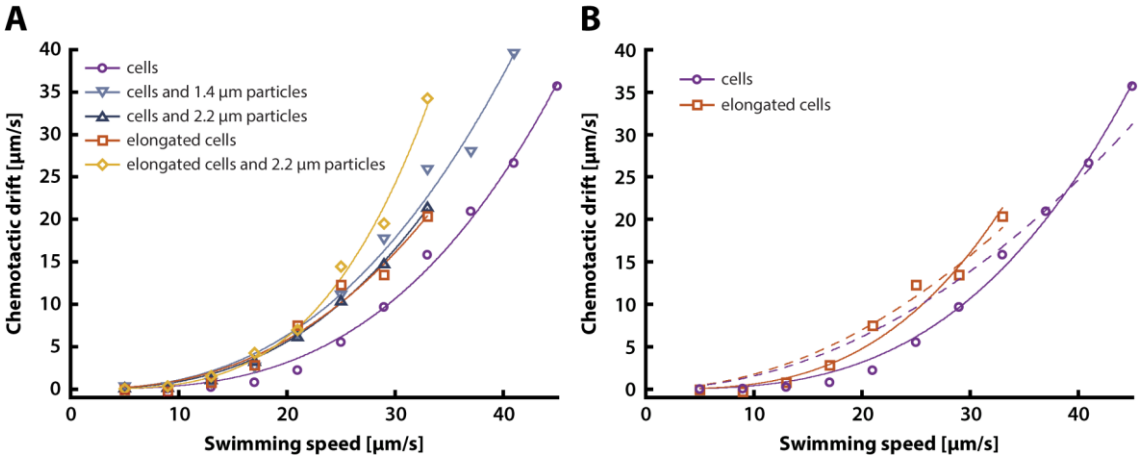

Appendix-Figure 4 Fits of the chemotactic drift as a function of swimming speed. (A) Fit by a power law $v_{ch} = K_\alpha v_0^\alpha$ yielded exponents close to 3: $\alpha = 3.0 \pm 0.1$ (normal cells), 2.5 ± 0.2 (normal cells and 1.4 µm particles), 2.7 ± 0.1 (normal cells and 2.2-µm particles), 2.5 ± 0.3 (elongated cells), 3.4 ± 0.2 (elongated cells and 2.2-µm particles), with $K_\alpha = 0.4$ (normal cells), 3 (normal cells and 1.4-µm particles), 2 (normal cells and 2.2-µm particles), 3 (elongated cells), 0.2 (elongated cells and 2.2-µm particles), in 10^{-3} $(\mu m/s)^{1-\alpha}$. **(B)** Fits by a square ($v_{ch} = K_2 v_0^2$, dotted line) and cubic ($v_{ch} = K_3 v_0^3$, solid line) dependence of the chemotactic drift on swimming speed, for normal cells ($K_2 = 0.015 \pm 0.001$ s/µm, $R_2 = 0.970$, $K_3 = (3.95 \pm 0.07)10^{-4}$ s^2/µm^2, $R_3 = 0.997$) and elongated cells ($K_2 = 0.017 \pm 0.001$ s/µm, $R_2 = 0.977$, $K_3 = (6.0 \pm 0.3)10^{-4}$ s^2/µm^2, $R_3 = 0.981$). In the context of the publication Schauer, *et al.* (2018)[192] the fitting was done by Dr. Remy Colin.

Appendix-Tables

Appendix-Table 1 Typical surface display systems for *E. coli*. Obtained and modified form van Bloois, *et al.* (2011)[13].

Scaffold	Type of fusion	Passenger size (kDa)	Application	Verification of surface display
Outer membrane proteins				
eCPX derived from OmpX	Biterminal	0.8 – 1.6	Peptide library screening	Flow cytometry, fluorescence microscopy
FhuA	Insertional	1.1 – 3.3	Peptide library screening	Flow cytometry
LamB	Insertional	1.2 –25.5	Bioremediation, peptide library screening, vaccine development	Cell fractionation, immunoblotting, functional assays
Omp1	C-terminal	56	Biocatalysis	Cell fractionation, immunoblotting, functional assays
OmpA	Insertional	1 – 50	Peptide library screening, peptide display, vaccine development	Cell fractionation, immunoblotting, fluorescence microscopy, flow cytometry
OmpC	Insertional, C-terminal	18-52	Bioremediation, biocatalysis	Functional assays
OmpT		35	Directed evolution, substrate profiling	Flow cytometry
OprF	C-terminal	50	Biocatalysis	Cell fractionation, immunoblotting, fluorescence microscopy, functional assays
PgsA	C-terminal	34-77	Biocatalysis	Cell fractionation, immunoblotting, fluorescence microscopy, flow cytometry
Wza-omp orf1/ OmpU/Omp26La	C-terminal	27-50	Translocation studies	Cell fractionation, immunoblotting, functional assays
Surface appendages				
F pillin	Insertional	1.6	Peptide antigen display	Functional assays
Fimbriae (FimH and FimA)	Insertional	1-4	Peptide library screening, immunogenic peptide display, bioremediation	Functional assays, fluorescence microscopy
Flagellin (FliC and FliD)	Insertional	1.2-33	Peptide display, peptide library screening, vaccines, bioremediation, exploring protein-protein interactions	Immunoelectron microscopy, flow cytometry
Lipoproteins				
INP	C-terminal	7-119	Epitope mapping, biocatalysis, vaccines, protein library screening	Cell fractionation, immunoblotting, flow cytometry, functional assays
Lpp-OmpA	C-terminal	27 – 74	Bioremediation, biocatalysis, antibody library screening,	Cell fractionation, immunoblotting, fluorescence microscopy, functional assays
PAL	N-terminal	29	Display antibody fragments, bioremediation	Flow cytometry, functional assays
Tat-dependent lipoprotein	C-terminal	27	Translocation studies	Cell fractionation, immunoblotting, fluorescence microscopy
TraT	Insertional, C-terminal	1.2 – 11	Antigen display	Dot blot, fluorescence microscopy
Virulence factors				
AIDA-I	N-terminal	12-65	Biocatalysis, protein library screening, vaccine development	Cell fractionation, immunoblotting, fluorescence microscopy, flow cytometry, functional assays
EaeA	C-terminal	3.9 – 31.6	Translocation studies	Cell fractionation, immunoblotting, fluorescence microscopy, flow cytometry
EspP	N-terminal	20	Protein library screening	Cell fractionation, immunoblotting, flow cytometry
EstA	N-terminal	38-60	Biocatalysis, protein library screening	Flow cytometry, functional assays
Invasin	C-terminal	1.1	Peptide library screening	Flow cytometry, fluorescence microscopy
MSP1a	N-terminal	4.6	Immunogenic peptide display	Cellular fractionation, fluorescence microscopy, functional assays

Appendix-Table 2 Parameters used for calculations of swimming speed in the model.

Parameter	Value	Reference
$\boldsymbol{\lambda}$	2.3 μm	[136]
$\boldsymbol{R}$	0.2 μm	[136]
$\boldsymbol{r}$	40 nm	[201]
$\boldsymbol{\gamma_k}$	0.7	[161]
$\boldsymbol{\sin\psi}$	0.88	$\boldsymbol{\tan\psi = \lambda/2\pi R}$
$\boldsymbol{\omega^m}$	$\boldsymbol{2\pi \times 140}$ rad/s	[160]
$\boldsymbol{l}$, cpx-	10 μm	[201]
$\boldsymbol{l}$, cpx+	17 μm	This study

REFERENCES

1. Yim SK, Kim DH, Jung HC, Pan JG, Kang HS, Ahn T, Yun CH (2010) Surface display of heme- and diflavin-containing cytochrome P450 BM3 in *Escherichia coli*: a whole cell biocatalyst for oxidation. *J Microbiol Biotechnol* 20(4):712-717.
2. Jose J, Bernhardt R, Hannemann F (2001) Functional display of active bovine adrenodoxin on the surface of *E. coli* by chemical incorporation of the [2Fe-2S] cluster. *Chembiochem* 2(9):695-701.
3. Wernerus H, Stahl S (2004) Biotechnological applications for surface-engineered bacteria. *Biotechnol Appl Biochem* 40(Pt 3):209-228.
4. Ribeiro LA, Azevedo V, Le Loir Y, Oliveira SC, Dieye Y, Piard JC, Gruss A, Langella P (2002) Production and targeting of the *Brucella abortus* antigen L7/L12 in *Lactococcus lactis*: a first step towards food-grade live vaccines against brucellosis. *Appl Environ Microbiol* 68(2):910-916.
5. Kornacker MG, Pugsley AP (1990) The normally periplasmic enzyme beta-lactamase is specifically and efficiently translocated through the *Escherichia coli* outer membrane when it is fused to the cell-surface enzyme pullulanase. *Mol Microbiol* 4(7):1101-1109.
6. Samuelson P, Gunneriusson E, Nygren PA, Stahl S (2002) Display of proteins on bacteria. *J Biotechnol* 96(2):129-154.
7. Ho M, Pastan I (2009) Mammalian cell display for antibody engineering. *Methods Mol Biol* 525:337-352, xiv.
8. Boder ET, Wittrup KD (1997) Yeast surface display for screening combinatorial polypeptide libraries. *Nat Biotechnol* 15(6):553-557.
9. Tanaka T, Yamada R, Ogino C, Kondo A (2012) Recent developments in yeast cell surface display toward extended applications in biotechnology. *Appl Microbiol Biotechnol* 95(3):577-591.
10. Liew PX, Wang CL, Wong SL (2012) Functional characterization and localization of a *Bacillus subtilis* sortase and its substrate and use of this sortase system to covalently anchor a heterologous protein to the B. subtilis cell wall for surface display. *J Bacteriol* 194(1):161-175.
11. Schneewind O, Missiakas DM (2012) Protein secretion and surface display in Gram-positive bacteria. *Philos Trans R Soc Lond B Biol Sci* 367(1592):1123-1139.

12. Freudl R, MacIntyre S, Degen M, Henning U (1986) Cell surface exposure of the outer membrane protein OmpA of *Escherichia coli* K-12. *J Mol Biol* 188(3):491-494.

13. van Bloois E, Winter RT, Kolmar H, Fraaije MW (2011) Decorating microbes: surface display of proteins on *Escherichia coli*. *Trends Biotechnol* 29(2):79-86.

14. Hartl FU, Lecker S, Schiebel E, Hendrick JP, Wickner W (1990) The binding cascade of SecB to SecA to SecY/E mediates preprotein targeting to the *E. coli* plasma membrane. *Cell* 63(2):269-279.

15. Knowles TJ, Scott-Tucker A, Overduin M, Henderson IR (2009) Membrane protein architects: the role of the BAM complex in outer membrane protein assembly. *Nat Rev Microbiol* 7(3):206-214.

16. Henderson IR, Navarro-Garcia F, Desvaux M, Fernandez RC, Ala'Aldeen D (2004) Type V protein secretion pathway: the autotransporter story. *Microbiol Mol Biol Rev* 68(4):692-744.

17. Maurer J, Jose J, Meyer TF (1997) Autodisplay: one-component system for efficient surface display and release of soluble recombinant proteins from *Escherichia coli*. *J Bacteriol* 179(3):794-804.

18. Freudl R, Schwarz H, Klose M, Movva NR, Henning U (1985) The nature of information, required for export and sorting, present within the outer membrane protein OmpA of *Escherichia coli* K-12. *EMBO J* 4(13A):3593-3598.

19. Earhart CF (2000) Use of an Lpp-OmpA fusion vehicle for bacterial surface display. *Methods Enzymol* 326:506-516.

20. Francisco JA, Earhart CF, Georgiou G (1992) Transport and anchoring of beta-lactamase to the external surface of *Escherichia coli*. *Proc Natl Acad Sci U S A* 89(7):2713-2717.

21. Wang AA, Mulchandani A, Chen W (2001) Whole-cell immobilization using cell surface-exposed cellulose-binding domain. *Biotechnol Prog* 17(3):407-411.

22. Wang AA, Mulchandani A, Chen W (2002) Specific Adhesion to Cellulose and Hydrolysis of Organophosphate Nerve Agents by a Genetically Engineered *Escherichia coli* Strain with a Surface-Expressed Cellulose-Binding Domain and Organophosphorus Hydrolase. *Applied and Environmental Microbiology* 68(4):1684-1689.

23. Jose J, von Schwichow S (2004) Autodisplay of active sorbitol dehydrogenase (SDH) yields a whole cell biocatalyst for the synthesis of rare sugars. *Chembiochem* 5(4):491-499.

24. Kjaergaard K, Hasman H, Schembri MA, Klemm P (2002) Antigen 43-mediated autotransporter display, a versatile bacterial cell surface presentation system. *J Bacteriol* 184(15):4197-4204.

25. Benz I, Schmidt MA (1992) AIDA-I, the adhesin involved in diffuse adherence of the diarrhoeagenic *Escherichia coli* strain 2787 (O126:H27), is synthesized via a precursor molecule. *Mol Microbiol* 6(11):1539-1546.

26. Maurer J, Jose J, Meyer TF (1999) Characterization of the essential transport function of the AIDA-I autotransporter and evidence supporting structural predictions. *J Bacteriol* 181(22):7014-7020.

27. van der Woude MW, Henderson IR (2008) Regulation and function of Ag43 (flu). *Annu Rev Microbiol* 62:153-169.

28. Jung HC, Park JH, Park SH, Lebeault JM, Pan JG (1998) Expression of carboxymethylcellulase on the surface of *Escherichia coli* using Pseudomonas syringae ice nucleation protein. *Enzyme Microb Technol* 22(5):348-354.

29. Kozloff LM, Turner MA, Arellano F, Lute M (1991) Phosphatidylinositol, a phospholipid of ice-nucleating bacteria. *J Bacteriol* 173(6):2053-2060.

30. Turner MA, Arellano F, Kozloff LM (1991) Components of ice nucleation structures of bacteria. *J Bacteriol* 173(20):6515-6527.

31. Wilson DR, Beveridge TJ (1993) Bacterial flagellar filaments and their component flagellins. *Can J Microbiol* 39(5):451-472.

32. Yonekura K, Maki-Yonekura S, Namba K (2003) Complete atomic model of the bacterial flagellar filament by electron cryomicroscopy. *Nature* 424(6949):643-650.

33. Kuwajima G, Asaka J-I, Fujiwara T, Fujiwara T, Nakano K, Kondoh E (1988) Presentation of an Antigenic Determinant from Hen Egg-White Lysozyme on the Flagellar Filament of *Escherichia coli*. *Bio/Technology* 6:1080.

34. Westerlund-Wikstrom B (2000) Peptide display on bacterial flagella: principles and applications. *Int J Med Microbiol* 290(3):223-230.

35. Kuwajima G (1988) Construction of a minimum-size functional flagellin of *Escherichia coli*. *J Bacteriol* 170(7):3305-3309.

36. Westerlund-Wikstrom B, Tanskanen J, Virkola R, Hacker J, Lindberg M, Skurnik M, Korhonen TK (1997) Functional expression of adhesive peptides as fusions to *Escherichia coli* flagellin. *Protein Eng* 10(11):1319-1326.

37. Diderichsen B (1980) flu, a metastable gene controlling surface properties of *Escherichia coli*. *J Bacteriol* 141(2):858-867.

38. Owen P, Caffrey P, Josefsson LG (1987) Identification and partial characterization of a novel bipartite protein antigen associated with the outer membrane of *Escherichia coli*. *J Bacteriol* 169(8):3770-3777.

39. Heras B, Totsika M, Peters KM, Paxman JJ, Gee CL, Jarrott RJ, Perugini MA, Whitten AE, Schembri MA (2014) The antigen 43 structure reveals a molecular Velcro-like mechanism of autotransporter-mediated bacterial clumping. *Proc Natl Acad Sci USA* 111(1):457-462.

40. Yuan X, Johnson MD, Zhang J, Lo AW, Schembri MA, Wijeyewickrema LC, Pike RN, Huysmans GHM, Henderson IR, Leyton DL (2018) Molecular basis for the folding of beta-helical autotransporter passenger domains. *Nat Commun* 9(1):1395.

41. Henderson IR, Meehan M, Owen P (1997) Antigen 43, a phase-variable bipartite outer membrane protein, determines colony morphology and autoaggregation in *Escherichia coli* K-12. *FEMS Microbiol Lett* 149(1):115-120.

42. Ieva R, Bernstein HD (2009) Interaction of an autotransporter passenger domain with BamA during its translocation across the bacterial outer membrane. *Proc Natl Acad Sci U S A* 106(45):19120-19125.

43. Wells TJ, Totsika M, Schembri MA (2010) Autotransporters of *Escherichia coli*: a sequence-based characterization. *Microbiology* 156(Pt 8):2459-2469.

44. Selkrig J, Mosbahi K, Webb CT, Belousoff MJ, Perry AJ, Wells TJ, Morris F, Leyton DL, Totsika M, Phan MD, Celik N, Kelly M, Oates C, Hartland EL, Robins-Browne RM, Ramarathinam SH, Purcell AW, Schembri MA, Strugnell RA, Henderson IR, Walker D, Lithgow T (2012) Discovery of an archetypal protein transport system in bacterial outer membranes. *Nat Struct Mol Biol* 19(5):506-510, S501.

45. Jain S, van Ulsen P, Benz I, Schmidt MA, Fernandez R, Tommassen J, Goldberg MB (2006) Polar localization of the autotransporter family of large bacterial virulence proteins. *J Bacteriol* 188(13):4841-4850.

46. Wallecha A, Munster V, Correnti J, Chan T, van der Woude M (2002) Dam- and OxyR-dependent phase variation of agn43: essential elements and evidence for a new role of DNA methylation. *J Bacteriol* 184(12):3338-3347.

47. Henderson IR, Meehan M, Owen P (1997) A novel regulatory mechanism for a novel phase-variable outer membrane protein of *Escherichia coli*. *Adv Exp Med Biol* 412:349-355.

48. Waldron DE, Owen P, Dorman CJ (2002) Competitive interaction of the OxyR DNA-binding protein and the Dam methylase at the antigen 43 gene regulatory region in *Escherichia coli*. *Mol Microbiol* 44(2):509-520.

49. Danese PN, Pratt LA, Dove SL, Kolter R (2000) The outer membrane protein, antigen 43, mediates cell-to-cell interactions within *Escherichia coli* biofilms. *Mol Microbiol* 37(2):424-432.

50. Kjaergaard K, Schembri MA, Hasman H, Klemm P (2000) Antigen 43 from *Escherichia coli* induces inter- and intraspecies cell aggregation and changes in colony morphology of Pseudomonas fluorescens. *J Bacteriol* 182(17):4789-4796.

51. Schembri MA, Kjaergaard K, Klemm P (2003) Global gene expression in *Escherichia coli* biofilms. *Mol Microbiol* 48(1):253-267.

52. Tong L (2013) Structure and function of biotin-dependent carboxylases. *Cell Mol Life Sci* 70(5):863-891.

53. Hassan YI, Zempleni J (2006) Epigenetic regulation of chromatin structure and gene function by biotin. *J Nutr* 136(7):1763-1765.

54. Barker DF, Campbell AM (1980) Use of bio-lac fusion strains to study regulation of biotin biosynthesis in *Escherichia coli*. *J Bacteriol* 143(2):789-800.

55. Cronan JE, Jr. (1988) Expression of the biotin biosynthetic operon of *Escherichia coli* is regulated by the rate of protein biotination. *J Biol Chem* 263(21):10332-10336.

56. Ringlstetter SL (2011) Identification of the biotin transporter in *Escherichia coli*, biotinylation of histones in *Saccharomyces cerevisiae* and analysis of biotin sensing in *Saccharomyces cerevisiae*. Ph.D. thesis. Universität Regensburg, Regensburg, Germany. http://epub.uni-regensburg.de/15822/1/Diss_R_S.pdf.

57. Barker DF, Campbell AM (1981) The birA gene of *Escherichia coli* encodes a biotin holoenzyme synthetase. *J Mol Biol* 146(4):451-467.

58. Barker DF, Campbell AM (1981) Genetic and biochemical characterization of the birA gene and its product: evidence for a direct role of biotin holoenzyme synthetase in repression of the biotin operon in *Escherichia coli*. *J Mol Biol* 146(4):469-492.

59. Chapman-Smith A, Cronan JE, Jr. (1999) The enzymatic biotinylation of proteins: a post-translational modification of exceptional specificity. *Trends Biochem Sci* 24(9):359-363.

60. Cronan JE, Jr., Waldrop GL (2002) Multi-subunit acetyl-CoA carboxylases. *Prog Lipid Res* 41(5):407-435.

61. Abdel-Hamid AM, Cronan JE (2007) Coordinate expression of the acetyl coenzyme A carboxylase genes, accB and accC, is necessary for normal regulation of biotin synthesis in *Escherichia coli*. *J Bacteriol* 189(2):369-376.

62. Xu Y, Beckett D (1994) Kinetics of biotinyl-5'-adenylate synthesis catalyzed by the *Escherichia coli* repressor of biotin biosynthesis and the stability of the enzyme-product complex. *Biochemistry* 33(23):7354-7360.

63. Cronan JE, Jr. (1989) The *E. coli* bio operon: transcriptional repression by an essential protein modification enzyme. *Cell* 58(3):427-429.

64. Beckett D (2005) The *Escherichia coli* biotin regulatory system: a transcriptional switch. *J Nutr Biochem* 16(7):411-415.

65. Schatz PJ (1993) Use of peptide libraries to map the substrate specificity of a peptide-modifying enzyme: a 13 residue consensus peptide specifies biotinylation in *Escherichia coli*. *Biotechnology* 11(10):1138-1143.

66. Solbiati J, Cronan JE (2010) The switch regulating transcription of the *Escherichia coli* biotin operon does not require extensive protein-protein interactions. *Chem Biol* 17(1):11-17.

67. Achermann M, Jeong S, Balet L, Montano GA, Hollingsworth JA (2011) Efficient quantum dot-quantum dot and quantum dot-dye energy transfer in biotemplated assemblies. *ACS Nano* 5(3):1761-1768.

68. Carlsen AT, Zahid OK, Ruzicka JA, Taylor EW, Hall AR (2014) Selective detection and quantification of modified DNA with solid-state nanopores. *Nano Lett* 14(10):5488-5492.

69. Jain A, Cheng K (2017) The principles and applications of avidin-based nanoparticles in drug delivery and diagnosis. *J Control Release* 245:27-40.

70. Bayer EA, Wilchek M (1990) Application of avidin-biotin technology to affinity-based separations. *J Chromatogr* 510:3-11.

71. Diamandis EP, Christopoulos TK (1991) The biotin-(strept)avidin system: principles and applications in biotechnology. *Clin Chem* 37(5):625-636.

72. Beckett D, Kovaleva E, Schatz PJ (1999) A minimal peptide substrate in biotin holoenzyme synthetase-catalyzed biotinylation. *Protein Sci* 8(4):921-929.

73. Parrott MB, Barry MA (2001) Metabolic biotinylation of secreted and cell surface proteins from mammalian cells. *Biochem Biophys Res Commun* 281(4):993-1000.

74. de Boer E, Rodriguez P, Bonte E, Krijgsveld J, Katsantoni E, Heck A, Grosveld F, Strouboulis J (2003) Efficient biotinylation and single-step purification of tagged transcription factors in mammalian cells and transgenic mice. *Proc Natl Acad Sci U S A* 100(13):7480-7485.

75. Tanaka T, Masunari S, Ishii J, Wakamura K, Segawa M, Fukuda H, Kondo A (2010) Displaying non-natural, functional molecules on yeast surfaces via biotin-streptavidin interaction. *J Biotechnol* 145(1):79-83.

76. Green NM (1963) Avidin. 1. The Use of (14-C) Biotin for Kinetic Studies and for Assay. *Biochem J* 89:585-591.

77. Green NM (1990) Avidin and streptavidin. *Methods Enzymol* 184:51-67.

78. Chilkoti A, Stayton PS (1995) Molecular-Origins of the Slow Streptavidin-Biotin Dissociation Kinetics. *Journal of the American Chemical Society* 117(43):10622-10628.

79. Merkel R, Nassoy P, Leung A, Ritchie K, Evans E (1999) Energy landscapes of receptor-ligand bonds explored with dynamic force spectroscopy. *Nature* 397(6714):50-53.

80. Kuntz ID, Chen K, Sharp KA, Kollman PA (1999) The maximal affinity of ligands. *Proc Natl Acad Sci U S A* 96(18):9997-10002.

81. Hyre DE, Le Trong I, Merritt EA, Eccleston JF, Green NM, Stenkamp RE, Stayton PS (2006) Cooperative hydrogen bond interactions in the streptavidin-biotin system. *Protein Sci* 15(3):459-467.

82. DeChancie J, Houk KN (2007) The origins of femtomolar protein-ligand binding: hydrogen-bond cooperativity and desolvation energetics in the biotin-(strept)avidin binding site. *J Am Chem Soc* 129(17):5419-5429.

83. Zeng J, Jia X, Zhang JZ, Mei Y (2013) The F130L mutation in streptavidin reduces its binding affinity to biotin through electronic polarization effect. *J Comput Chem* 34(31):2677-2686.

84. Liu F, Zhang JZ, Mei Y (2016) The origin of the cooperativity in the streptavidin-biotin system: A computational investigation through molecular dynamics simulations. *Sci Rep* 6:27190.

85. Weber PC, Ohlendorf DH, Wendoloski JJ, Salemme FR (1989) Structural origins of high-affinity biotin binding to streptavidin. *Science* 243(4887):85-88.

86. Livnah O, Bayer EA, Wilchek M, Sussman JL (1993) Three-dimensional structures of avidin and the avidin-biotin complex. *Proc Natl Acad Sci U S A* 90(11):5076-5080.

87. Pierce Biotechnology. Instructions for NeutrAvidin, Product No.31000

88. Altin JG, Pagler EB (1995) A one-step procedure for biotinylation and chemical cross-linking of lymphocyte surface and intracellular membrane-associated molecules. *Anal Biochem* 224(1):382-389.

89. Scheurer SB, Rybak JN, Roesli C, Brunisholz RA, Potthast F, Schlapbach R, Neri D, Elia G (2005) Identification and relative quantification of membrane proteins by surface biotinylation and two-dimensional peptide mapping. *Proteomics* 5(11):2718-2728.

90. Tannous BA, Grimm J, Perry KF, Chen JW, Weissleder R, Breakefield XO (2006) Metabolic biotinylation of cell surface receptors for in vivo imaging. *Nat Methods* 3(5):391-396.

91. Cole JN, Ramirez RD, Currie BJ, Cordwell SJ, Djordjevic SP, Walker MJ (2005) Surface analyses and immune reactivities of major cell wall-associated proteins of group a streptococcus. *Infect Immun* 73(5):3137-3146.

92. Bradburne JA, Godfrey P, Choi JH, Mathis JN (1993) In vivo labeling of *Escherichia coli* cell envelope proteins with N-hydroxysuccinimide esters of biotin. *Appl Environ Microbiol* 59(3):663-668.

93. Verhoeven GS, Alexeeva S, Dogterom M, den Blaauwen T (2009) Differential bacterial surface display of peptides by the transmembrane domain of OmpA. *PLoS One* 4(8):e6739.

94. Singh AV, Hosseinidoust Z, Park BW, Yasa O, Sitti M (2017) Microemulsion-Based Soft Bacteria-Driven Microswimmers for Active Cargo Delivery. *ACS Nano* 11(10):9759-9769.

95. Lee MY, Lufkin T (2012) Development of the "Three-step MACS": a novel strategy for isolating rare cell populations in the absence of known cell surface markers from complex animal tissue. *J Biomol Tech* 23(2):69-77.

96. Krager KJ, Sarkar M, Twait EC, Lill NL, Koland JG (2012) A novel biotinylated lipid raft reporter for electron microscopic imaging of plasma membrane microdomains. *J Lipid Res* 53(10):2214-2225.

97. Sabarth N, Lamer S, Zimny-Arndt U, Jungblut PR, Meyer TF, Bumann D (2002) Identification of surface proteins of Helicobacter pylori by selective biotinylation, affinity purification, and two-dimensional gel electrophoresis. *J Biol Chem* 277(31):27896-27902.

98. Smither SJ, Hill J, van Baar BL, Hulst AG, de Jong AL, Titball RW (2007) Identification of outer membrane proteins of Yersinia pestis through biotinylation. *J Microbiol Methods* 68(1):26-31.

99. Madler S, Bich C, Touboul D, Zenobi R (2009) Chemical cross-linking with NHS esters: a systematic study on amino acid reactivities. *J Mass Spectrom* 44(5):694-706.

100. Odeyale CO, Kang YH (1988) Biotinylation of bacterial lipopolysaccharide and its applications to electron microscopy. *J Histochem Cytochem* 36(9):1131-1137.

101. Kojima N, Matsuo T, Sakai Y (2006) Rapid hepatic cell attachment onto biodegradable polymer surfaces without toxicity using an avidin-biotin binding system. *Biomaterials* 27(28):4904-4910.

102. Singh AV, Sitti M (2016) Patterned and Specific Attachment of Bacteria on Biohybrid Bacteria-Driven Microswimmers. *Adv Healthc Mater* 5(18):2325-2331.

103. Park SJ, Park SH, Cho S, Kim DM, Lee Y, Ko SY, Hong Y, Choy HE, Min JJ, Park JO, Park S (2013) New paradigm for tumor theranostic methodology using bacteria-based microrobot. *Sci Rep.* 3. 3394; 10.1038/srep03394.

104. Chen I, Howarth M, Lin W, Ting AY (2005) Site-specific labeling of cell surface proteins with biophysical probes using biotin ligase. *Nat Methods* 2(2):99-104.

105. Furukawa H, Tanino T, Fukuda H, Kondo A (2006) Development of novel yeast cell surface display system for homo-oligomeric protein by coexpression of native and anchored subunits. *Biotechnol Prog* 22(4):994-997.

106. Howarth M, Takao K, Hayashi Y, Ting AY (2005) Targeting quantum dots to surface proteins in living cells with biotin ligase. *Proc Natl Acad Sci U S A* 102(21):7583-7588.

107. Carlsen RW, Sitti M (2014) Bio-Hybrid Cell-Based Actuators for Microsystems. *Small* 10(19):3831-3851.

108. Martel S (2012) Bacterial microsystems and microrobots. *Biomed Microdevices* 14(6):1033-1045.

109. Felfoul O, Mohammadi M, Taherkhani S, de Lanauze D, Xu YZ, Loghin D, Essa S, Jancik S, Houle D, Lafleur M, Gaboury L, Tabrizian M, Kaou N, Atkin M, Vuong T, Batist G, Beauchemin N, Radzioch D, Martel S (2016) Magneto-aerotactic bacteria deliver drug-containing nanoliposomes to tumour hypoxic regions. *Nat Nanotechnol* 11(11):941-947.

110. Nguyen VD, Han JW, Choi YJ, Cho S, Zheng S, Ko SY, Park JO, Park S (2016) Active tumor-therapeutic liposomal bacteriobot combining a drug (paclitaxel)-encapsulated liposome with targeting bacteria (*Salmonella Typhimurium*). *Sensor Actuat B-Chem* 224:217-224.

111. Ceylan H, Giltinan J, Kozielski K, Sitti M (2017) Mobile microrobots for bioengineering applications. *Lab Chip* 17(10):1705-1724.

112. Park BW, Zhuang J, Yasa O, Sitti M (2017) Multifunctional Bacteria-Driven Microswimmers for Targeted Active Drug Delivery. *ACS Nano* 11(9):8910-8923.

113. Sitti M (2017) *Mobile Microrobotics* (MIT Press, Cambridge, MA) pp xxviii, 271 pages.

114. Xu H, Medina-Sanchez M, Magdanz V, Schwarz L, Hebenstreit F, Schmidt OG (2018) Sperm-Hybrid Micromotor for Targeted Drug Delivery. *ACS Nano* 12(1):327-337.

115. Hosseinidoust Z, Mostaghaci B, Yasa O, Park BW, Singh AV, Sitti M (2016) Bioengineered and biohybrid bacteria-based systems for drug delivery. *Adv Drug Deliver Rev* 106:27-44.

116. Hong JW, Song S, Shin JH (2013) A novel microfluidic co-culture system for investigation of bacterial cancer targeting. *Lab Chip* 13(15):3033-3040.

117. Danino T, Prindle A, Kwong GA, Skalak M, Li H, Allen K, Hasty J, Bhatia SN (2015) Programmable probiotics for detection of cancer in urine. *Sci Transl Med.* 7(289). 289ra84; 10.1126/scitranslmed.aaa3519.

118. Sahari A, Traore MA, Scharf BE, Behkam B (2014) Directed transport of bacteria-based drug delivery vehicles: bacterial chemotaxis dominates particle shape. *Biomed Microdevices* 16(5):717-725.

119. Zhuang J, Sitti M (2016) Chemotaxis of bio-hybrid multiple bacteria-driven microswimmers. *Sci Rep.* 6. 32135; 10.1038/srep32135.

120. Park D, Park SJ, Cho S, Lee Y, Lee YK, Min JJ, Park BJ, Ko SY, Park JO, Park S (2014) Motility analysis of bacteria-based microrobot (bacteriobot) using chemical gradient microchamber. *Biotechnol Bioeng* 111(1):134-143.

121. Kim D, Liu A, Diller E, Sitti M (2012) Chemotactic steering of bacteria propelled microbeads. *Biomed Microdevices* 14(6):1009-1017.

122. Traore MA, Sahari A, Behkam B (2011) Computational and experimental study of chemotaxis of an ensemble of bacteria attached to a microbead. *Phys Rev E Stat Nonlin Soft Matter Phys* 84(6 Pt 1):061908.

123. Behkam B, Sitti M (2007) Bacterial flagella-based propulsion and on/off motion control of microscale objects. *Appl Phys Lett.* 90(2). 023902; 10.1063/1.2431454.

124. Darnton N, Turner L, Breuer K, Berg HC (2004) Moving fluid with bacterial carpets. *Biophys J* 86(3):1863-1870.

125. Stanton MM, Park BW, Miguel-Lopez A, Ma X, Sitti M, Sanchez S (2017) Biohybrid Microtube Swimmers Driven by Single Captured Bacteria. *Small.* 13(19). 1603679; 10.1002/Smll.201603679.

126. Sahari A, Headen D, Behkam B (2012) Effect of body shape on the motile behavior of bacteria-powered swimming microrobots (BacteriaBots). *Biomed Microdevices* 14(6):999-1007.

127. Reddington SC, Howarth M (2015) Secrets of a covalent interaction for biomaterials and biotechnology: SpyTag and SpyCatcher. *Curr Opin Chem Biol* 29:94-99.

128. Veiga E, de Lorenzo V, Fernandez LA (2003) Autotransporters as scaffolds for novel bacterial adhesins: surface properties of *Escherichia coli* cells displaying Jun/Fos dimerization domains. *J Bacteriol* 185(18):5585-5590.

129. Traore MA, Damico CM, Behkam B (2014) Biomanufacturing and self-propulsion dynamics of nanoscale bacteria-enabled autonomous delivery systems. *Appl Phys Lett.* 105(17). 173702; 10.1063/1.4900641.

130. Mostaghaci B, Yasa O, Zhuang J, Sitti M (2017) Bioadhesive Bacterial Microswimmers for Targeted Drug Delivery in the Urinary and Gastrointestinal Tracts. *Adv Sci* 4(6):1700058.

131. Adler J (2011) My life with nature. *Annu Rev Biochem* 80:42-70.

132. Sourjik V, Berg HC (2004) Functional interactions between receptors in bacterial chemotaxis. *Nature* 428(6981):437-441.

133. Harshey RM (2003) Bacterial motility on a surface: many ways to a common goal. *Annu Rev Microbiol* 57:249-273.

134. Macnab RM (2003) How bacteria assemble flagella. *Annu Rev Microbiol* 57:77-100.

135. Colin R, Sourjik V (2017) Emergent properties of bacterial chemotaxis pathway. *Curr Opin Microbiol* 39:24-33.

136. Darnton NC, Turner L, Rojevsky S, Berg HC (2007) On torque and tumbling in swimming *Escherichia coli*. *J Bacteriol* 189(5):1756-1764.

137. Berg HC, Brown DA (1972) Chemotaxis in *Escherichia coli* analysed by three-dimensional tracking. *Nature* 239(5374):500-504.

138. Segall JE, Block SM, Berg HC (1986) Temporal comparisons in bacterial chemotaxis. *Proc Natl Acad Sci USA* 83(23):8987-8991.

139. Macnab RM, Koshland DE, Jr. (1972) The gradient-sensing mechanism in bacterial chemotaxis. *Proc Natl Acad Sci USA* 69(9):2509-2512.

140. Hazelbauer GL, Falke JJ, Parkinson JS (2008) Bacterial chemoreceptors: high-performance signaling in networked arrays. *Trends Biochem Sci* 33(1):9-19.

141. Briegel A, Li X, Bilwes AM, Hughes KT, Jensen GJ, Crane BR (2012) Bacterial chemoreceptor arrays are hexagonally packed trimers of receptor dimers networked by rings of kinase and coupling proteins. *Proc Natl Acad Sci USA* 109(10):3766-3771.

142. Sourjik V, Wingreen NS (2012) Responding to chemical gradients: bacterial chemotaxis. *Curr Opin Cell Biol* 24(2):262-268.

143. Porter SL, Wadhams GH, Armitage JP (2011) Signal processing in complex chemotaxis pathways. *Nat Rev Microbiol* 9(3):153-165.

144. Friedlander RS, Vogel N, Aizenberg J (2015) Role of Flagella in Adhesion of *Escherichia coli* to Abiotic Surfaces. *Langmuir* 31(22):6137-6144.

145. Zhou M, Duan Q, Zhu X, Guo Z, Li Y, Hardwidge PR, Zhu G (2013) Both flagella and F4 fimbriae from F4ac+ enterotoxigenic *Escherichia coli* contribute to attachment to IPEC-J2 cells in vitro. *Vet Res* 44:30.

146. Holden MA, Cremer PS (2003) Light activated patterning of dye-labeled molecules on surfaces. *J Am Chem Soc* 125(27):8074-8075.

147. Belisle JM, Correia JP, Wiseman PW, Kennedy TE, Costantino S (2008) Patterning protein concentration using laser-assisted adsorption by photobleaching, LAPAP. *Lab Chip* 8(12):2164-2167.

148. Song L, Varma CA, Verhoeven JW, Tanke HJ (1996) Influence of the triplet excited state on the photobleaching kinetics of fluorescein in microscopy. *Biophys J* 70(6):2959-2968.

149. Kogelnik H, Li T (1966) Laser beams and resonators. *Appl Opt* 5(10):1550-1567.

150. Suhr M, Benz I, Schmidt MA (1996) Processing of the AIDA-I precursor: removal of AIDAc and evidence for the outer membrane anchoring as a beta-barrel structure. *Mol Microbiol* 22(1):31-42.

151. Benz I, Schmidt MA (1989) Cloning and expression of an adhesin (AIDA-I) involved in diffuse adherence of enteropathogenic *Escherichia coli*. *Infect Immun* 57(5):1506-1511.

152. Kuwajima G, Asaka J, Fujiwara T, Fujiwara T, Node K, Kondo E (1986) Nucleotide sequence of the hag gene encoding flagellin of *Escherichia coli*. *J Bacteriol* 168(3):1479-1483.

153. Lu Z, Murray KS, Van Cleave V, LaVallie ER, Stahl ML, McCoy JM (1995) Expression of thioredoxin random peptide libraries on the *Escherichia coli* cell surface as functional fusions to flagellin: a system designed for exploring protein-protein interactions. *Biotechnology (N Y)* 13(4):366-372.

154. Huala E, Oeller PW, Liscum E, Han IS, Larsen E, Briggs WR (1997) Arabidopsis NPH1: a protein kinase with a putative redox-sensing domain. *Science* 278(5346):2120-2123.

155. Harper SM, Neil LC, Gardner KH (2003) Structural basis of a phototropin light switch. *Science* 301(5639):1541-1544.

156. Konold PE, Mathes T, Weibetaenborn J, Groot ML, Hegemann P, Kennis JT (2016) Unfolding of the C-Terminal Jalpha Helix in the LOV2 Photoreceptor Domain Observed by Time-Resolved Vibrational Spectroscopy. *J Phys Chem Lett* 7(17):3472-3476.

157. Zayner JP, Antoniou C, Sosnick TR (2012) The amino-terminal helix modulates light-activated conformational changes in AsLOV2. *J Mol Biol* 419(1-2):61-74.

158. Pudasaini A, El-Arab KK, Zoltowski BD (2015) LOV-based optogenetic devices: light-driven modules to impart photoregulated control of cellular signaling. *Front Mol Biosci* 2:18.

159. Purcell EM (1997) The efficiency of propulsion by a rotating flagellum. *Proc Natl Acad Sci USA* 94(21):11307-11311.

160. Guadayol O, Thornton KL, Humphries S (2017) Cell morphology governs directional control in swimming bacteria. *Sci Rep* 7(1):2061.

161. Chattopadhyay S, Moldovan R, Yeung C, Wu XL (2006) Swimming efficiency of bacterium *Escherichia coli*. *Proc Natl Acad Sci USA* 103(37):13712-13717.

162. Curtis NA, Orr D, Ross GW, Boulton MG (1979) Affinities of penicillins and cephalosporins for the penicillin-binding proteins of *Escherichia coli* K-12 and their antibacterial activity. *Antimicrob Agents Chemother* 16(5):533-539.

163. Yao Z, Kahne D, Kishony R (2012) Distinct single-cell morphological dynamics under beta-lactam antibiotics. *Mol cell* 48(5):705-712.

164. Maki N, Gestwicki JE, Lake EM, Kiessling LL, Adler J (2000) Motility and chemotaxis of filamentous cells of *Escherichia coli*. *J Bacteriol* 182(15):4337-4342.

165. Ni B, Ghosh B, Paldy FS, Colin R, Heimerl T, Sourjik V (2017) Evolutionary Remodeling of Bacterial Motility Checkpoint Control. *Cell Rep* 18(4):866-877.

166. Taute KM, Gude S, Tans SJ, Shimizu TS (2015) High-throughput 3D tracking of bacteria on a standard phase contrast microscope. *Nat Commun* 6:8776.

167. Pries AR, Neuhaus D, Gaehtgens P (1992) Blood viscosity in tube flow: dependence on diameter and hematocrit. *Am J Physiol* 263(6 Pt 2):H1770-1778.

168. Berg HC, Turner L (1979) Movement of microorganisms in viscous environments. *Nature* 278(5702):349-351.

169. Smith PA, Tripp BC, DiBlasio-Smith EA, Lu Z, LaVallie ER, McCoy JM (1998) A plasmid expression system for quantitative in vivo biotinylation of thioredoxin fusion proteins in *Escherichia coli*. *Nucleic Acids Res* 26(6):1414-1420.

170. Delli-Bovi TA, Spalding MD, Prigge ST (2010) Overexpression of biotin synthase and biotin ligase is required for efficient generation of sulfur-35 labeled biotin in *E. coli*. *BMC Biotechnol* 10:73.

171. Hasman H, Chakraborty T, Klemm P (1999) Antigen-43-mediated autoaggregation of *Escherichia coli* is blocked by fimbriation. *J Bacteriol* 181(16):4834-4841.

172. Kato N, Ohta M, Kido N, Ito H, Naito S, Hasegawa T, Watabe T, Sasaki K (1990) Crystallization of R-form lipopolysaccharides from *Salmonella minnesota* and *Escherichia coli*. *J Bacteriol* 172(3):1516-1528.

173. Kastowsky M, Gutberlet T, Bradaczek H (1992) Molecular modelling of the three-dimensional structure and conformational flexibility of bacterial lipopolysaccharide. *J Bacteriol* 174(14):4798-4806.

174. Kato N, Sugiyama T, Naito S, Arakawa Y, Ito H, Kido N, Ohta M, Sasaki K (2000) Molecular structure of bacterial endotoxin (*Escherichia coli* Re

lipopolysaccharide): implications for formation of a novel heterogeneous lattice structure. *Mol Microbiol* 36(4):796-805.

175. Strauss J, Burnham NA, Camesano TA (2009) Atomic force microscopy study of the role of LPS O-antigen on adhesion of *E. coli*. *J Mol Recognit* 22(5):347-355.

176. Schembri MA, Dalsgaard D, Klemm P (2004) Capsule shields the function of short bacterial adhesins. *J Bacteriol* 186(5):1249-1257.

177. Korea CG, Badouraly R, Prevost MC, Ghigo JM, Beloin C (2010) *Escherichia coli* K-12 possesses multiple cryptic but functional chaperone-usher fimbriae with distinct surface specificities. *Environ Microbiol* 12(7):1957-1977.

178. Flores-Mireles AL, Walker JN, Caparon M, Hultgren SJ (2015) Urinary tract infections: epidemiology, mechanisms of infection and treatment options. *Nat Rev Microbiol* 13(5):269-284.

179. Justice SS, Hunstad DA, Cegelski L, Hultgren SJ (2008) Morphological plasticity as a bacterial survival strategy. *Nat Rev Microbiol* 6(2):162-168.

180. Wadhams GH, Armitage JP (2004) Making sense of it all: bacterial chemotaxis. *Nat Rev Mol Cell Biol* 5(12):1024-1037.

181. Bestebroer J, De Haas CJ, Van Strijp JA (2010) How microorganisms avoid phagocyte attraction. *FEMS Microbiol Rev* 34(3):395-414.

182. Schuurmann J, Quehl P, Festel G, Jose J (2014) Bacterial whole-cell biocatalysts by surface display of enzymes: toward industrial application. *Appl Microbiol Biotechnol* 98(19):8031-8046.

183. Eiteman MA, Lee SA, Altman E (2008) A co-fermentation strategy to consume sugar mixtures effectively. *Journal of Biological Engineering* 2:3-3.

184. Marmann A, Aly AH, Lin W, Wang B, Proksch P (2014) Co-Cultivation—A Powerful Emerging Tool for Enhancing the Chemical Diversity of Microorganisms. *Marine Drugs* 12(2):1043-1065.

185. Park J, Kerner A, Burns MA, Lin XN (2011) Microdroplet-enabled highly parallel co-cultivation of microbial communities. *PLoS One* 6(2):e17019.

186. Song H, Ding MZ, Jia XQ, Ma Q, Yuan YJ (2014) Synthetic microbial consortia: from systematic analysis to construction and applications. *Chem Soc Rev* 43(20):6954-6981.

187. Behkam B, Sitti M (2008) Effect of quantity and configuration of attached bacteria on bacterial propulsion of microbeads. *Appl Phys Lett.* 93(22). 223901; 10.1063/1.3040318.

188. Turner L, Ryu WS, Berg HC (2000) Real-time imaging of fluorescent flagellar filaments. *J Bacteriol* 182(10):2793-2801.

189. Zhuang J, Wright Carlsen R, Sitti M (2015) pH-Taxis of Biohybrid Microsystems. *Sci Rep* 5:11403.

190. Suh S, Traore MA, Behkam B (2016) Bacterial chemotaxis-enabled autonomous sorting of nanoparticles of comparable sizes. *Lab Chip* 16(7):1254-1260.

191. Alapan Y, Yasa O, Schauer O, Giltinan J, Tabak AF, Sourjik V, Sitti M (2018) Soft erythrocyte-based bacterial microswimmers for cargo delivery. *Science Robotics* 3(17).

192. Schauer O, Mostaghaci B, Colin R, Hurtgen D, Kraus D, Sitti M, Sourjik V (2018) Motility and chemotaxis of bacteria-driven microswimmers fabricated using antigen 43-mediated biotin display. *Sci Rep* 8(1):9801.

193. Blattner FR, Plunkett G, 3rd, Bloch CA, Perna NT, Burland V, Riley M, Collado-Vides J, Glasner JD, Rode CK, Mayhew GF, Gregor J, Davis NW, Kirkpatrick HA, Goeden MA, Rose DJ, Mau B, Shao Y (1997) The complete genome sequence of *Escherichia coli* K-12. *Science* 277(5331):1453-1462.

194. Guzman LM, Belin D, Carson MJ, Beckwith J (1995) Tight regulation, modulation, and high-level expression by vectors containing the arabinose PBAD promoter. *J Bacteriol* 177(14):4121-4130.

195. Ksenzenko VN, Kamynina TP, Pustoshilova NM, Kryukov VM, Bayev AA (1982) Cloning of bacteriophage T5 promoters. *Mol Gen Genet* 185(3):520-522.

196. Cherepanov PP, Wackernagel W (1995) Gene disruption in *Escherichia coli*: TcR and KmR cassettes with the option of Flp-catalyzed excision of the antibiotic-resistance determinant. *Gene* 158(1):9-14.

197. Inoue H, Nojima H, Okayama H (1990) High efficiency transformation of *Escherichia coli* with plasmids. *Gene* 96(1):23-28.

198. Colin R, Zhang R, Wilson LG (2014) Fast, high-throughput measurement of collective behaviour in a bacterial population. *J R Soc Interface* 11(98):20140486.

199. Schindelin J, Arganda-Carreras I, Frise E, Kaynig V, Longair M, Pietzsch T, Preibisch S, Rueden C, Saalfeld S, Schmid B, Tinevez JY, White DJ, Hartenstein V, Eliceiri K, Tomancak P, Cardona A (2012) Fiji: an open-source platform for biological-image analysis. *Nat Methods* 9(7):676-682.

200. Crocker JC, Grier DG (1996) Methods of digital video microscopy for colloidal studies. *J Colloid Interf Sci* 179(1):298-310.

201. Purcell EM (1977) Life at Low Reynolds-Number. *Am J Phys* 45(1):3-11.

202. Tirado MM, Martinez CL, Delatorre JG (1984) Comparison of Theories for the Translational and Rotational Diffusion-Coefficients of Rod-Like Macromolecules - Application to Short DNA Fragments. *J Chem Phys* 81(4):2047-2052.

203. Chen X, Berg HC (2000) Torque-speed relationship of the flagellar rotary motor of *Escherichia coli*. *Biophys J* 78(2):1036-1041.

204. Espinosa-Garcia J, Lauga E, Zenit R (2013) Fluid elasticity increases the locomotion of flexible swimmers. *Phys Fluids*. 25(3). 031701; 10.1063/1.4795166.

ACKNOWLEDGEMENTS

I want to thank everyone supporting and helping me with this work.

First of all, I would like to thank Prof. Dr. Victor Sourjik for the opportunity to work in his lab, the support he gave me over all these years and the encouragement to pursue my own ideas.

Big thanks to my thesis committee members Prof. Dr. Anke Becker, Prof. Dr. Martin Thanbichler and in particular Prof. Dr. Michael Bölker who thankfully agreed to become the second reviewer of this thesis.

Furthermore, I want to thank Prof. Dr. Metin Sitti and Dr. Babak Mostaghaci from the Max Planck Institute for Intelligent Systems for the great collaboration and discussions on the bacteriabot project.

I would also like to thank my great group for a wonderful working atmosphere and also for all the great conversations at lunch time. Special thanks go to Remy for reading my thesis and all the support he gave me with the microsfluidic system and cell tracking and to David for helping me with the data analysis.

Thanks of cause all my friends which supported me over these years, making my PhD a great time which I enjoyed a lot, especially thanks to Daniel for joining me on this long journey and keeping my spirit up not only with elaborate scientific discussions but also with all our awesome nights out and trips around the world. You became one of my closest friends, which makes our PhD time even more worth it =); Dr. Joana Lopes for all the fun we had over the years in great and silly moments captured on numerous videos, the fruitful conversations during sober nights and for being an amazing friend (plus for not killing me or snapping); Silvia - aka the world's first class FACS wizard! - for all the great conversations and laughter I had with you and best of good luck with baby Olli ^^ (it's a great German name for a German baby, think about it!); Ela for the good times we had and all the support you gave me over all these years; Delia for being my awesome dance partner, Adrian to controlling our craziness and to support me

against the chicas ;D (and yes, both of you officially progressed from more or less proper to more German than Merkel).

More than a special thanks to María and Limón! You make me laugh every day (yes you have all the hilarious jokes), even when I have my grumpy face on after a long and tiring day. You are just awesome and my 42! I enjoy exploring with you exotic countries and cultures, meeting random people in the streets and being free and crazy as I am. And last but not least, showing me that an ice-cold beer can bring so much peace into life.

Zum Schluss danke ich meiner ganzen Familie recht herzlich, vor allem meinen Eltern Heike und Hartmut und meinem Bruder Jens für den seelischen und moralischen Rückhalt den ihr mir in der ganzen Zeit gegeben habt. Danke, dass ihr nie an mir gezweifelt, jede Entscheidung mit allen Kräften unterstützt und mir die Gewissheit gebt immer ein Zuhause zu haben.

DANKE

"*So long and thanks for all the fish*"

Douglas Adams, The Hitchhiker's Guide to the Galaxy

Wissenschaftlicher Werdegang

Erklärung

Hiermit erkläre ich, dass ich die vorliegende Dissertation mit dem Titel:

„**Antigen 43-mediated biotin display and fabrication of bacteria-driven microswimmers**“

selbstständig verfasst, keine anderen als die im Text angegebenen Hilfsmittel verwendet und sämtliche Stellen, die im Wortlaut oder dem Sinn nach anderen Werken entnommen sind, mit Quellenangaben kenntlich gemacht habe.

Die Arbeit wurde in dieser oder ähnlicher Form noch keiner Prüfungskommission vorgelegt.

Marburg, ___.___._____

_____

(Oliver Schauer)